2020
~ September ~
No. 3

HIDRAULICA

HYDRAULICS-PNEUMATICS-TRIBOLOGY-ECOLOGY-SENSORICS-MECHATRONICS

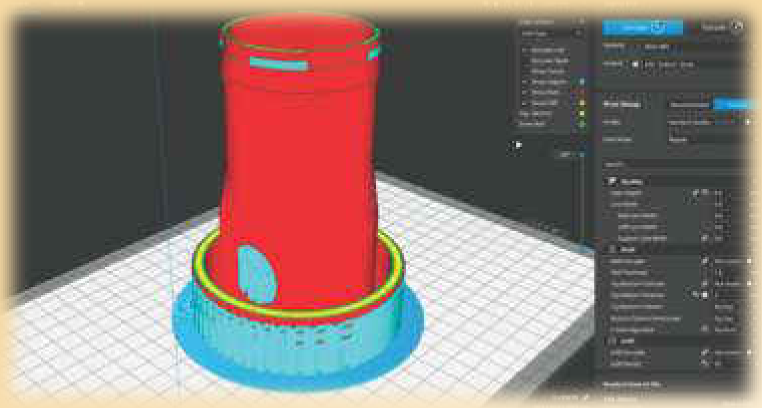

ISSN 1453-7303
ISSN-L 1453-7303

Available online at
hidraulica.fluidas.ro

CONTENTS

Published by:
Hydraulics and Pneumatics Research Institute, Bucharest-Romania
Address: 14 Cuţitul de Argint, district 4, Bucharest, 040558, Romania
Phone: +40 21 336 39 91; Fax: +40 21 337 30 40; e-Mail: ihp@fluidas.ro; Web: www.ihp.ro
with support from:
National Professional Association of Hydraulics and Pneumatics in Romania - FLUIDAS
e-Mail: fluidas@fluidas.ro; Web: www.fluidas.ro

HIDRAULICA Magazine is indexed by international databases

ISSN 1453 – 7303; ISSN – L 1453 – 7303

EDITORIAL

De noutăți cine se ocupă și, mai ales, când?

Dr. Ing. Petrin DRUMEA
DIRECTOR PUBLICAȚIE

Dacă în ultimul timp am tot încercat să conving lumea că dezvoltarea domeniului se face cu foarte mare efort și cu o aplecare specială spre cercetarea aplicativă practică, tradițională, în editorialul de astăzi o să mă preocup de cercetarea aplicativă modernă și cu puternic iz teoretic. Nu o să încerc să definesc aceste nuanțe ale noțiunii de cercetare aplicativă, în speranța că voi fi corect înțeles fără probleme.

Două direcții noi în domeniul tehnologic s-au impus în zilele noastre, ambele influențând acționările hidraulice, dar și folosindu-le. Cele două direcții sunt interconectate și mai ales au intrat în vocabularul zilnic al tuturor oamenilor, chiar și atunci când nu înțeleg aceste noțiuni.

În primul rând discutam de digitalizare, care a cunoscut o dezvoltare foarte rapidă, devenind un accelerator al dezvoltarii și care reprezintă – într-o încercare de a sintetiza mai multe păreri – folosirea tehnologiei de stocare și procesare, căutare și regăsire a informațiilor între utilizatorii on-line. Suportul tehnic al digitalizării e reprezentat de o infrastructură electronică ce permite transmiterea și primirea de informații la distanță. Internetul este suportul tehnologic al digitalizării. După procesul de digitizare a informațiilor urmează faza de integrare și de folosire a lor în diverse aplicații software cu premise bune pentru automatizări, deci digitalizarea.

O a doua direcție des și uneori neclar invocată în spațiul public, dar foarte serios discutată în spațiul tehnico-științific este tehnologia, în cazul nostru - acționarea hidraulică inteligentă. Hidraulica inteligentă în comparație cu actionarea electrică are un cost mai bun, o eficiență energetică mai bună, o densitate de putere mai bună, dar o controlabilitate ceva mai scazută. Pe plan mondial această orientare spre combinația dintre hidraulică, electronică, senzorică și informatică a făcut și face pași uriași, în timp ce pe plaiurile noastre și - aș putea îndrăzni să spun - și la nivel european lucrurile merg greoi și cu multe poticneli. Problema mare în țara noastră este că nu știm cine se ocupă cu aceste noutăți tehnice, unde se vor face pasii necesari și mai ales când? Dacă vom miza doar pe activitatea studențească este clar că am cam renunțat la crearea de specialiști în domeniu și la implicarea acestora în cercetarea serioasă în domeniul hidraulicii inteligente și al digitalizării. Primul pas spre renunțarea la noutăți este deja făcut de cei care gestionează fondurile țării, care au bani pentru orice, dar nu pentru cercetare.

Nu uitați că în hidraulica trebuie făcute și racorduri și bazine și conducte, precum și mentenanța sistemelor, dar nu în detrimentul noutăților de tipul digitalizării sistemelor hidraulice sau al dezvoltării hidraulicii inteligente.

Multă sănătate!

EDITORIAL

Who deals with novelty and, above all, when?

Ph.D.Eng. Petrin DRUMEA
MANAGING EDITOR

While lately I have been trying to convince the people that the development of the field is done with great effort and with a special inclination towards practical, traditional applied research, in today's editorial I will focus on modern applied research with a strong theoretical flavour. I will not try to define these nuances of the notion of applied research, in the hope that I will be correctly understood without problems.

Two new directions in the technological field have emerged nowadays, both influencing the hydraulic drives, but also using them. The two directions are interconnected and especially have entered the daily vocabulary of all people, even when they do not understand these notions.

First of all we are talking about digitalization, which has experienced a very rapid growth, becoming an accelerator of development, and is - in an attempt to synthesize multiple opinions - the use of technology for storing, processing, searching and retrieving information among online users. The technical support of digitalization is represented by an electronic infrastructure that allows sending and receiving information remotely. The Internet is the technological support of digitalization. The process of digitizing the information is followed by the phase of integrating and using it in various software applications with good prerequisites for automation - that is the digitalization.

A second direction often and sometimes unclearly invoked in the public space, but very seriously discussed in the technical and scientific space is technology, in our case - the intelligent hydraulic drive. Intelligent hydraulics compared to electric drive has a better cost, better energy efficiency, better power density, but a slightly lower controllability. Globally, this focus on the combination of hydraulics, electronics, sensorics and computing has made and continues to make huge strides, while on our lands and - I dare say - at European level things are moving slowly and with many stumbles. The big problem in our country is that we do not know who deals with these technical novelties, where will the necessary steps be taken and especially when? If we rely only on student activity, it is clear that we have given up the creation of specialists in the field and their involvement in serious research in the field of intelligent hydraulics and digitalization. The first step towards giving up the novelty is already made by those who manage the country's funds, who have money for anything but research.

Remember that in hydraulics one must make fittings and tanks and pipes, and also provide system maintenance, but not to the detriment of novelties such as the digitalization of hydraulic systems or the development of intelligent hydraulics.

I wish you all good health.

Wave Energy Recovery System Based on the Hydrostatic Principle

Assistant professor **Fănel Dorel ȘCHEAUA**[1]*

[1] "Dunărea de Jos" University of Galați

* fanel.scheaua@ugal.ro

Abstract: *Due to the certainly fact that the energy needs are constantly increasing at the present time, the handy production methods and also constituting environmentally friendly methods must be considered. Thus, processes and devices for energy production based on our planet renewable sources, constituted in water flows, solar energy, wind power and not at least the waves and tides force, have been continuously invented and developed. A solution for wave energy capture operating on the hydrostatic principle is presented in this paper. The solution particularity is represented by the operating principle of a constructive variant of wave energy recovery plant that has to be located directly on the seafront in order to have direct access at the waves continuously motion which drive the installation's floats. A set of large volume floats are located directly on the water surface, which by the cyclical movement in vertical direction drives the hydraulic cylinders of the plant producing hydraulic energy in the form of volumetric flow rate and fluid pressure. This energy flow stream has the possibility to drive hydrostatic motors that provide axis rotational motion and rotation torque necessary for the operation of the electricity generators.*

Keywords: *Wave energy recovery, hydrostatic actuation, circuit model*

1. Introduction

The production of energy from renewable sources represents the optimal option to be applied for an environment not irreparably affected. Whether we are talking about applications using solar energy, wind energy, wave or tidal power, it should be emphasized that the contribution of all these methods for obtaining green energy has gained increasing importance in the total energy produced today in the world, thus replacing the traditional energy production methods that bring inevitable changes in the environment.
Of the procedures for obtaining energy from renewable sources, the waves force is of particular importance because by wave continuous movement a significant amount of mechanical energy can be recovered that can be transformed into electricity.
There are multiple applications that have been developed over time regarding the wave energy recovery. It represents a method of use the large amount of energy provided by the wave motion worldwide over seas and oceans coastal regions. This existent potential based on cyclic motion described by wave motion must be used at the real value in order to recovery and convert the energy amounts in electrical energy for human communities needs. The power plant concept uses this potential motion to achieve a continuous hydraulic fluid power stream within a closed circuit necessary for a rotary engine motion that provide angular velocity and torque at the shaft necessary for a generator to convert the mechanical energy into electric energy.
The constructive solution for a generative power plant based on the waves force is presented, which can be located on the shore, having direct access to the sea. This concept uses a set of large floats positioned at the water level near the shore, having the possibility to make repeated cyclical movements in the vertical direction dictated by the waves force. These floats have the connections with hydrostatic systems anchored on the shore and which receive the mechanical energy required to move the piston due to the continuous floats cyclic movement. Through this process the working fluid existing inside the hydrostatic systems is entrained within the circuit having the possibility to transmit the energy flow to a hydrostatic motor that transforms the taken energy in the form of volumetric flow rate and pressure into mechanical energy of rotation at the motor shaft.
There are presented aspects related to the possibilities of realization and location of such a power plant in the sea immediate vicinity. The plant facility must be located so that it has an adequate depth of water (steep bank) and at a very small distance from the water so that the floats are

located not too far from the central unit. The mechanical connections between the floats and the hydrostatic systems must be made in such a way as to ensure the floats moving possibility, pushing the hydrostatic systems rods, with a very low coefficient of friction between the components in contact so as not to affect the installation efficiency.0

2. Wave energy concept

Marine waves are formed at the contact surface between water and atmospheric air. Due to the atmospheric air forced movement as a result of the uneven atmosphere heating levels in different areas, the winds are occur acting on the large water surfaces and causing the water movement.
The combined frictional and pressure forces action on the water surface have results in the mechanical energy transfer from the air movement to water. Thus, the waves are formed with a significant amount of energy stored dependent of wind velocity, time and acting surface.
Depending on the sinusoidal functions, the behavior of the deep-sea waves can be modeled. The approximate shape of the deep-sea waves is shown as a sinusoidal curve, and the wave-specific parameters are shown in Figure 1. 00

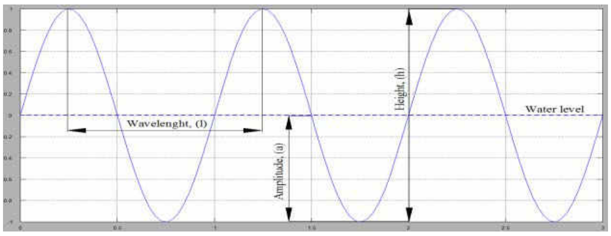

Fig. 1. Sine wave approximation curve

Starting from the concept of fluid mechanics that considers the displacement of a single fluid particle on a given trajectory (Lagrange) the velocity field can be shaped at a certain time (Euler).
Using the Lagrange method, the fluid particle motion reported to an OXYZ reference axis system can be studied, where the position of the particle depends on the time t and the initial position given by its coordinates (x_0, y_0, z_0) at time (t_0).
The trajectory equations are as follows: 0

$$x = x(x_0, y_0, z_0, t);\ y = y(x_0, y_0, z_0, t);\ z = z(x_0, y_0, z_0, t) \tag{1}$$

Velocities and accelerations are expressed as: 0

$$\begin{aligned} & u = \frac{\partial x}{\partial t};\ v = \frac{\partial y}{\partial t};\ w = \frac{\partial z}{\partial t} \\ & a_x = \frac{\partial u}{\partial t} = \frac{\partial^2 x}{\partial t^2};\ a_y = \frac{\partial v}{\partial t} = \frac{\partial^2 y}{\partial t^2};\ a_z = \frac{\partial w}{\partial t} = \frac{\partial^2 z}{\partial t^2} \end{aligned} \tag{2}$$

The Euler method determines the motion elements of all fluid particles passing through a point in space reported by its coordinates to a fixed trihedral in time. Thus, the field velocity values are obtained at the points of the space occupied by the fluid movement as well as the velocities variation at these points as a time function.
The velocity field and accelerations are given by the following relations: 0

$$u = u(x, y, z, t);\ v = v(x, y, z, t);\ w = w(x, y, z, t) \tag{3}$$

Where x, y, z represent the space points coordinates and not of the fluid particle.

$$du = \frac{\partial u}{\partial t}dt + \frac{\partial u}{\partial x}dx + \frac{\partial u}{\partial y}dy + \frac{\partial u}{\partial z}dz \qquad (4)$$

$$\begin{aligned} a_x &= \frac{du}{dt} = \frac{\partial u}{\partial t} + u\frac{\partial u}{\partial x} + v\frac{\partial u}{\partial y} + w\frac{\partial u}{\partial z} \\ a_y &= \frac{dv}{dt} = \frac{\partial v}{\partial t} + u\frac{\partial v}{\partial x} + v\frac{\partial v}{\partial y} + w\frac{\partial v}{\partial z} \\ a_z &= \frac{dw}{dt} = \frac{\partial w}{\partial t} + u\frac{\partial w}{\partial x} + v\frac{\partial w}{\partial y} + w\frac{\partial w}{\partial z} \end{aligned} \qquad (5)$$

Details of the fluid particle motion using the Lagrange and Euler methods are shown in the figure 2.

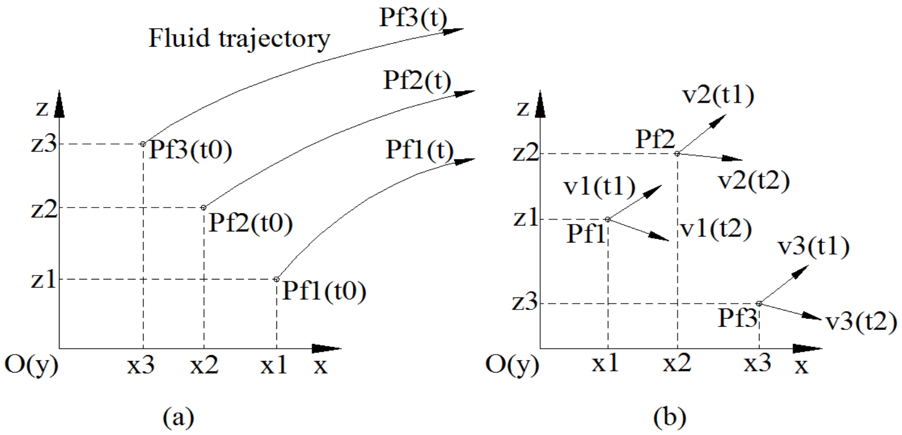

Fig. 2. Description of fluid motion: Lagrange method (a) and Euler method (b)

For the case of the fluid considered incompressible having $(\rho = 0)$ and $\left(\frac{\partial \rho}{\partial t} = 0\right)$ the continuity equation is written: 00

$$\frac{\partial u}{\partial x} + \frac{\partial v}{\partial y} + \frac{\partial w}{\partial z} = 0 \qquad (6)$$

If fluid motion is considered as irrotational, the velocity forms may be expressed in terms of velocity potential (ϕ):

$$u = \frac{\partial \phi}{\partial x};\ v = \frac{\partial \phi}{\partial y};\ w = \frac{\partial \phi}{\partial z} \qquad (7)$$

By making the substitutions in the continuity equation is obtained:

$$\frac{\partial^2 \phi}{\partial x^2} + \frac{\partial^2 \phi}{\partial y^2} + \frac{\partial^2 \phi}{\partial z^2} = 0 \qquad (8)$$

The obtained equation is known as the Laplace equation, which describes the wave motion of the deep water regions.

3. Model of hydrostatic circuit used for energy recovery

For the wave energy recovery plant basic unit, a constructive solution is presented which allow the take over of wave energy and its conversion into hydraulic energy of the working fluid used in a closed circuit. For this purpose, a hydraulic circuit is designed in order to use linear motors that acquire cyclic motion from the sea wave providing a continuous fluid stream to a rotary hydraulic motor of the system, ensuring rotational movement at the motor axis, necessary for driving the electric current generator. 0

The installation composition shown in figure 3, based on the specific symbols of industrial hydraulics, is being made up of drive floats, linear motors for working fluid transport, hydraulic accumulators for fluid pressure accumulation, distribution and directional fluid flow apparatus inside circuit, a rotary hydraulic motor with variable displacement that operates based on the fluid flow rate received as a result of the forced displacement of the floats corresponding to the wave motion. 0

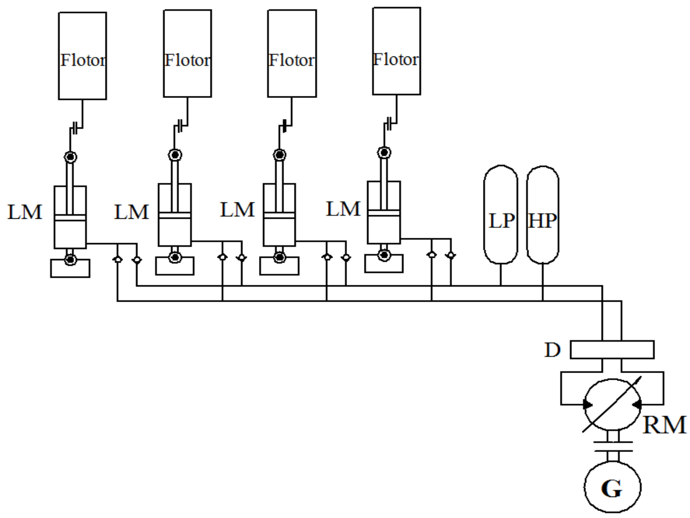

Fig. 3. Schematically representation of wave energy recovery power plant (WERP).

Depending on the waves amplitude is possible to obtain optimal results regarding the energy recovered using the hydrostatic method proposed.

The operating principle based on the hydraulic drive implies high operation efficiency due to the reliability of the installation components.

The system performs two types of energy conversion functions corresponding to changing the waves mechanical energy into hydraulic energy of the moving fluid being converted again into mechanical energy as motor shaft rotation.

4. Hydrostatic wave energy conversion method

A hydrostatic method of wave energy recovery is presented that involves phenomena of energy transfer between the component elements of the installation recovery unit. Theoretical aspects of calculation that underlie these phenomena dictate the operating principle of the wave energy recovery plant.

The primary energy conversion function ensures the retrieval of the mechanical energy from the power source represented by linear motors and the energy amount transfer to the installation rotary motor through the working fluid. The basic fluid parameters inside the hydrostatic drive are represented by volumetric flow rate and hydrostatic pressure.

The primary conversion function type (PCF) made with linear motors is required for this type of recovery circuit and the working phases characteristic of the operation describe the working cycle of the linear pumps.

The principle diagram of the drive system with linear motors is shown in Figure 4. 0

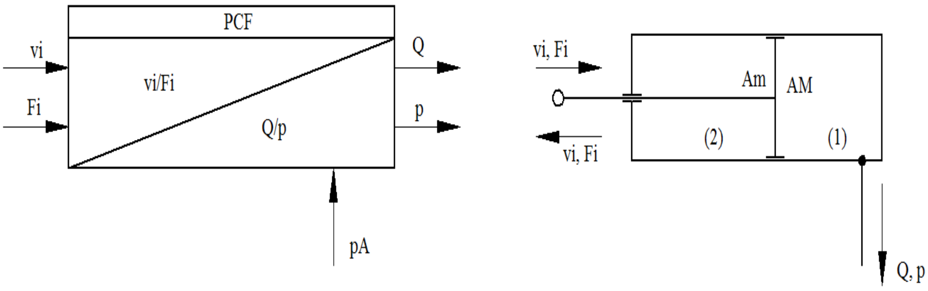

Fig. 4. Primary conversion function (PCF)

The linear motors constructive characteristics involving the piston working areas, the characteristic piston stroke, the fluid flow conveyed at the maximum piston stroke ensure the hydraulic power values obtained through the use of the linear motor.

The multi-polar model of the primary conversion function (PCF) performed with the linear motor comprises the characteristic equations for the input and output parameters represented by the input force and velocity, as well as the fluid flow rate and pressure at the output. 0

$$Q = 6\eta_v A_M v_i \tag{9}$$

$$F_i = \frac{1}{\eta_{mh}}\left(A_M p - A_m p_A\right) \tag{10}$$

By applying the principle of fluid flow continuity and the association with the differential equation of motion of the active components involved in energy transmission, the dynamic model of the primary conversion function (PCF) is obtained.0

$$\begin{aligned} Q &= A_M \frac{dx}{dt} - a_M\left(p - p_A\right) - \frac{V_{0M}}{E}\frac{dp}{dt} \\ F_i &= m_r \frac{d^2x}{dt^2} - b_M \frac{dx}{dt} - C_f \frac{\dot{x}}{|x|}\left(A_M p - A_m p_A\right) \end{aligned} \tag{11}$$

Based on the cyclical and continuous action of the linear motors dictated by the waves movement, the working fluid flow inside the circuit is provided, which ensures an energy flux necessary to drive the hydrostatic motor. This motor takes the energy from the working fluid in the form of energy components flow rate (Q) and pressure (p), further converting it into mechanical energy, through the components moment (torque) and angular velocity at the axis, necessary to drive the electric current generator.

This energy conversion is considered as the secondary conversion function (SCF) presented schematically in figure 5. 0

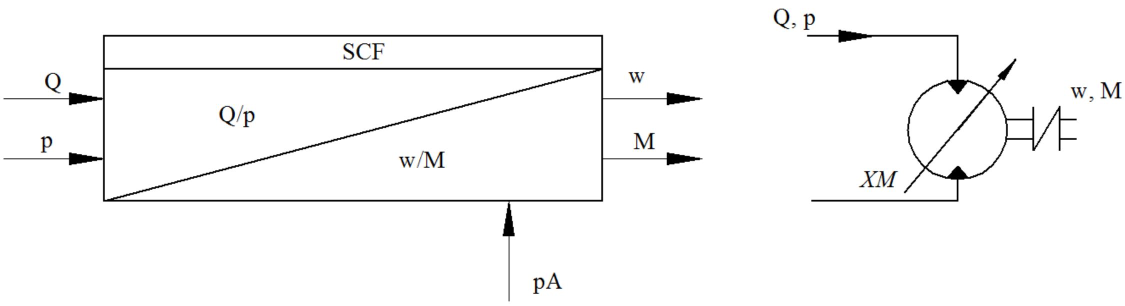

Fig. 5. Second conversion function (SCF)

The theoretical flow rate value received by the hydraulic motor taking into account the XM command and its momentary and maximum cylinder rates is of the form: 0

$$Q = V_m \frac{w}{2\pi} = XM \frac{1}{2\pi} V_0 w \tag{12}$$

The real flow rate taking into account the engine volumetric efficiency will be of the form: 0

$$Q = XM \frac{1}{2\pi\eta_v} V_0 w \tag{13}$$

The relations for mechanical and hydraulic power are: 0

$$P_m = M \frac{w}{2\pi};\ P_h = Q\left(p - p_A\right) \tag{14}$$

where:

$$P_m = \eta_t P_h \tag{15}$$

$$M \frac{w}{2\pi} = \eta_v \eta_{mh} XM \frac{1}{2\pi\eta_v} V_0 w\left(p - p_A\right) \tag{16}$$

$$M = \eta_{mh} XMV_0 \left(p - p_A\right) \tag{17}$$

From the obtained equation can be determined the pressure necessary value for achieving the mechanical torque (M) at the motor shaft: 0

$$p = p_A + \frac{M}{\eta_{mh} XMV_0} \tag{18}$$

For angular velocity the relation is: 0

$$w = \frac{2\pi\eta_v Q}{XMV_0} \tag{19}$$

The multi-polar model of the secondary conversion function (SCF) is thus obtained: 0

$$n = \eta_v \frac{1000Q}{XMV_0} \left[rot / \min\right];\ p = p_A + \frac{10M}{\eta_{mh} XMV_0} \left[bar\right] \tag{20}$$

The presented model provides information on the modality to convert the input parameters $\left(Q, p\right)$ into output parameters $\left(M, w\right)$ depending on the hydraulic motor cylinder control mode $\left(XM\right)$.

5. Conclusion

Current methods of obtaining energy from alternative sources have been developed and improved in order to be able to provide higher amounts of green energy, thus reducing the energy consumption that comes from the sources that have a direct effect on the environment.

Of all used methods, the sea and ocean waves energy must be highlighted as a viable energy source to be recovered and converted into electrical energy.
A constructive variant for a wave energy recovery plant was presented in this paper. It is a concept of using a hydrostatic drive system powered by the cyclical movement of a set of floats positioned directly on the water surface.
Due to the waves continuous movement the floats press directly on the pistons of the hydrostatic systems through the rods, forcing the fluid to circulate in the circuit. This results in a volumetric flow rate and pressure that constitutes the flow energy necessary for a hydrostatic motor that performs axial rotational movement with a certain velocity value.
It represents a working principle that can be used in the construction of such generative energy units based on the waves motion.

References

[1] Florea, J., and V. Panaitescu. *Fluid Mechanics / Mecanica fluidelor*. Bucahrest, Didactic and Pedagogical Publishing House, 1979.
[2] Axinti, G., and A.S. Axinti. *Hydraulic and pneumatic drives - Components and systems, functions and characteristics / Actionari hidraulice si pneumatice – Componente si sisteme, functii si caracteristici.* Chisinau, Tehnica-Info Publishing House, 2008.
[3] Vasilescu, Al.A. *Fluid Mechanics / Mecanica fluidelor.* Galati, Ministry of Education and Tuition, University of Galati, 1979.
[4] Spînu, I., and C.D. Deac. “Valorificarea energiei valurilor.” Paper presented at Multidisciplinary National Conference, Sebeș, Romania, June 1–2, 2012.
[5] Dean, R.G., and R.A. Dalrymple. *Water wave mechanics for engineers and scientists.* World Scientific Publishing Company, 1991.
[6] Krogstad, Harald E., and Oivind A. Arntsen. *Linear Wave Theory. Part A. Regular Waves*. Norwegian University of Science and Technology, Trondheim, Norway, 2000.
[7] Scurtu, I.C. “A survey of developments in wave energy." *Analele Universitatii Maritime Constanta* 14, no. 20 (2013): 103-106.
[8] Scurtu, I.C. “CFD Simulation Approach for Semisubmersible Response in Waves Based on Advanced Techniques.” *Applied Mechanics and Materials* 772 (2015): 108-113.
[9] Goanta, A.M. “Innovative methods of knowledge transfer by multimedia library.” *IOP Conference Series: Materials Science and Engineering* 145, no. 4 (2016): 042002.
[10] Goanta, A.M., L. Daschievici, and D. Ghelase. “Modern PLM integrated design tools that meet the of principles of concurrent engineering.” Paper presented at the 9-th WSEAS International Conference on System Science and Simulation in Engineering – ICOSSSE'10, Iwate, Japan, 4-6 October, 2010.

Modeling the Flow through the Wastewater Installation Bioreactor

Prof.PhD.Eng. **Mariana PANAITESCU**[1*], Prof.PhD.Eng. **Fănel-Viorel PANAITESCU**[1],
student **Nicolae-Marian IACOB**[1]

[1] Constanta Maritime University

* panaitescumariana1@gmail.com

Abstract: *The paper presents the wastewater treatment processes circulating on board cruise ship and modeling the flow through the wastewater installation bioreactor.*

Keywords: *Wastewater, modeling, bioreactor, oil separator, hydrocarbon, emulsion*

1. Introduction

Norwegian Joy is a cruise ship (Figure 1) [1].

Fig. 1. Norwegian Joy cruise ship

The characteristic data of the ship, as well as the installations and the afferent equipments are the result of the designer [2]. The total installed power of the ship is 76800 kW and is equipped with two MAN B & W 14V48 / 60CR engines of 16800 kW and three diesel generators of MAN B & W 12V48 / 60CR with a power of 14400 kW. The propulsion system is two ABB Azipod XO units with a total power of 40 MW. The power supply installation of the ship and the Azipod is divided into two large groups bow and stern, which allow the operation of the installations on the ship and the propulsion.
Regarding the wastewater treatment, on board the cruise ship is operated with the Scanship AWP system (Advanced waste purification) (Figure 2).

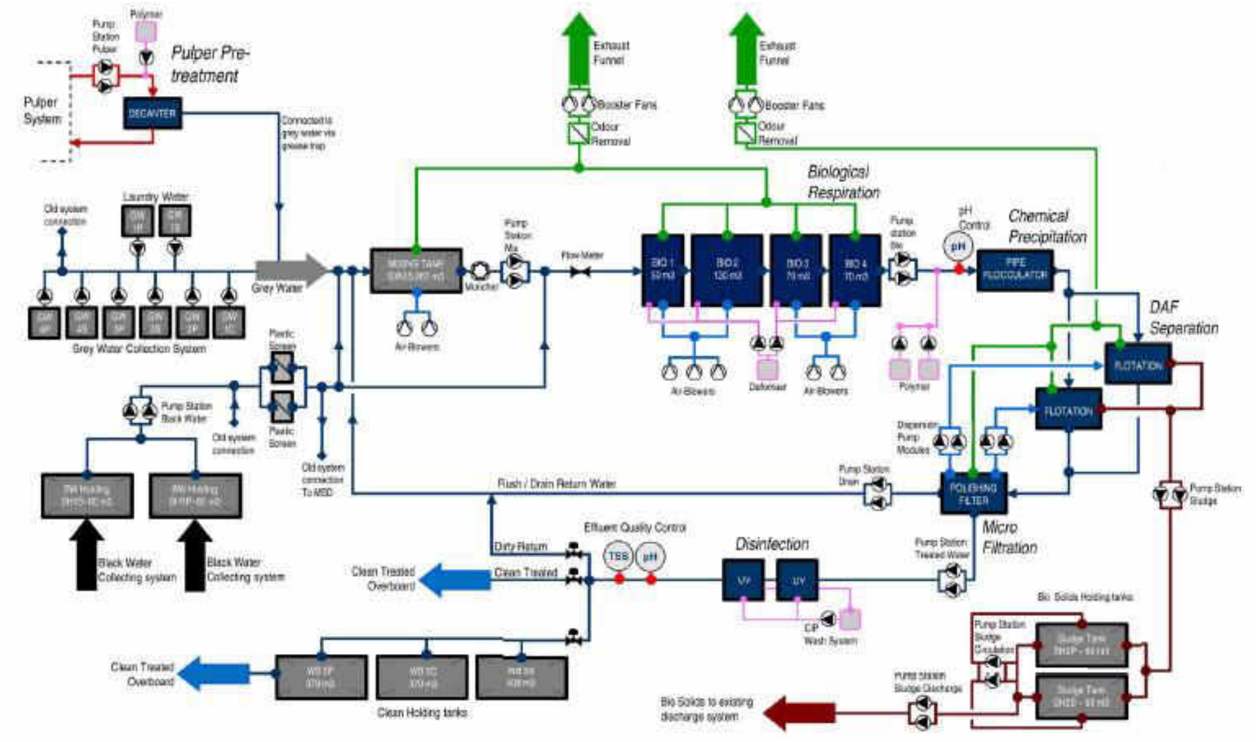

Fig. 2. Advanced waste purification system on cruise ship JOY

The wastewater treatment processes circulating on board of the JOY are shown in the diagram below (Figure.3) [1]:

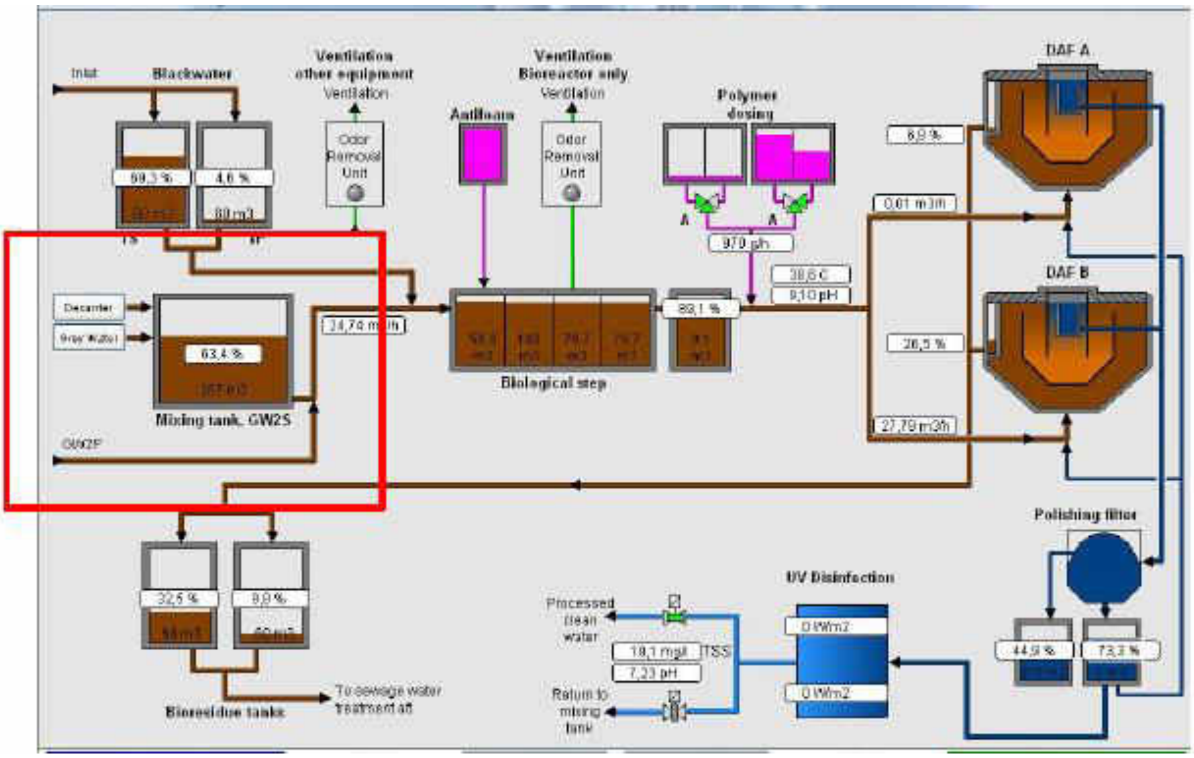

Fig. 3. JOY wastewater treatment processes

The wastewater comes from: the Engine room (ER), from the ER bilge, where the treatment of oil residues from the ship's facilities is done with the bilge separator, through an automated circuit and from all decks, crew cabins, passenger cabins, recreation rooms, gyms, swimming pools, restaurants, medical offices, shops, etc. In the ER, wastewater goes through several treatment processes:

- *Separation of residues by bilge separator type: 3SEP OWSF* (Figure 4) [2]

Fig. 4. JOY 3SEP OWS bilge separator

The elimination of hydrocarbon residues occurs in 3 points: tanks T_1, T_2 and T_3. The removed hydrocarbon residues are directed to the residue tank. In the first phase (tank T_1), the disposal of residues is controlled by a hydrocarbon sensor. The sensitivity of the sensor is adjustable to reduce the amount of bilge water removed from T_1. Hydrocarbons are accumulated at the top of tanks T_2 and T_3, the water coming from T_1. The removal of hydrocarbons from the filter tanks T_2 and T_3 occurs automatically. These hydrocarbons are removed by the pneumatically operated valves $V0_2$ (T_2) and $V0_3$ (T_3). The time interval between hydrocarbon removals for $V0_2$ and $V0_3$ is fixed. Hydrocarbons are removed from $V0_2$ every 5 minutes for a period of 20 seconds, which can be adjusted. Hydrocarbons removed from $V0_3$ every hour for a fixed period of 5 seconds. When the separator is switched on, automatic removal of hydrocarbons by $V0_2$ and $V0_3$ occurs for a fixed period of 3 seconds. This ensures that hydrocarbons that have accumulated at the top of the tanks while the separator has been turned off are removed.

- *Separation of residues through the JOWA type bilge separator*

The JOWA bilge separator is a two-stage separation system designed to separate and remove hydrocarbons from wastewater (Figure 5) [3].

In the first stage, the separator removes free hydrocarbons by gravity using coalescing plates. An adjustable hydrocarbon sensor controls the pneumatic valve for automatic discharge into the sludge tank or any dedicated tank. This sensor makes it possible to minimize the amount of water discharged into the waste tank. In the second stage the emulsified hydrocarbons are discharged into the two filter tanks and the value of the quantity in PPM (parts per million) is monitored by a PPM-meter also called ODM (oil discharge monitor) (Figure 6) [2], before the water is discharged overboard.

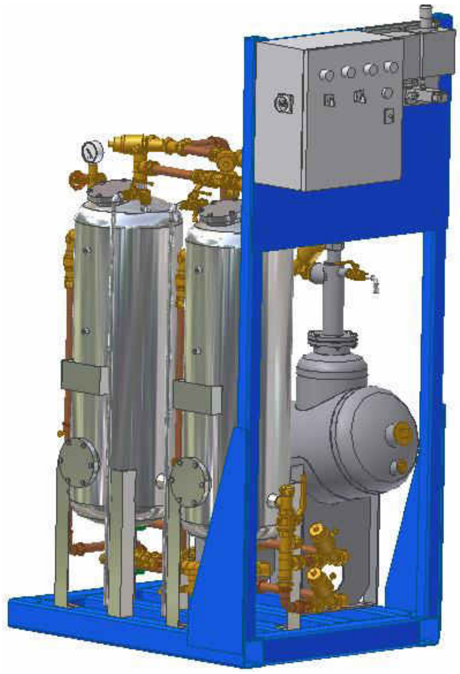

Fig. 5. JOWA bilge separator

Fig. 6. JOWA type separator control panel together with PPM meter

The free hydrocarbons collected at the top of each tank are automatically discharged into the waste tank at a predetermined interval. When the PPM meter alarm sounds, the separator automatically closes the overflow valve and recirculates the treated water into the bilge. When the degree of contamination drops below 15 ppm, the overflow discharge valve opens again without human intervention (Figure 7) [3].

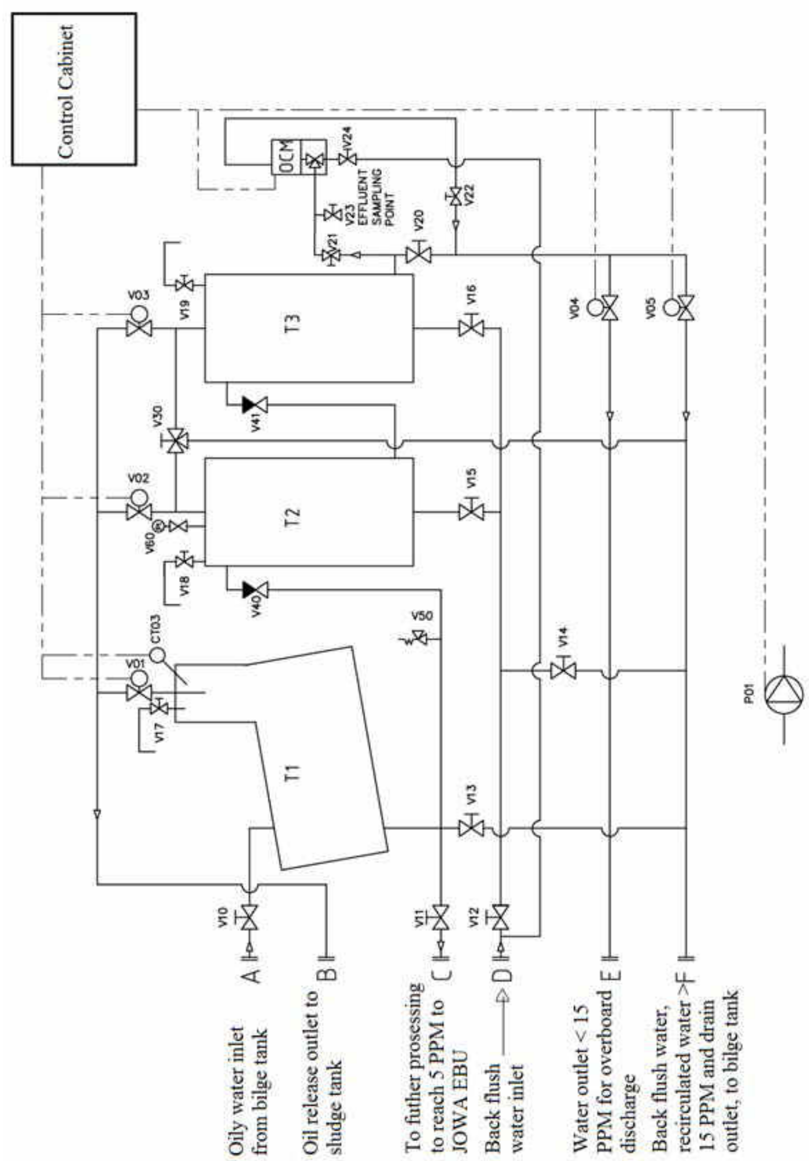

Fig. 7. Operating scheme of hydrocarbon separation

- *Anti-emulsion system. Constructive features of the separator - EBU*

The JOWA anti-emulsion system is designed to act as a pre-treatment of emulsions in bilge water before it enters the separator. The main function of the unit is to flocculate and remove hydrocarbon emulsions from bilge water (Figure.8) [4]. The EBU is specially designed to be connected to the bilge separator as a combined treatment system. When connected to the separator, the EBU system uses its own bilge pump [5].

The bilge pump of the EBU system ($P0_1$) is a screw or multi-screw type pump depending on the capacity of the treatment system 6m3 / 24h, $8m^3$ / 24h, $10m^3$ / 24h. It operates at a power of 0.55kW - 1.74kW with a current of 1.55A - 3.5A.

In addition to the bilge pump and two dosing pumps $P0_2$ and $P0_3$ are introduced into the system. These two pumps are diaphragm and operate with a power consumption of 16 W, at a working pressure of 0-2 bar.

Fig. 8. EBU anti-emulsion system

The B01 storage tank has a volume of 1000 liters. The anti-emulsion system coupled to the separator removes up to 80% of the water from the emulsions, then this water called treated water is discharged into the separator.

2. Methods and researches

The ANSYS-FLUENT v13 program was used to simulate the process of separating hydrocarbons from water.

2.1 Drawing geometry

A two-dimensional model was created, a rectangle 0.1 m wide and 0.2 m long. This is the reservoir where the two fluids, water and hydrocarbon, will separate gravitationally. To make the geometry we used the program tools (Figure 9) and dimensioned the study system (Figure 10). In the end, the study model was generated in an axonometric system and with the units of measurement.

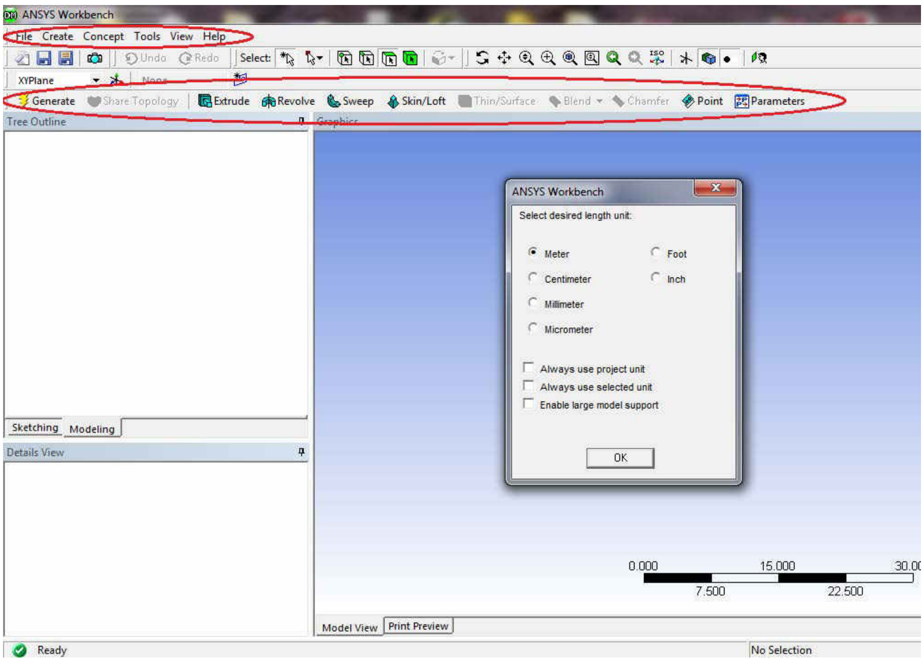

Fig. 9. Geometric module

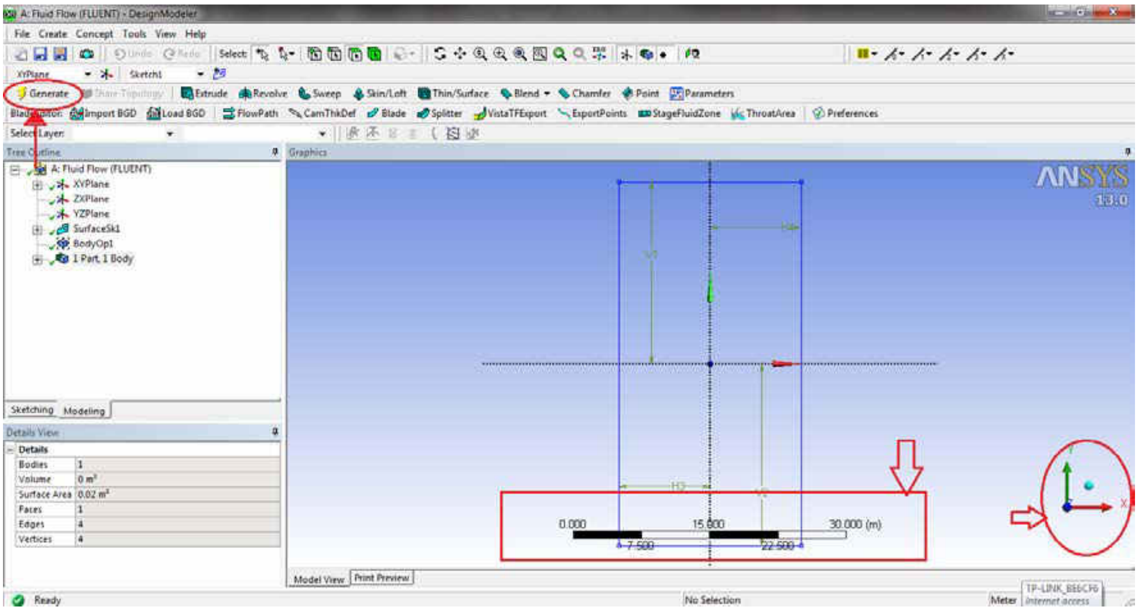

Fig. 10. Geometry completion

2.2. Profile discretization

At this stage, we have made the tank discretized. We discretized the tank into 5000 simple units, namely squares measuring 0.002 meters (Figure 11).

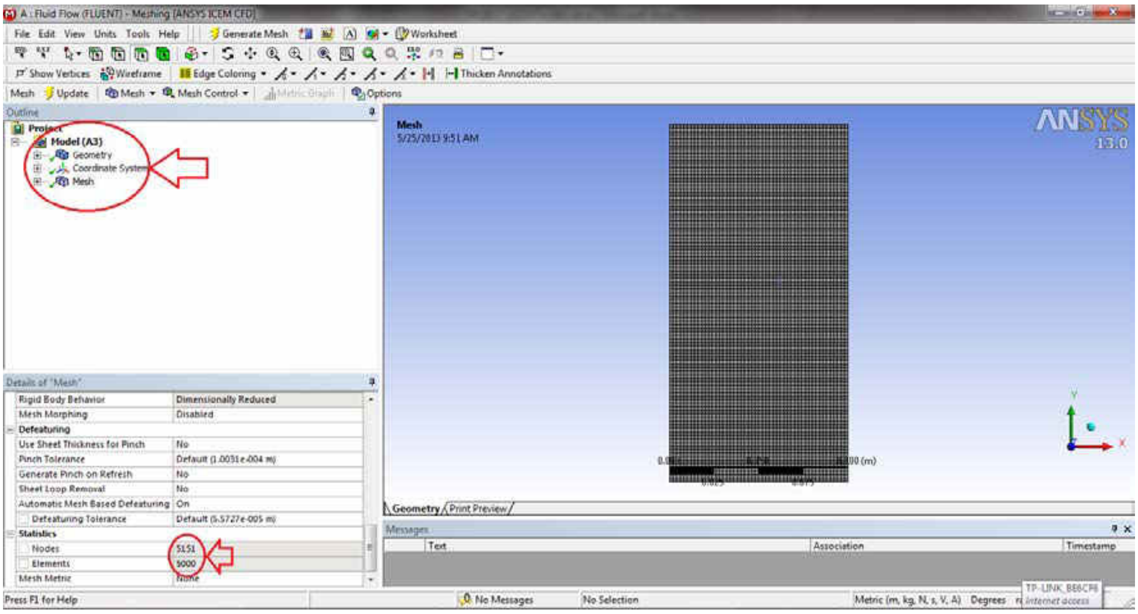

Fig. 11. Discretization of the field of study

2. 3. Calculation of fluid parameters

2.3.1. Using the Solution function

Opening the solution module leads to the window in Figure 12, where the parameters and settings are entered for a more suggestive display.

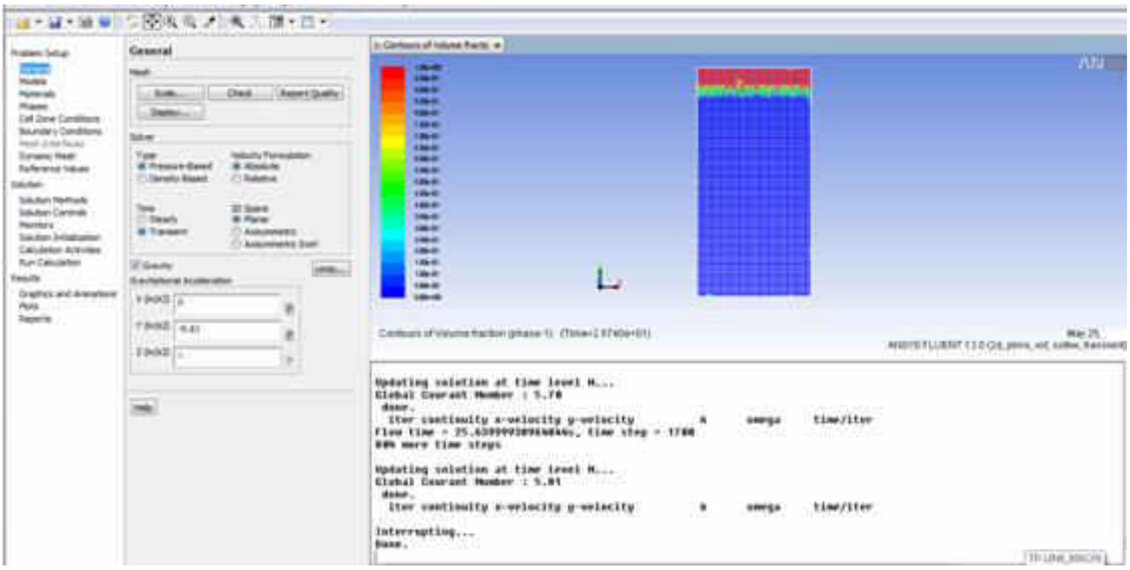

Fig. 12. Calculation of solutions

3. Results and interpretations

After initialization, an effective calculation is made, establishing for the first time 1000 iterations with the size of the iteration interval of 0.001 seconds (Figure 13).

As results after the flow simulation were obtained:
- representation of water relative to hydrocarbon after 1 second (Figure 14);
- representation of water relative to hydrocarbon after 11 seconds (Figure 15);
- representation of water relative to hydrocarbon after 111 seconds (Figure 16);
- representation of the circulation speed of fluid cells (Figure 17)
- representation of the density of working fluids (Figure 18);
- representation of the turbulence of kinetic energy (Figure 19);
- representation of the dynamic pressure of moving fluids (Figure 20).

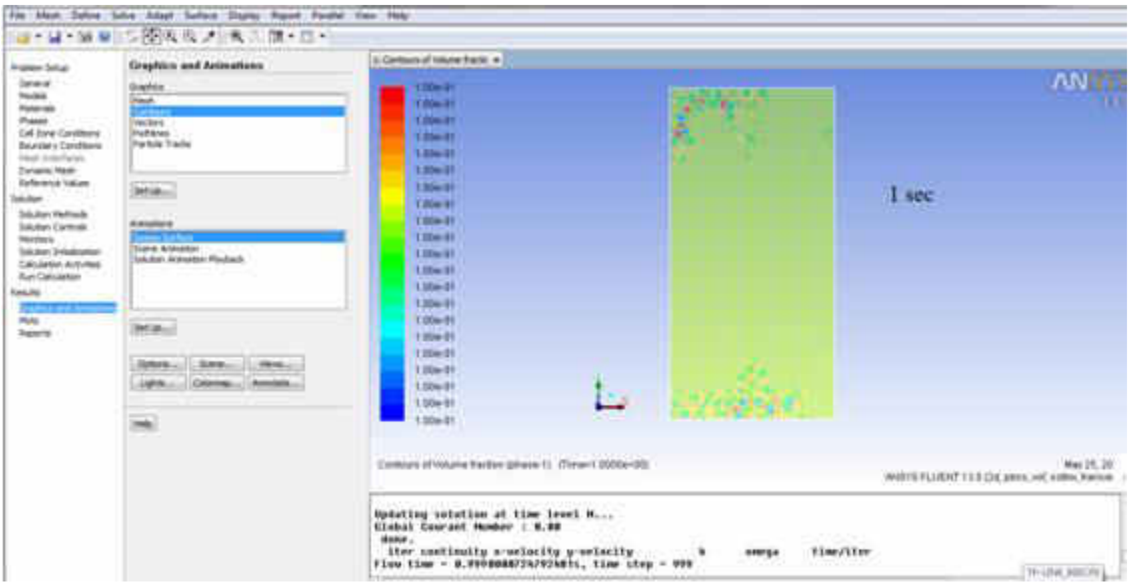

Fig. 13. Representation of water to hydrocarbon after 1 second

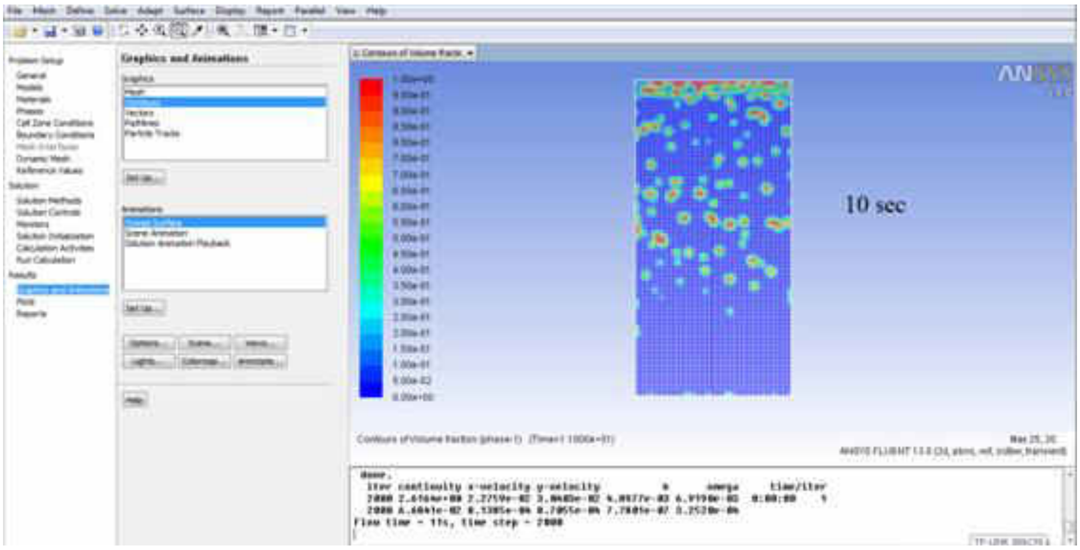

Fig. 14. Representation of water to hydrocarbon after 11 seconds

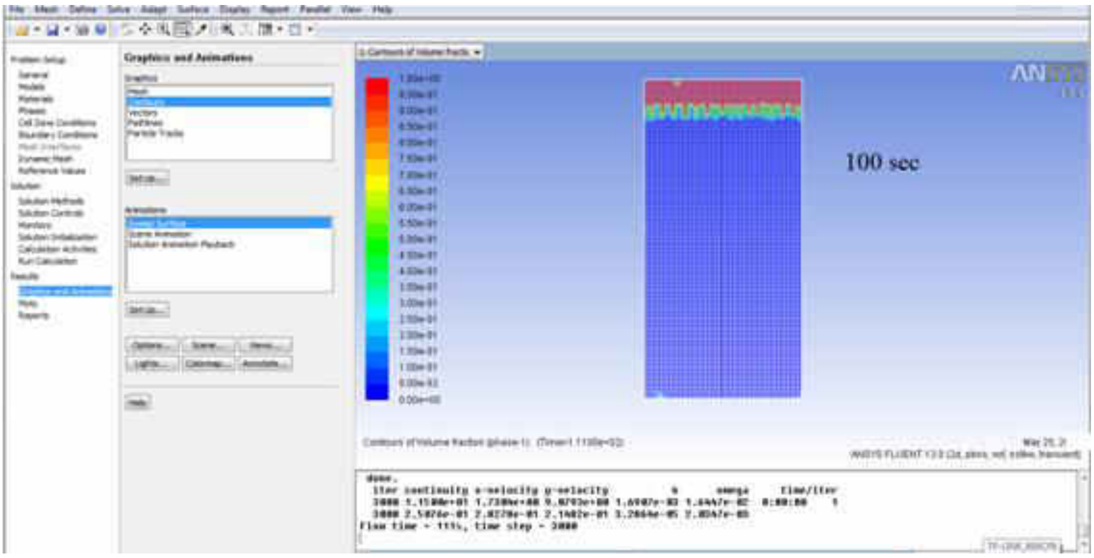

Fig. 15. Representation of water to hydrocarbon after 111 seconds

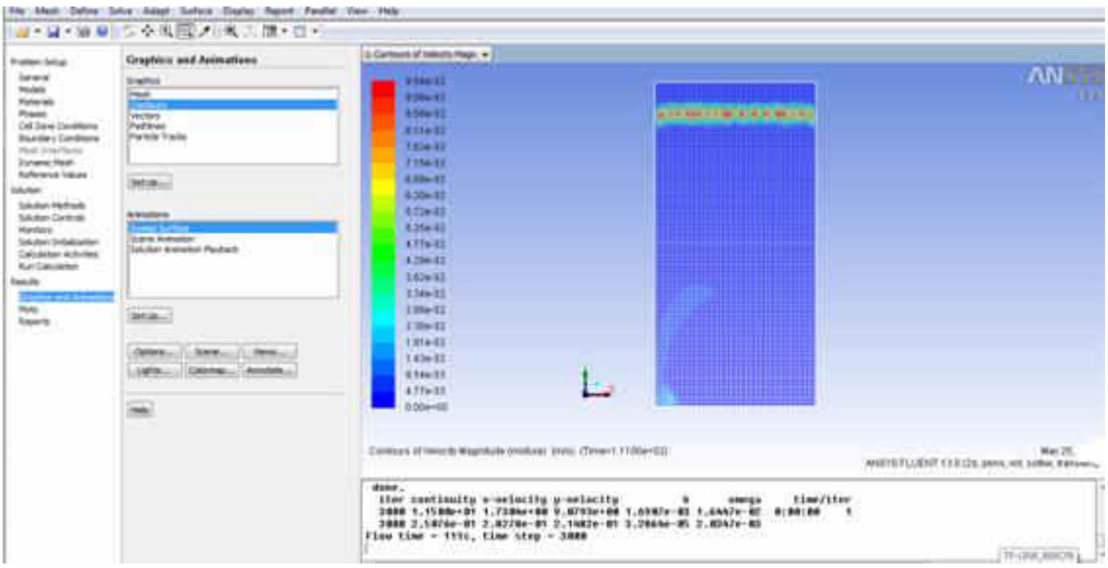

Fig. 16. Representation of the circulation speed of fluid cells

As one can see, the minimum value of the circulation speed of fluid cells is 0.0 m/s and the maximum value is $9.54{*}10^{-02}$ m/s.

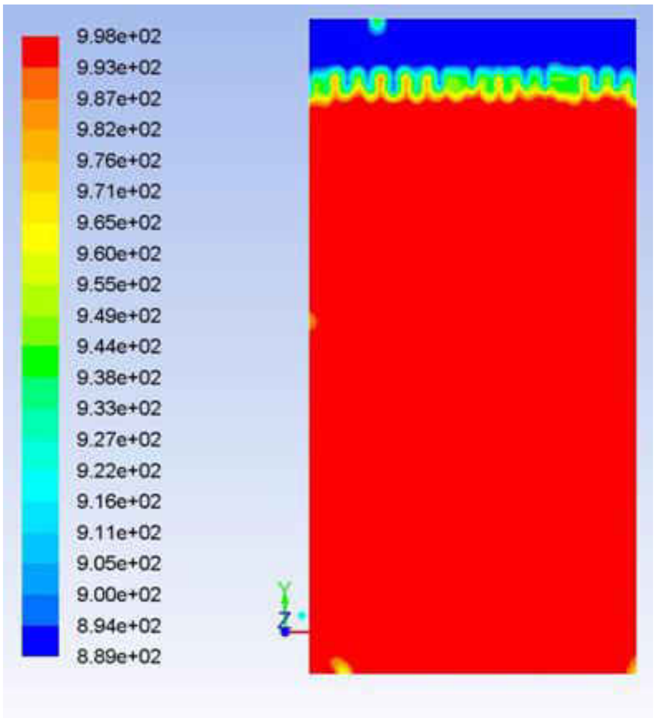

Fig. 17. Representation of working fluid density

As one can see, the minimum value of working fluid density is $8.89{*}10^{+02}$ kg/m^3 and the maximum value is $9.96{*}10^{+02}$ kg/m^3.

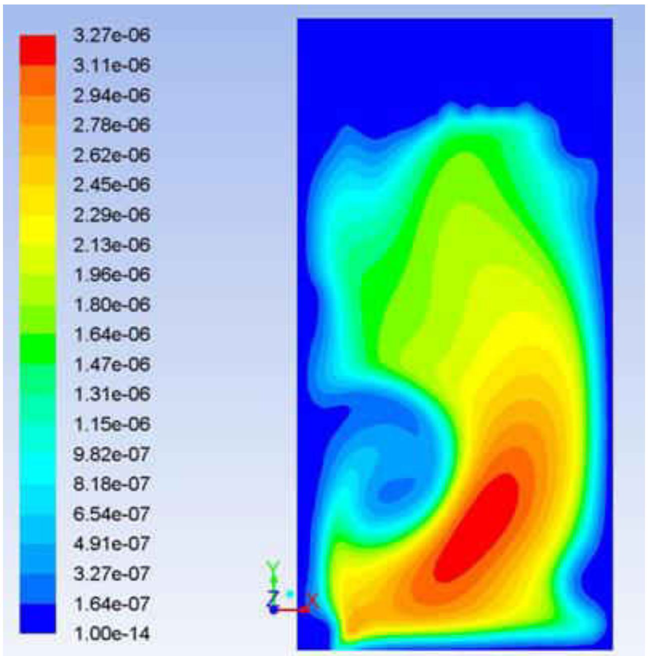

Fig. 18. Representation of kinetic energy turbulence

As one can see, the minimum value of kinetic energy turbulence is $1.00{*}10^{-14}$ J and the maximum value is $3.27{*}10^{-6}$ J.

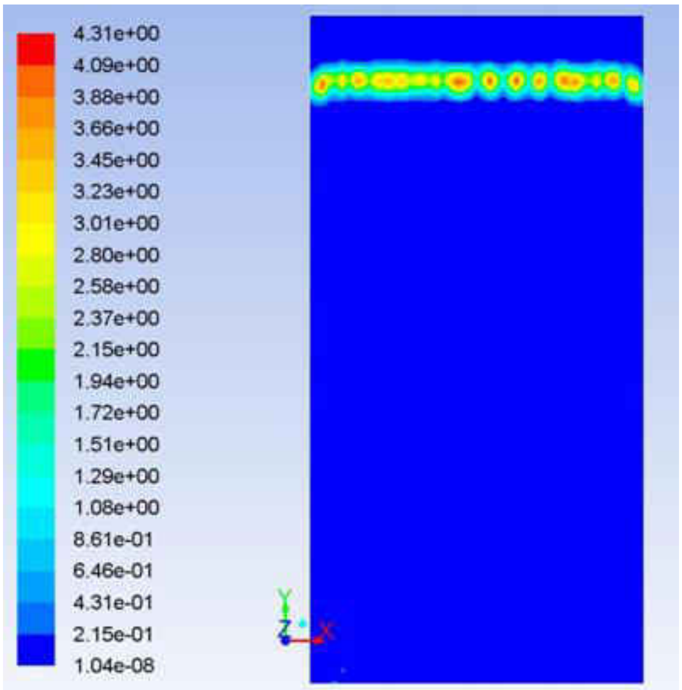

Fig. 19. Representation of the dynamic pressure of moving fluids

As one can see, the minimum value for dynamic pressure of moving fluids is $1.04*10^{-8}$ Pa and the maximum value is 4.31 Pa.

4. Conclusions

Marine oil pollution due to the carelessness and unpreparedness of seafarers is becoming an increasingly harsh reality. However, the interventions, measures and limitation of these actions are up to us. The violation of the rules by the navigators of the sea transport companies imposed the appearance of new combat provisions. Part of these is the security of all facilities and means by which crimes can be committed and the mode of operation. The start of the separation installation, respectively of the bilge separator is done by noting in the Logbook. Opening the overboard valves (which are sealed) and not only is also done by noting in the Logbook. All these measures were taken as a result of the increase in crime.
The water in the bilge tanks can also come from leaks through the glands of the shut-off valves and the etambou tube, purging the level bottles, condensation on the side of the water vapor in the air, washing the decks below the waterline, extinguishing fires and much more.
Technological availability allows us to design and build increasingly efficient bilge installations with a high degree of automation.

References

[1] Iacob, Nicolae-Marian. *Wastewater treatment on board cruise ships*. Dissertation thesis. Constanta, Maritime University, 2020.
[2] Papanikolaou, A. *Ship Design.* Netherlands, Springer Publishing House, 2014.
[3] ***. Scan Ship AWB Operation Guide-level 2, Ship documentation, 2015.
[4] Ramli, Liyana, Z. Mohamed, Auwalu M. Abdullahi, H.I. Jaafar, and Izzuddin M. Lazim. "Control strategies for crane systems: A comprehensive review." *Mechanical Systems and Signal Processing* 95 (October 2017): 1-23.
[5] Borisov, A.M., G.I. Drachev, and N.E. Lyakh. "Revamping the crane electric drive." *Russian Electrical Engineering* 85 (December 2014): 630-633.
[6] Panaitescu, M., F.V. Panaitescu, and A. Draganoiu. *Experimental techniques for water analysis / Tehnici experimentale de analiza a apei*. Constanta, EXPONTO Publishing House, 2010.
[7] Panaitescu, M., F.V. Panaitescu, and I.I. Panaitescu. "Modeling the equipment shape of the technological flow of the waste water treatment station." *HIDRAULICA Magazine,* no. 2 (June 2019): 16-22.

Analysis of Vibrations and Noise in a Centrifugal Pump for Predictive Maintenance

PhD eng. **Sanda BUDEA**[1*]

[1] University Politehnica of Bucharest, Department of Hydraulics, Hydraulic machines and Environment Engineering

* sanda.budea@upb.ro

Abstract: *The article makes an analysis of the experimental results regarding the noises and vibrations that appear in the operation of a centrifugal pump, both on the pump and the electric drive motor, as well as on the elements of the installation. Noises and vibrations have both mechanical and hydraulic causes, in close connection with the flow rate of fluid or with the occurrence of the cavitation phenomenon. The maximum values of the noises and vibrations are tracking, their compliance with the limits of the specific standards is verified, and in case of exceeding the values, remedial solutions are proposed. Monitoring the operation of hydraulic machines in installations has the purpose of a correct operation, but also of a preventive maintenance.*

Keywords: *Vibrations, noises, centrifugal pump, cavitation, maintenance*

1. Introduction

The appearance of vibrations in hydraulic machines is due to mechanical causes (imperfections in bearings, bearings, eccentricities, friction, etc.) and hydraulic (detachment of the boundary layer on the blades, cavitation operation, imbalance of hydraulic forces, etc.). Vibrations and noises emitted into the atmosphere by machines and installations consume additional energy and have a detrimental influence on the service life of this equipment. Vibrations and noises also have an unfavorable effect on human health.
Vibration analysis is important for pump fault detection and predictive maintenance and was studied by D. Jung in [1], D. Siano in [2] and others. Vibration and cavitation in pumps are directly related and have been previously studied in [3-8].
Ahmed Ramadhan Al-Obaidi in [3] says that the hydraulic and mechanical sources of vibration in centrifugal pumps occur as a result from several problems: flow distribution, high velocity, interaction between the impeller and the volute through the rotation of the impeller in the pump particularly at volute tongue region.
Hydraulic sources of vibration in centrifugal pumps include blades passing forces, hydraulic imbalance, recirculation flow, cavitation, system instabilities, or water hammer in installation pipes [4]. The pumping installation includes the centrifugal pump, the electrical motor and its piping system with pipes, elbows, fittings, and valves. J. Tuzson in [5] says that "even through regular operation conditions, various kinds of physical processes create vibration such as hydraulic interaction with the piping system, improper installation or maintenance, application for the pump, and manufacturing designs and different types of faults".
"Typically, the mechanical vibration sources in the pump include several sources such as pressure fluctuations created in the fluid, imbalance, misalignment between shafts connections, and damaged bearings" [6].
In addition, other mechanical sources incorporate mechanical forces, improper usage of the pump as provided in the installation manual and the conditions emerging from the pumps' incorrect assembly and from wear [7, 8]. When cavitation occurs in the different types of machines, it leads to dropping in pressure at the impeller inlet below the water vapour pressure. This leads to increasing the level of noise and vibration due to unstable flow which, in turn, causes an increase in the pressure fluctuations within a pump [5].
For the purpose of correct operation, but also of preventive maintenance, this article makes an analysis of the experimental results regarding the noises and vibrations that appear in the

operation of a centrifugal pump, both on the pump and the electric drive motor, as well as on the installation elements.
The article is structured in 5 chapters: after the introduction, a theoretical approach to the phenomenon, with reference to amplitude, velocity vibration, accelerations, analysis with the RMS method (Root mean square) for pulsating and periodic phenomena. Chapter 3 presents the presentation of the experiment stand and the measuring devices, and in chapter 4 the author presents results and makes an analysis of them. The final chapter is dedicated to the conclusions and solutions to improve the operation of the pump in the installation. The work consists in the measurement and analysis of vibrations and noises emitted by a single-stage centrifugal pump type LCC of medium size, often used in pumping stations.
The operation of the pump is at variable speed, by frequency converter n = 2900-2500 rpm. Vibration measurements are made in 3 directions (horizontal x, vertical y and axial z).

2. Theoretical approach

Vibrations are pulsating and periodic phenomena, with the following characteristic quantities:

X – displacement [*mm*];

a - amplitude; *t* – time [*s*]

$\dot{x}$ - velocity vibration [*mm/s*];

$\ddot{x}$ - acceleration $[mm/s^2]$

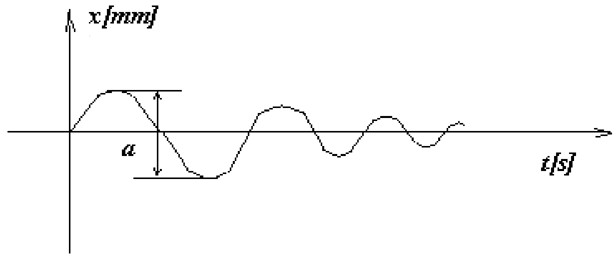

$$x = a \cdot \sin(\omega \cdot t + \varphi); \tag{1}$$

$$\dot{x} = a \cdot \cos(\omega \cdot t + \varphi); \tag{2}$$

$$\ddot{x} = -a \cdot \omega^2 \cdot \sin(\omega \cdot t + \varphi); \tag{3}$$

If the phenomena have a T-period, several measurements are made for the whole range of flows and their mean square deviation is calculated RMS (root mean square) [9]:

$$x_{MP} = \sqrt{\frac{1}{T} \cdot \int_0^T x^2(t)dt} \tag{4}$$

Methods used in theoretical analysis to understand the pattern of the vibration refer to FFT (Fast Fourier Transform) spectrum and are analysed with RMS (root mean square).
Also H. Ahmadi in [10] makes a theoretical but also experimental analysis on a centrifugal pump of comparable size with the pump used in the present experimental study, a useful study for comparing the results.

3. Experimental setup

The experimental stand consists in a centrifugal pump LCC 65-50-200, having suction pipe diameter 65 mm, discharge pipe diameter 50 mm and the diameter of the impeller 200 mm.
The experimental installation is shown in figure 1 and consists of a single-stage centrifugal pump for water *1*, driven by the asynchronous electric motor *2*, 5 kW at 2880 rpm equipped with frequency converter, an electromagnetic flow meter *3* on the discharge pipe, manometers *5* and pressure transducers *4*, for pumping head.

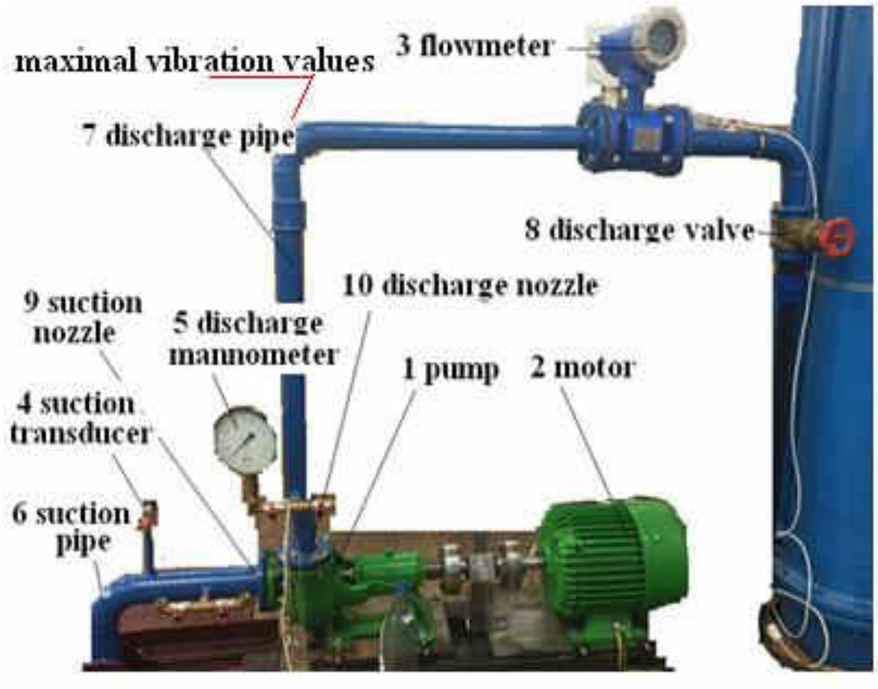

Fig. 1. Experimental stand

Vibration measuring transducers are built on the principle of accelerometers and are fixed with a magnet. Depending on the mode of transmission of the relative displacements, the transducers can be mechanical, electrical, or piezoelectric (figure 2), with a permanent magnet that is fixed on the machine housing.
Noises, with higher frequencies, are measured with a microphone built on various principles: mechanical, electro-dynamic or piezoelectric.
The location of the transducers is made in the most sensitive places for measurements, of maximum vibrations or of special interest.
The installation is equipped with a piezoelectric vibration transducer, figure 2, which takes over the movement and a Bruel and Kaer accelerometer, which indicates the speed of movement (mm / s), as well as with a microphone for recording noises. The accuracy of the measuring instruments is ±2%.
The vibration transducer is placed on the horizontal, vertical and axial direction of the pump, the electric motor, in different sensitive points or on elements in the installation, and the microphone for measuring the noise intensity is fixed consecutively at different azimuth angles, on a virtual circle of radius R = 1 m perpendicular to this plane.

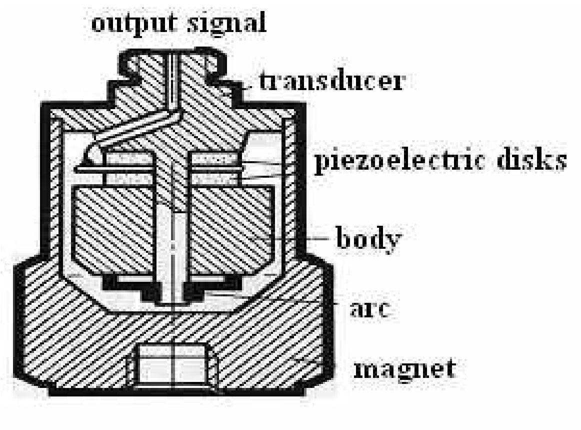

Fig. 2. The piezoelectric vibration transducer [9]

Operation procedure

One measures the velocity vibration in the horizontal x, vertical y and axial z directions and calculates the accelerations and displacements in the 3 directions. We are interested in the maximum values of vibrations, those for which the value of the sine is 1 [9].

$$\dot{x} = a\omega \,, \quad \ddot{x} = \dot{x}\omega \quad , \quad x = \frac{\dot{x}}{\omega} \tag{5}$$

The impeller of the centrifugal pump has z = 6 blades and variable rotation speed
n =2875-2552 rot/min.

The angular speed is

$$\omega = \frac{\pi \cdot n}{30} \tag{6}$$

And the oscillation frequency is:

$$f_v = \frac{z \cdot n}{60} \tag{7}$$

4. Results and discussion

The main tested characteristic sizes of the centrifugal pump - flow rate, head, rotational speed, angular speed and oscillation - are presented in Table 1.

Table 1: Centrifugal pump characteristics

Q (mc/h)	1.7	8.5	13.62	20.5	26.33	31.78
H (m)	32.5	30	27.2	21	14.3	3.8
n (rot/min)	2875	2820	2765	2656	2562	2552
ω (s^{-1})	300.92	295.16	289.40	277.99	268.16	267.11
f (Hz)	287.5	282	276.5	265.6	256.2	255.2

In the following we have exemplified for the suction flange of the pump, velocity vibration (mm / s) recorded with the measuring device in the 3 directions, the maximum amplitudes that are identical to the maximum displacements - Table 2 and a calculation example for the mean square deviation of the values of the velocity vibration, respectively the amplitudes / vibrations on the 3 directions – Table 3.

Table 2: Velocity vibration and amplitude / maximal displacement at suction nozzle

$\dot{x}$	1.3	1.4	1.8	1.8	1.4	1.7
$\dot{y}$	5.9	5.2	9.8	5.3	7.7	7.7
$\dot{z}$	1.3	1	1	1.2	1.3	1.5
ax	0.0043	0.0047	0.0062	0.0065	0.0052	0.0064
ay	0.0196	0.0176	0.0339	0.0191	0.0287	0.0288
az	0.0043	0.0034	0.0035	0.0043	0.0048	0.0056

Table 3: Root mean square of vibration for suction nozzle

	RMS
$\dot{x}$	0.198139
$\dot{y}$	1.609635
$\dot{z}$	0.134199
ax	0.000773
ay	0.005876
az	0.000563

The verification is done using the ISO 10816-3 vibration standard [11]. If the pump has an RMS vibration above the ISO 10816-3 vibration standard, it is necessary to do a more detailed analysis to determine the cause of the condition. Therefore, analysis of the vibration spectrum was performed to obtain the causes of vibrations that exceeded the standard values.
In figures 3-7 there are presented the results of the experimental determinations of vibrations in the form of velocity vibration (mm/s) for suction nozzle, discharge nozzle, discharge pipe, pump bearing house and electric motor casing, versus pump flow rate (m^3/h).

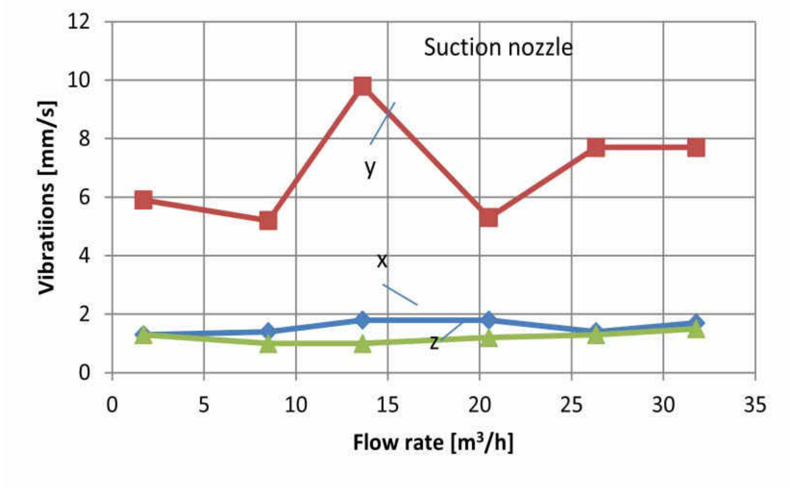

Fig. 3. Velocity vibration (mm/s) for suction nozzle

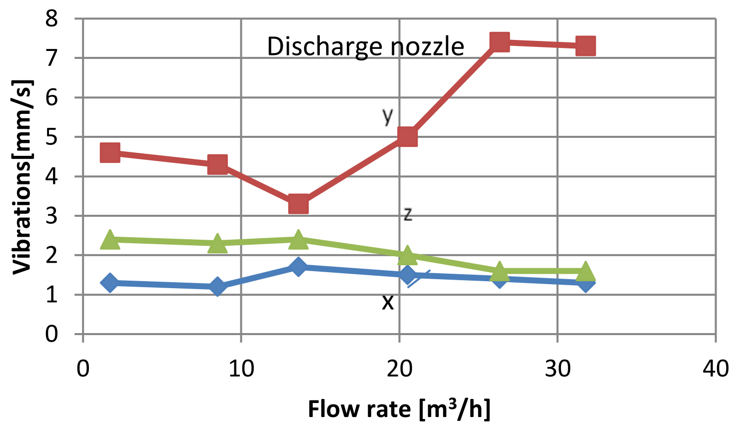

Fig. 4. Velocity vibration (mm/s) for discharge nozzle

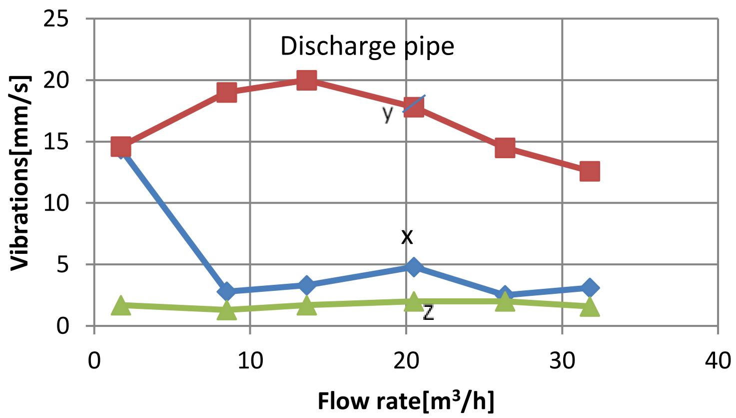

Fig. 5. Velocity vibration (mm/s) for discharge pipe

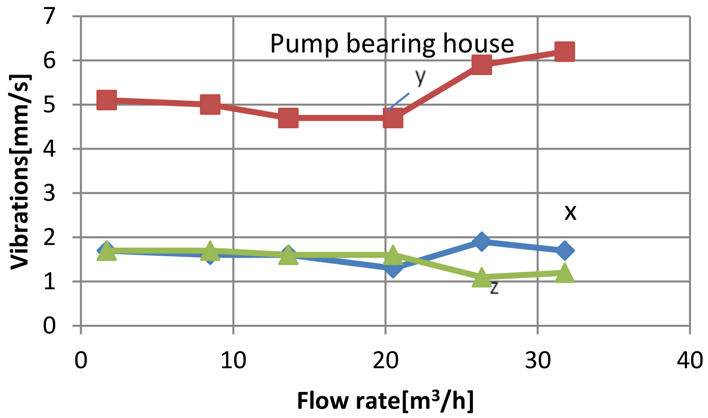

Fig. 6. Velocity vibration (mm/s) for pump bearing house

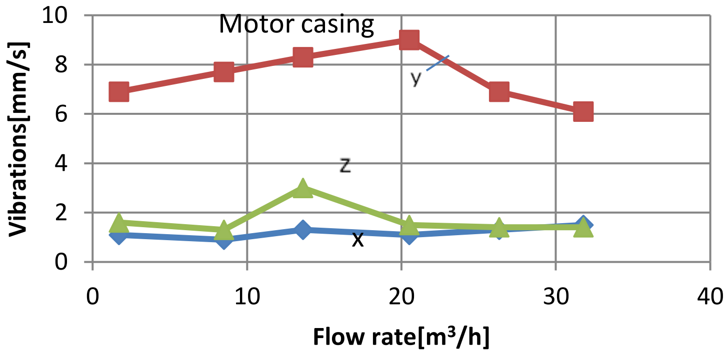

Fig. 7. Velocity vibration (mm/s) for electric motor casing

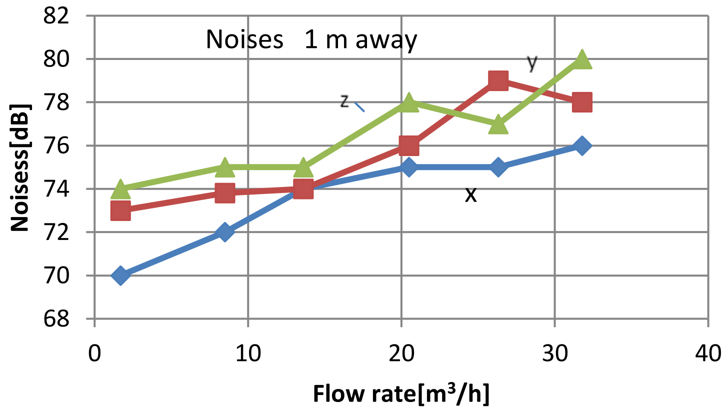

Fig. 8. Noises (dB)) at 1 m away from pump

Figure 8 shows the results of noise measurements at 1 m distance from the installation. Noise values at maximum flow rates are at the limit of the norms provided for hydraulic machines (75-80 dB) [12].

At the fully open valve (maximal flow rate) the noises are maximal and the vibrations on the discharge flange and the bearing body of the pump are also maximal.

The results show that the motor casing in the vertical and horizontal directions has the highest vibration value compared to other measurement directions. The highest velocity vibration value in the motor comes from the y direction which is 9 mm/s.
Regarding the pump bearing house, the highest velocity vibration value is 6.2 mm/s in vertical direction, 1.9 mm/s for horizontal and 1.7 mm/s for axial.
The highest velocity vibration values are at discharge pipe: 20 mm/s for vertical, 14.4 mm/s for horizontal and 2 mm/s for axial direction. Here the cause can be the water hammer phenomenon in the elbow of the installation, by the sudden change of the direction of movement. The results are comparable to those obtained on a pump of similar dimensions H Ahmadi in [10].
Based on the ISO 10816), in the studied pump installation, the average vibration value of the RMS velocity in few cases do not exceeded the standard limit. Only for discharge pipe the standard limit is exceeded. The solution for limiting the vibrations in the elbow consists in stiffening / fixing the installation elbow with clamps.
High vibration is a characteristic of damage to the pump. Analysis of the signal amplitude in the time and frequency domains carried out in the pump has been presented to predict and diagnose cavitation [13]. If left unchecked, this vibration will cause damage to the main components of the pump.
In the industry there are applications dedicated to monitoring and diagnosing pump faults based on vibration and noise analysis [14-15].

5. Conclusions

The following conclusions can be drawn from the analysis of vibrations on the installation of a centrifugal pump:

- In the vertical direction the vibrations are higher than in the horizontal and axial direction, the explanation being the sudden change of the flow direction in the radial rotor of the pump;
- On the suction flange the vibrations increase with the flow and as a result of the cavitation phenomenon that appears at the fully open valve;
- On the discharge pipe the vibrations are maximum, even 3 times higher than on the other parts of the pump and the installation, due to the ram blow phenomenon.
- On the motor housing the vibrations are higher than on the pump bearing, which leads us to the conclusion that the pump rotor is well balanced hydraulically;
- Noises are continuously increasing with flow, in all directions.

By monitoring the pump bearings in terms of vibration, but also the temperature, one can ensure a good operation of the pump, a correct maintenance when values appear outside the limit indicated by the standards and one can ensure a predictive maintenance.

References

[1] Jung, D., Z. Zhang, and M. Winslett. "Vibration Analysis for IoT Enabled Predictive Maintenance." Paper presented at IEEE 33rd International Conference on Data Engineering (ICDE), San Diego, CA, 2017, 1271-1282, doi: 10.1109/ICDE.2017.170. 2017.
[2] Siano, D., and M.A. Panza. "Diagnosis method by using vibration analysis for pump fault detection." *Energy Procedia* 148 (August 2018): 10-17.
[3] Al-Obaidi, Ahmed Ramadhan. "Investigation of effect of pump rotational speed on performance and detection of cavitation within a centrifugal pump using vibration analysis." *Heliyon* 5, no. 6 (June 2019): e01910, 1-19.
[4] Kim, J., K. Oh, K. Pyun, C. Kim, Y. Choi, and J. Yoon. "Design optimization of a centrifugal pump impeller and volute using computational fluid dynamics." *IOP Conference Series: Earth and Environmental Science* 15, no. 3 (November 2012): 032025.
[5] Tuzson, J. *Centrifugal Pump Design*. John Wiley & Sons, 2000.
[6] Schmitz, S. "Reducing pump noise in cooling tower applications." *World Pumps* 456 (September 2004): 24–29.
[7] Hernandez-Solis, A. *Diagnosis of Centrifugal Pumps*. Kungliga Tekniska högskolan, 2006.
[8] Goyal, D., and B. Pabla. "The vibration monitoring methods and signal processing techniques for structural health monitoring: a review." *Arch. Comput. Methods Eng*. 23, no. 4 (2016): 585–594.

[9] Budea, Sanda. *Hydraulic measurements and experiments for hydraulic machines like pumps, fans and blowers – lab works / Măsurări hidraulice şi încercarea unor maşini hidraulice din categoria pompe, ventilatoare şi suflante – lucrări de laborator*. Bucharest, Printech Publishing House, ISBN 978-606-521-559-7, 127-131, 2010.
[10] Ahmadi, H., M. Subchan, R.E. Rachmanita, R.D. Audora, and A. Wibuana. “Vibration analysis of Kartini reactor secondary cooling pump using FFT analyzer.” *Journal of Physics*: *Conference Series* 1511 (2020): 012080, doi:10.1088/1742-6596/1511/1/012080.
[11] I.S.O. Standard. ‘Mechanical Vibration-Evaluation of Machine Vibration by Measurements on Non-Rotating Parts.’ p. 24, 1996.
[12] SR ISO 1996-2:2018. ’Acoustics. Description, measurement and assessment of ambient noise. Part 2: Determination of ambient noise levels.’ 2018.
[13] ***. ”Pump cavitation and how to avoid it.” *World Pumps* 2018, no. 2 (February 2018): 34-38, ISSN 0262-1762, https://doi.org/10.1016/S0262-1762(18)30146-9.
[14] ABB discrete operations management software. *[online] Available:* https://new.abb.com/products/measurement-products/wireless-products-and-solutions/integrated-solutions/condition-monitoring-and-wireless-vibration-transmitter-copy20140702_151332. Accessed July 2020.
[15] Siemens SIMATIC IT for Discrete Manufacturing. *[online] Available:* http://w3.siemens.com/mcms/mes/enlindustry/discretemanufacturing/Pages/Default.aspx. Accessed July 2020.

Microwave Drying of Biomass

Dipl. Eng. **Roxana APOLZAN**[1*], Dipl. Eng. **Adrian PEREBICEANU**[1], Dipl. Eng. **Florica MATEIAS**[1]

[1] S.C. LAMBDA MAT BUCURESTI S.R.L.

* roxana.apolzan@yahoo.com

Abstract: *Pilot studies were performed on the identification of drying conditions in the microwave field leading to the obtaining of dry biomass with humidity in the range of 5… 8%, starting from initial humidity of 14… 20%.*
Sets of tests were performed with biomass sample masses of 5 and 10 kg for which the applied microwave power was varied, recording: variation of drying time with microwave power, average value of the final moisture in the sawdust (7.075, 60.6%) and variation of power density with drying time.
The existence of the direct relationship between the applied power density and the drying time allows the optimization of energy consumption. Thus, one can choose the amount of biomass to be dried at a target humidity, while setting the equipment at the appropriate power of the process.

Keywords: *Dying, dry biomass, microwave drying, microwave power*

1. Introduction

Drying is not only an energy-intensive operation, but also a complex phenomenon of the process of heat transfer and mass transfer, including that related to the drying of hygroscopic and porous materials such as wood and agri-food [1]. Consequently, improving knowledge about the interconnected physical, chemical and thermodynamic processes involved in drying, as well as the energy efficiency of drying equipment are the most relevant objectives of future research and development worldwide.

The main objective of the development of drying technology is to further improve the biomass drying process by applying new technologies and advanced measurement, modeling and simulation techniques.

Biomass refers to a non-fossilized biological material derived from living / recently living organisms and from biodegradable organic or carbon-based materials from plants, animals, plant matter and microorganisms. The most common industrial biomass can be grown from many types of plants, including miscanthus, hemp, corn, poplar, willow, sorghum, bamboo, sugar cane and a variety of tree species.

Regardless of the source, biomass materials can be divided into two broad categories: woody and non-woody. Forests provide only wood materials; agricultural sources provide both woody biomass and non-woody biomass for bioenergy production. The main source of wood biomass comes from forest and agricultural residues. Agriculture is a source of non-wood materials used to obtain bioenergy. Biomass-based materials from agriculture are represented by annual crops such as maize and soybeans, residues collected after harvesting annual crops for food or feed and perennial crops such as grass and fruit trees.

The use of biomass as a source of renewable energy is attracting even more attention nowadays due to concerns about heating and care for fossil fuel depletion. However, not all biomass is suitable for direct combustion, except for dry biomass.

In the past, biomass, such as wood or rice straw, was naturally dried before being burned. Recently, due to high energy costs and environmental concerns, some high-moisture organic wastes, such as microalgae, are used as fuel. They have a high moisture content so they must be mechanically and / or thermally dried before burning. Practice has shown that drying biofuels before burning can increase combustion efficiency. [2].

The high moisture content reduces the combustion temperature generating an incomplete combustion as well as a series of unwanted reaction products. In addition, a biofuel with a high moisture content requires a large amount of auxiliary fuel to burn [3]. Some data on how moisture content affects combustion efficiency as well as other combustion parameters, such as flame temperature, were reported by Voima et al. [4].

Basic knowledge of microwave heating refers to heat dissipation and the typical propagation of microwaves in which dipoles begin to vibrate and rotate angrily through the electric field. When the microwave energy emitted from a microwave oscillator (Pin) is irradiated in the microwave applicator, dielectric materials that have a dielectric loss factor absorb energy and are heated with a dielectric loss factor. Then the internal heat generation takes place. The basic equation for calculating the density of the microwave power absorbed by the dielectric material (P1) is given by the relation:

$$P_1 = \omega \varepsilon_0 \varepsilon_r'' E^2 = 2\pi f \varepsilon_0 \varepsilon_r (\tan\delta) E^2 \tag{1}$$

where E is the intensity of the electromagnetic field; f is the microwave frequency; ω is the angular velocity of the microwave; ε_r is a relative dielectric constant; ε_0 is the dielectric constant of the air and tan δ is the tangent coefficient of the dielectric loss.

As it results from the equation, the power P1 is directly proportional to the frequency applied to the electric field and the tangent coefficient of the dielectric loss and the average root - the square value of the electric field. This means that an increase in the tan, of the object, energy absorption and heat generation are also increased. While the tan δ is small, the microwaves will penetrate the object without generating heat. However, the increase in temperature probably depends on other factors, such as the specific heat, size and characteristics of the object.

When the material is heated unilaterally, it is found that as the dielectric constant and the loss coefficient vary, the penetration depth will change and the electric field in the dielectric material will change. The penetration depth is used to indicate the depth at which the power density has decreased to 37% of its initial surface value.

$$D_p = \frac{1}{(2\pi f/\upsilon)\sqrt{\left[\varepsilon_r'\left(\sqrt{1+\left(\varepsilon_r''/\varepsilon_r'\right)^2}-1\right)\right]/2}} = \frac{1}{(2\pi f/\upsilon)\sqrt{\left[\varepsilon_r'\left(\sqrt{1+(\tan\delta)^2}-1\right)\right]/2}} \tag{2}$$

$$P_2(W) = \frac{4.18 W C_p \Delta T}{t} \tag{3}$$

where W is the weight of the dielectric material (g), CP is the specific heat of the dielectric material (Cal / gr ◦C), ΔT is the temperature rise (T2 −T1) (◦C), t is the heating time [s].

Assuming an ideal condition, all the oscillating energy of the microwave (P_in) is absorbed in the dielectric material; internal heat generation as Equation (1). In this case, the relationship between P_in and ηP2 is presented below:

P = in (W) = P2

However, from a practical point of view, the transformation energy (η) in the applicator exists due to the rate of absorption of microwave energy by the dielectric factor.

Green biomass is an organic, hygroscopic, capillary, porous, anisotropic, non-uniform and heterogeneous mixture of solids, liquids and gases. It contains considerable amounts of moisture (water and liquid vapor) depending on the relative humidity of the surrounding air. For many industrial applications, many national laws require the removal of moisture from biomass / wood for minimal damage, quality preservation and reduction of transport costs [5].

Drying techniques generally refer to the use of energy depending on how the drying medium is heated (for example by fuel or electricity), how the residual energy is recovered from the exhaust air and how the control system is used to maximize energy use etc. Specialized drying techniques such as direct heat, radio frequency and microwave, infrared, vacuum, solar (more attractive in remote locations for small ovens) and assisted heat pumps (dehumidification) are usually more expensive and oriented towards special final products. In addition, some of these technologies use higher energy (electricity), which is generally expensive [6, 7]. Heat pumps can also include auxiliary heating sources, such as electromagnetic radiation, radio frequency, microwave, infrared and solar energy.

One of the important properties of biomass in terms of combustion process and thermo-chemical conversion processes is the moisture content, which influences the energy content (calorific value) of the fuel. The moisture content of biomass is given by the amount of water in the product, expressed as a percentage by mass. Currently, two methods (dry and wet) are used to express total humidity.

For most fuels it is used dry. This is due to the fact that different types of biomass have different moisture contents, because the humidity of the wood depends on the place, type and duration of storage and preparation of the fuel. Dry moisture reports moisture to the mass of dry material. Moisture is related to the total mass of the material. It varies from less than 10% (by-products of the wood processing industry) to 50% (forest residues). The moisture content is relevant not only for the calorific value but also for the storage conditions, the combustion temperature and the amount of flue gases.

In the case of waste in heterogeneous mixtures - urban and similar - in addition to its influence on the specific mass, moisture has a direct influence on the calorific value and fermentation processes, when they are intended for the formation of compost. Humidity is directly influenced by the climate of the region, being different from one season to another.

Microwave heating is an efficient method for transferring energy to water molecules inside biomass pieces.

Water molecules are dipolar in nature (i.e. have an asymmetric center of charge) and are normally randomly oriented. The rapidly changing polarity of the radio frequency and microwave field tries to bring these dipoles into alignment with the field. As the field changes polarity, the dipoles return to a random orientation before being pulled in another direction. This accumulation and degradation of the field and the resulting stress on the molecules determine a conversion of the energy of the electric field to the stored potential energy, then to the random kinetic or thermal energy. Therefore, dipole molecules, such as water, absorb energy in these frequency ranges. The field strength and frequency are fixed by the equipment, while the dielectric constant, dissipation factor and loss factor are material dependent. The actual power of the electric field also depends on the location of the material inside the microwave / radio frequency cavity.

The dielectric constant of water is more than an order of magnitude larger than most basic materials (such as wood pulp), moisture is preferentially heated, a process that leads to a more uniformly moist product over time, while the overall dielectric density of most materials usually almost proportional to the moisture content up to a critical value, often around 0.2 0.3. Therefore, microwave and radio frequency methods prefer to heat and dry wetlands in most materials, processes that tend to lead to a more uniform final moisture content. For water and other small molecules, the effect of increasing the temperature is a slight decrease in the heating rate, which leads to a self-limiting effect [6, 8]. The force and frequency of the field are fixed by the equipment, while other parameters are dependent on the material. If the energy requirement is higher than 50 kW, the use of tubes with higher power in the radio frequency range seems to be economically favourable. The least expensive guides are the microwave oven guides, which have an output power of 750 W.

Microwave heating works on the same principles as radio frequency heating, but with higher frequencies in the range of 300 MHz-300 GHz; thus, the thermal power ratios of the heating can be significantly increased. The unit cost of drying wood for microwave drying is influenced by the initial moisture content and density of the wood, while for conventional drying, the unit cost of volume depends mainly on the length of the drying cycle required to reach the levels. acceptable degradation. The cost of the whole system, including the generator, The waveguide from generator to dryer, applicator, control system and conveyor is much higher, but lower unit costs are associated with higher power equipment [6]. Microwave drying seems to be suitable where hardwood species have a low initial moisture content, causing problems with degradation in conventional drying and / or is relatively valuable, so the capital load is significant. For example, microwave drying is economical for Douglas fir with an initial low moisture content of 40%, but not for wood with an initial moisture content of more than 86%. On this basis, microwave drying would find the most applications for hardwood species [9].

Electromagnetic radiation with varying wavelengths (0.2 m - 0.2 µm) can be combined with forced conventional air convection and / or vacuum wood drying [10]. The low frequency of electromagnetic radiation (generated by magnetroons and clystrons) covers the range 1-100 MHz, while the high frequencies range from 300 MHz to 300 GHz [6]. At radio frequency, the impedance of the wettest materials decreases dramatically, although they are poor conductors of 50-60 Hz current, thus reducing the internal resistance to heat transfer. Energy is selectively absorbed by water molecules and, as the product becomes drier, less energy is used.

The advantages of such methods of electric heating include (i) the direct supply of heat to the product, so that a drying environment is not required; (ii) the possibility of precise temperature control by drying; (iii) uniform control of the moisture content within a period of minutes without the development of defects, thus avoiding dangerous humidity gradients; (iv) the small size of the dryer is not required; (v) clean, easy to maintain and without handling flammable fuel; (vi) better quality, no contamination and no risk of combustion; (vii) short start and stop time; and (viii) may be used to complete the drying of conventionally dried timber that has not met the target moisture content.

2. Experimental activities

The biomass drying tests were performed in a microwave field with a frequency of 2.45 GHz. Fresh sawdust obtained after cutting softwood (pine) with an initial moisture content of 72% by mass was used as biomass.

Drying tests were performed in average quantities of 10 kg. After drying tests in which the biomass was placed in a layer with a thickness of 3 ... 5 cm, it was found that there are areas with microwave concentrations that generate thermal degradation. These areas can become biomass ignition points, taking into account that the sawdust has a dimensional distribution from dust to fragments with an average size of 2 mm.

Under these conditions, the concept of drying finely divided biomass was rethought, the identified solution consisting in the use of a cylindrical foil made of transparent material in the microwave, resistant to working temperatures up to 150ºC.

The working method consists in introducing in the microwave field a quantity of biomass (sawdust) limited by the length of the cavity and the diameter of the cylindrical foil. The cylindrical foil filled with sawdust is insulated at the ends with elastic systems that have the role of preventing the exit of biomass as well as the function of valves as the pressure of water vapor increases with increasing temperature in the sawdust mass. At a microwave power of 3 kW (3 magnetrons x 1000W), 13000g was heated from room temperature to 103ºC, within 25 minutes. The heated biomass was transferred to the conveyor belt for drying in hot air at 35 ° C. Following the drying step in a stream of hot air, a humidity of 12% in the sawdust mass was determined. Completion of drying is performed on the conveyor belt by entraining vapours from a stream of warm air with a temperature between 25 ... 40ºC, depending on the type of material subjected to drying.

Among the advantages of this new mode of operation can be mentioned:

- minimizing deposits of fine biomass powders inside the furnace, minimizing the risk of ignition,

- removal of the effect of local warming accompanied by carbonisation of the biomass and even its ignition, due to the existence of a controlled atmosphere of water vapour

- ensuring a controlled geometric shape (cylinder) of the material subjected to drying - biomass - with the possibility of optimizing the process following a series of tests

- optimizing the distribution of the electromagnetic field accompanied by the need to supplement the microwave power to reduce the duration of the drying process.

A type of dryer was developed which was based on several requirements identified in the application area:

- type of raw material: sawdust, biomass chop, corn cobs,
- raw material size: micronic range up to 50 mm
- dry biomass humidity: 5 - 8% by mass
- use of dry biomass: briquetting.

3. Microwave field heating oven

3.1 Geometry identification

A technological process of controlled drying of biomass in the microwave field was developed and studied.

The drying of biomass in a controlled dimensioned form is performed in a first stage inside a drying oven, under the action of microwaves. The processes in which microwave energy is used are characterized by a direct relationship between the nature and geometry of the body exposed to radiation and the efficiency of the process.

3.1.1 Planar geometry

In the case of biomass, the arrangement of the biomass in a layer with a thickness in the range 10… 50 mm was tested in a first stage, for which the surface exposed to irradiation was given by the surface generated by the width of the conveyor belt and the length of the furnace (800 x 1500 mm).

Under these conditions, drying tests were conducted in the following conditions:

- microwave power: 5 - 9 kW
- microwave frequency: 2.45 GHz
- thermal gradient: 1… 5 ºC / min.
- working temperature: 60… 110ºC
- layer thickness: 10… 50 mm
- type of biomass: softwood waste
- initial humidity of the biomass: 64.3%.

It was found that, although the distribution of the electric field in the plane of the biomass layer is homogeneous (see Fig.1), burned areas were observed in the drying layer. The study was conducted using a specialized software QuickWave Professional 2017. With this software you can draw 3D structures and simultaneously simulate the effects of the electromagnetic field in relation to the thermal field. The appearance of these burned areas was observed regardless of the thickness of the layers, noting in general, an accentuation of the phenomenon in case of reduction of thickness.

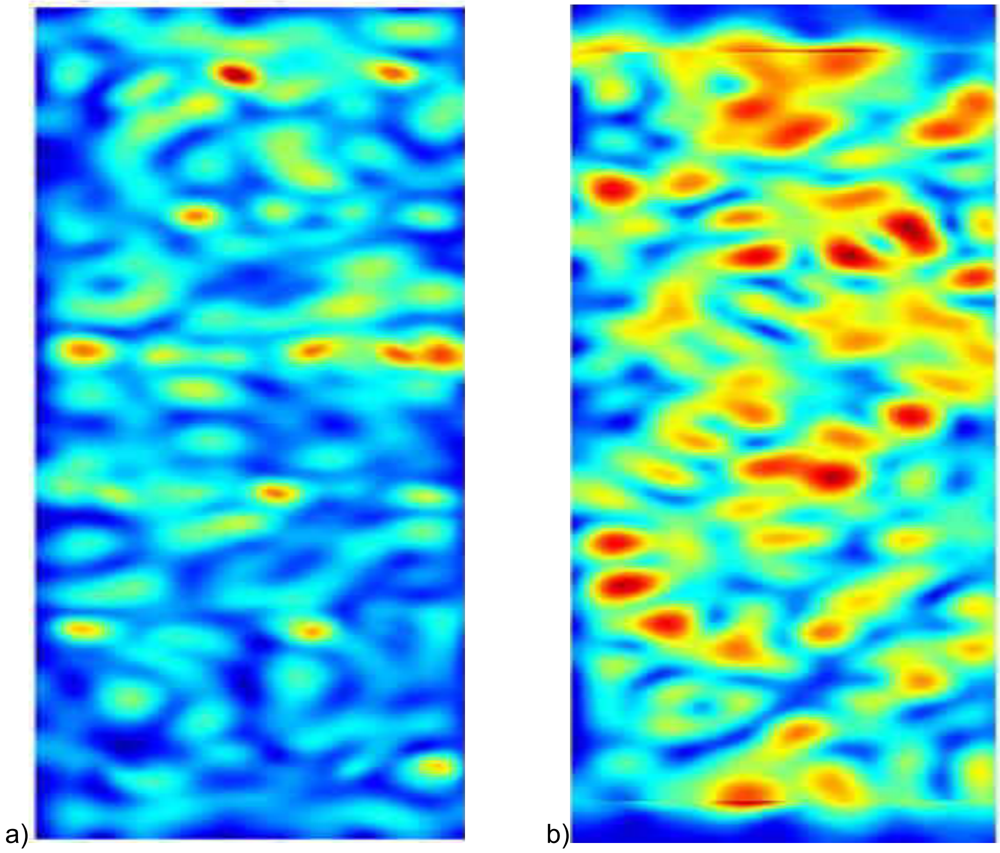

Fig. 1. Electric field distribution in the microwave - biomass arrangement plan: a) at 10 cm above b) at 1 cm above

From the analysis of the observations resulting from the development of 15 tests performed in planar geometry, the following were found:

- the use of high microwave powers is accompanied by rapid increases in temperature, reduction of drying time at the level of 5 precum 10 minutes as well as an increase in the incidence of burned areas in the biomass bed,

- the use of small microwave powers is characterized by longer drying times of 15… 50 minutes, lower temperature rises in irradiated biomass and a reduction in the incidence of burned areas in the biomass bed.

3.1.2 Cylindrical geometry

Bound moisture is associated with the hygroscopic nature of wood components. There are some uncertainties about the limits of hygroscopic behavior, especially in forests with high extractive content. For practical reasons, a maximum moisture content has been defined, called the fiber saturation point (PSF). If the effects of capillary condensation in pores larger than 0.1 mm in equivalent cylindrical diameter are ignored, the PSF of the wood can be defined as the equilibrium moisture content (CUE) in an environment of 99% relative humidity. This produces a value of 30 to 32% for most commercial species (Keey et al., 2000) [11] at room temperature. PSF decreases with increasing temperature. For a softwood such as Sitka spruce (Picea sitchensis), PSF decreases from about 31% at 25 ° C to 23% at 100 ° C (Stamm, 1964) [12].

The water absorbed from the cell wall has a lower enthalpy than liquid water. However, unlike other forms of water, such as the solid form, the enthalpy of bound water increases with increasing moisture content to PSF. Above this value, the enthalpy of wood water is essentially the same as that of liquid water.

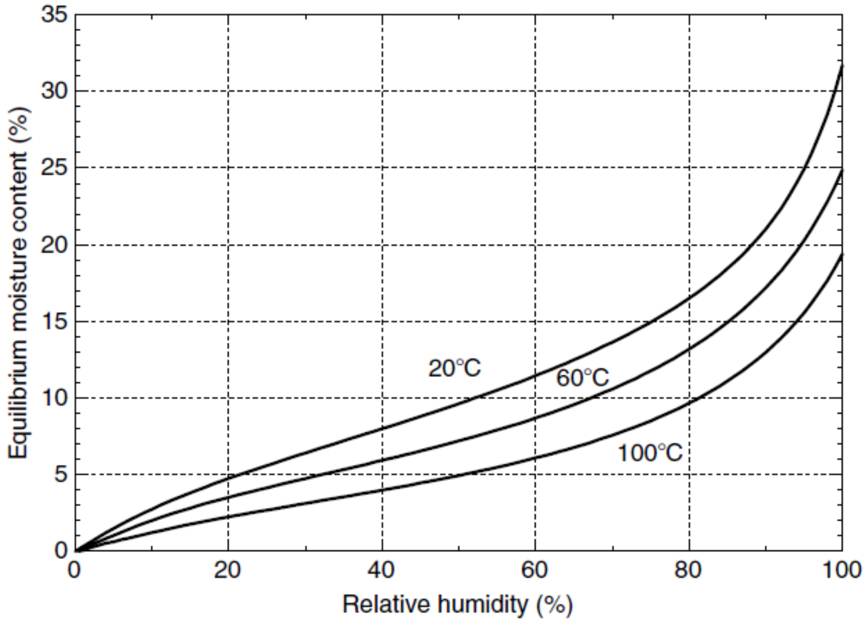

Fig. 2. Absorption isotherms calculated by a mathematical expression obtained from published data.

The drying process of the wood biomass can be differentiated by the operating temperature (low and high respectively) and by the operating pressure (vacuum and atmospheric).

3.1.3 Selecting the geometric pattern

As a result of the deepening of some theoretical and practical aspects specific to the drying of the wood material corroborated with the specific aspects of the drying in the microwave field, a specific drying process was developed. The specificity of this process consists in placing the biomass (wood waste) in powder or granular form in a controlled geometry that simultaneously fulfills the conditions:

- transparent in the microwave
- thermal resistance up to 165ºC
- resistance to lowered pressures (max. 3 bar)
- vapor resistance.

Several geometries were studied from the perspective of ergonomics and efficiency, finally choosing the cylindrical shape. As a material used to make the geometry, a partially cross-linked, heat-resistant polyethylene foil was used. Under filling conditions, the cylindrical geometry has the following dimensions: outer diameter approx. 300 mm, length of approx. 1500 mm, with a capacity of approx. 106 liters. For drying reasons, one end of the test geometry is sealed while at the other end the controlled evacuation of pressure is ensured by means of a valve. In Fig.3 the cylindrical geometry with the test material is presented, positioned inside the microwave assisted drying equipment.

Fig. 3. Microwave-assisted drying equipment before testing, with biomass sample in cylindrical geometry

Subsequent tests to optimize the microwave drying process were performed using cylindrical geometry.

3.2 Determination of drying time

As a result of the preliminary data accumulated, microwave heating was performed in the batch dryer variant (Fig. 1). The microwave cavity had a rectangular shape with a cross section of 80cm × 42 cm. The dryer operates at a frequency of 2.45 GHz and a maximum operating temperature of 200 ºC. Microwave power is generated by 10 air-cooled magnetrons by means of fans. The maximum microwave capacity is 11.2kW at 2.45 GHz. The power setting can be individually adjusted in 1000W steps. The measurement of the temperature inside the enclosure as well as in the biomass introduced in the cylindrical geometry is made with the help of some thermocouples. The equipment is equipped with a timer for setting the irradiation time after establishing the operating program for a certain type of material.

The tests performed after establishing the cylindrical geometry consisted in a first stage in determining the humidity profile for pine sawdust samples, freshly produced, with the humidity in the range of 75 ... 85%. The determination of the humidity was made by means of a thermobalance with the dedicated operating program for wood, the measuring temperature being 105ºC. Determinations were made between the duration of irradiation at a given power and the humidity in the irradiated biomass.

In this sense, for each power level a sample with a mass of 15 kg was used. Each sample was placed in a cylinder with a radius of 30 cm. At regular intervals (5 min.) 50 g of sawdust exposed to the microwave were taken. Each sample was exposed for 60 seconds to a 45C hot air stream to remove water from the sawdust particles. Subsequently, a small sample of the prepared sample (approximately 3-4 g) was used to determine the humidity with thermobalance. The results of these first tests are represented in graphical form in Fig.4.

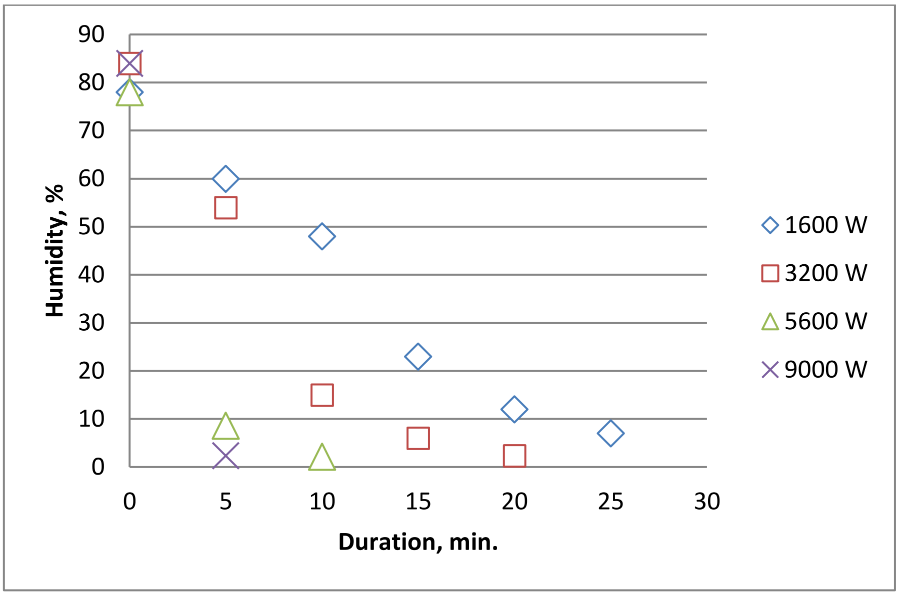

Fig. 4. Humidity profile depending on the duration for different microwave power levels

In the next step, the amount of pine sawdust was left to dry naturally in a bed with a thickness of 50.80 mm to dry naturally. The obtained humidity was between 15… 20%.

Using samples from this natural dry pine sawdust, determinations were made to reduce the humidity to values in the range of 5… 8%. This humidity range is necessary for processes such as briquetting, pyrolysis, being a strong energy-consuming and expensive to achieve through conventional heating.

Two drying sets were performed for which the operating parameters were:

- biomass material type: softwood sawdust
- quantity of biomass sample: 5 kg, 10 kg
- initial humidity of biomass samples: 14.55□0.6%
- proposed final humidity: 5… 8%
- applied microwave power: 3000, 5000, 7000, 9000 W.

Each sample was introduced in a cylindrical shape, according to the established geometry. The test results are represented in graphical form in Fig.5.

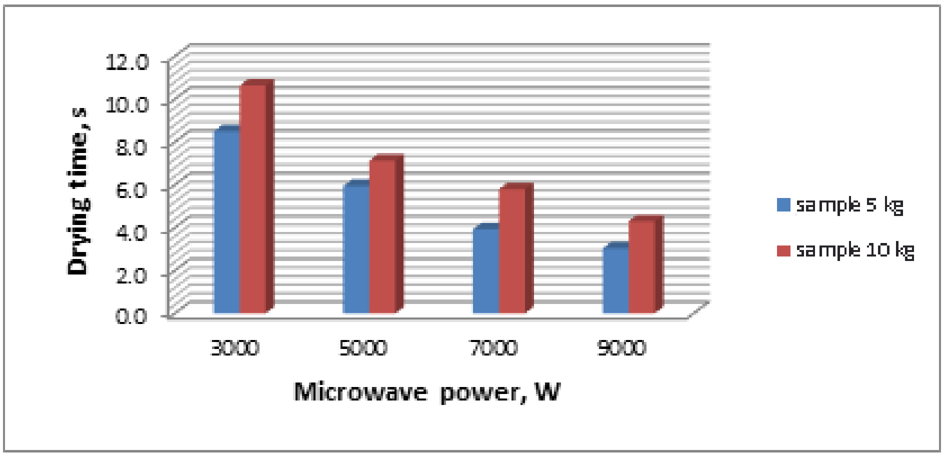

Fig. 5. Variation of drying time with microwave power

Following these tests, the average value of the final moisture in the sawdust was 7.075±0.6%.

3.3 Determining the optimal power

An important parameter in the drying process is the power density (DP) which is defined as the ratio between the microwave power and the sample mass exposed to microwave irradiation. The unit of measurement can be W / g, W / kg. The values of the power densities related to the samples and the applied microwave powers were calculated. Fig.6 shows graphically the variations of the power densities with the drying time for two sets of samples.

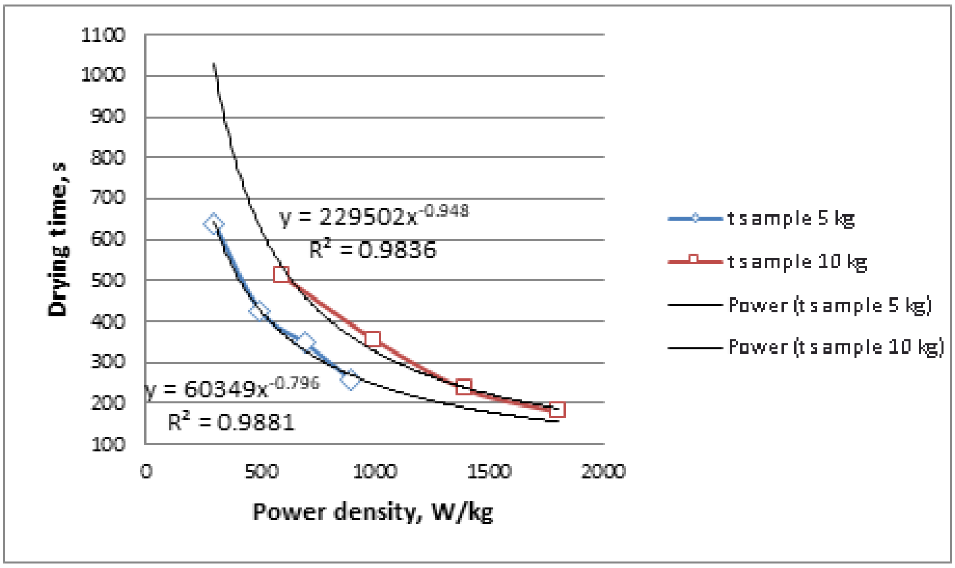

Fig. 6. Power density variation with drying time

Based on the test data, exponential equations were generated to mathematically describe the variation of power density with drying time.

It can be seen from the graphical representations that there are points on the theoretical curve that are not aligned. In this case, the set of measurements may be resumed in order to identify the nature of the causes which led to this aligned result, simultaneously with the use of statistical instruments.

The existence of the direct relationship between the applied power density and the drying time allows the optimization of energy consumption. Thus, you can choose the amount of biomass to be dried at a target humidity, while setting the equipment at the appropriate power of the process.

3.4 Possibilities for process optimization

Microwave drying of lignocellulosic biomass waste can be achieved under energy and process conditions by identifying the relationships between the various parameters encountered: nature of lignocellulosic biomass waste, initial and final humidity, sizing, microwave power density, geometry.

4. Conclusions

Pilot studies were performed on the identification of drying conditions in the microwave field leading to the obtaining of dry biomass with humidity in the range of 5… 8%, starting from initial humidity of 14… 20%.

The field of humidities with low values is the largest energy consumer. Under these conditions, the use of microwave drying equipment is preferable for this type of process by the specific heating mechanism, it being known that microwaves act inside the irradiated material.

For the microwave oven designed and made for drying biomass waste, the test conditions for establishing the biomass geometry in the cavity of the microwave oven were established. Two geometric models of planar and cylindrical type were analysed, choosing as performance criteria: homogeneity of heating, absence of burns, process safety, and quality of the finished product.

Based on the experimental data and the observations during the tests performed, the cylindrical geometry was selected.

The conditions for the material from which to make the cylindrical geometry were listed:
- transparent in the microwave
- thermal resistance up to 165ºC
- resistance to lowered pressures (max. 3 bar)
- vapor resistance.

Tests were performed to determine the drying time, performing tests to obtain humidity between 14 ... 20% followed by tests to obtain humidity of 5 ... 8% in biomass.

Sets of tests were performed with biomass sample masses of 5 and 10 kg for which the applied microwave power was varied, recording:
- variation of drying time with microwave power
- average value of the final moisture in the sawdust (7.075, 60.6%)
- variation of power density with drying time.

The existence of the direct relationship between the applied power density and the drying time allows the optimization of energy consumption. Thus, one can choose the amount of biomass to be dried at a target humidity, while setting the equipment at the appropriate power of the process.

Acknowledgments

This paper has been developed as part of a project co-financed by the European Union through the European Regional Development Fund, under Competitiveness Operational Programme 2014-2020, Priority Axis 1: Research, technological development and innovation (RD&I) to support economic competitiveness and business development, Action 1.2.3 – Partnerships for knowledge transfer, project title: *Eco-innovative technologies for recovery of biomass wastes*, project acronym: ECOVALDES, SMIS code: 105693-594, Financial agreement no. 129/23.09.2016.

References

[1] Chua, K.J., S.K. Chou, J.C. Ho, and N.A. Hawlader. "Heat pump drying: Recent developments and future trends." *Drying Technology* 20, no. 8 (2002): 1579–1610.
[2] Amos, W.A. *Report on biomass drying technology*. National Renewable Energy Laboratory, 1998.
[3] Khan, A.A., W. de Jong, P.J. Jansens, and H. Spliethoff. "Biomass combustion in fluidized bed boilers: potential problems and remedies." *Fuel Processing Technology* 90, no. 1 (2009): 21-50.
[4] Imatran Voima OY. HASL. *Thermal drying of wet fuels: opportunities and technology*. Prepared by H.A. Simons LTD. for Electric Power Research Institute of Canada, TR-107109 4269e0, 1996.
[5] Mujumdar, A.S. "Principles, classification, and selection of dryers." *Handbook of Industrial Drying*, 4th edition. Boca Raton, Florida, CRC Press, 2014.
[6] Keey, R.B., and J.J. Nijdam. "Moisture movement on drying softwood boards and kiln design." *Drying Technology* 20, no. 10 (2002): 1955–1974.
[7] McCurdy, M.C. *Efficient kiln drying of quality softwood timber*. Doctoral Thesis. Degree of Doctor of Philosophy in Chemical and Process Engineering, University of Canterbury, Christchurch, New Zealand, 2005.
[8] Schiffmann, R.F. "Microwave and dielectric drying." *Handbook of Industrial Drying*, vol. 1, 2nd edition. New York, Marcel Dekker, Inc., 1995.
[9] Barnes, D., L. Admiraal, R.L. Pike, and V.N.P. Mathur. "Continuous system for the drying of lumber with microwave energy." *Forest Products Journal* 26, no. 5 (1976): 31–42.
[10] Mujumdar, A.S. "An overview of innovation in industrial drying: Current status and R&D needs." *Transport Porous Media* 66 (2007): 3–18, doi:10.1007/s11242-006-90l8-y.
[11] Keey, R.B., T.A.G. Langrish, and J.C.F. Walker. *Kiln-Drying of Lumber*. New York, Springer, 2000.
[12] Stamm, A.J. *Wood and Cellulose Science*. New York, Ronald Press, 1964.

Considerations Regarding the Different Behaviour to Vibratory Cavitation Erosion-Corrosion of Brass and Bronze Used in the Cooling and Power Systems of Railway Engines

PhD. Eng. **Iosif LAZĂR[1]**, Prof. PhD. Eng. **Ilare BORDEAȘU[1*]**,
Lecturer PhD. Eng. **Gabriel Vasile URSU-NEAMȚ[1**]**

[1] University Politehnica Timisoara, Faculty of Mechanical Engineering, 1 Bd. Mihai Viteazul, 300222 – Timisoara, Romania

*ilarica59@gmail.com, **ursu.gabriel@gmail.com

Abstract: *Very many components operating in liquid environments are manufactured from copper-based alloys, i.e. brass and bronze. Most often, these alloys are selected based on their resistance to chemical corrosion and their high level of heat transfer capability. Some of these components are subject to cavitation stress. In consideration of the above, this paper presents the different resistances to vibratory cavitation erosion-corrosion of brass (CuZn39Pb3) and bronze (CuSn12-C) in semi-finished state, used to manufacture the components of valves installed in the cooling systems and hydrodynamic power transmission of railway vehicles. To show these differences in the behavior and resistance of the material when it is subject to cavitation microjets from the vibratory cavitation process, we are using SEM and photographic images of the eroded surface structure. The assessment of the difference in resistance is made based on the MDE(t) curves and the specific parameters: average erosion depth, cavitation resistance and the average roughness, as appearing in the profile diagram for the eroded surface. The experiments were performed using the standard piezoelectric crystal assembly, available in the Cavitation Research Laboratory at the Polytechnic University from Timisoara.*

Keywords: *Cavitation erosion-corrosion, microstructure, erosion depth, cavitation resistance, roughness, brass, bronze.*

1. Introduction

Copper-based alloys (brass and bronze) are largely used in the industry, especially in the construction of the vehicle water-cooling systems, due to their technological properties (allowing the production of semi-finished components by casting, rolling, forging, due to their adaptability to mechanical processing and heat treatments, etc.), and due to their physical and mechanical characteristics, which make them withstand the chemical corrosion during operation, as well as the thermal and hydrodynamic stress, such as cavitation. Thus, components manufactured out of brass and bronze alloys, in semi-finished state, can be found in all the equipment and installations processing liquids (hydraulic turbines and pumps, hydrodynamic transmissions, command and control equipment from the hydraulic drive systems, pipelines, valves, fittings and pumps on the water-supply and irrigating systems), where the hydrodynamic effect occurs as a result of pressure variations (i.e. decrease below vaporization threshold and sudden increase) [1]. In time, operation under cavitation determines the decommissioning for repairs or replacement, because of the damages caused by the erosion of cavitation microjets. According to the type of brass or bronze allow, the degree of damage is different. In consideration of the above, this paper presents the research results of the exposure to vibratory cavitation of brass (CuZn39Pb3) and bronze (CuSn12-C) in initial state (as delivered), in order to understand the damage mechanism and choose the best practical solution for components operating in cavitation conditions.

2. Materials under analysis

The materials used in our research are two alloys: a copper-zinc alloy (brass) and a copper-tin alloy (bronze). We have chosen these two alloys because they are used in the production of a wide range of components operating in low-intensity cavitation conditions (discharge tap and valve bodies), as well as in the production of pump rotors and hydrodynamic drive turbines, and ship propellers, where the cavitation forces exceed moderate values. For these reasons, it was necessary to know the behavior and resistance to cavitation erosion, as created in the piezoelectric crystal assembly, available in the Cavitation Research Laboratory at the Polytechnic University from Timisoara, which creates quite a high destruction intensity, much higher than the one in the real operating conditions for the above-mentioned components.

The brass (CuZn39Pb3) was made available by SC Color-Metal SRL, as a 20-mm rod which is mainly used for pipe fittings and valve stoppers.

The chemical composition, as determined by laboratory tests, is as follows: [2] 57.7 % Cu, 38.49 % Zn, 3.3 % Pb, 0.2 % Fe, 0.1 % Ni, 0.2 % Sn, 0.01 % Al.

The mechanical properties, as determined by laboratory tests, are as follows: tensile strength R_m = 502 MPa, fluid flow $R_{p0.2}$ = 365 MPa, Vickers hardness (average of 8 measurements) = 121.75 HV0.5, breaking elongation A5 = 18 %, coefficient of longitudinal elasticity E = 97 GPa, density ρ = 8.47 g/cm^3.

The two-phased structure made up of the solid solution α (approx. 60%) and the electronic compound β (approx. 40 %), figure 1, [2].

The bronze alloy (of the type CuSn12-C) was received from the "Dunărea de Jos" University from Galati, as a 20-mm diameter rod, turned from a cast semi-finished product. This alloy, in comparison with brass (CuZn39Pb3) is more widely used for components which need to withstand wear and tear by chemical corrosion and cavitation [2], such as: discharge valve bodies, fittings, hub for removable blade impellers, pump and turbine rotors for hydraulic machines, ship propellers.

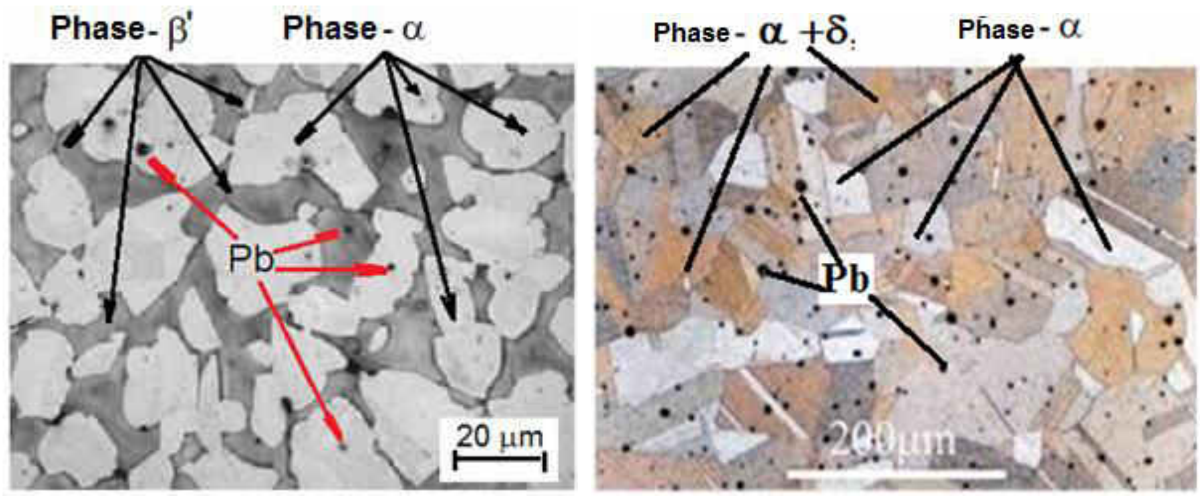

a) b)

Fig. 1. Structure of brass CuZn39Pb3 (a) and bronze CuSn12-C (b)

(image taken with [2])

The chemical composition, as determined by laboratory tests, is as follows [2]: 85.16 % Cu, 11.18 % Sn, 0.4856 % Zn, 0.7983 % Pb, 0.5226 % Fe, 0.6933 % Ni, 0.2 % Sn, 0.0304 % Mn, 0.0382 %S, 0.0714 %Sb, < 0.003 %P.

The mechanical properties, as determined by laboratory tests, are as follows [2]: tensile strength R_m = 312 MPa, fluid flow $R_{p0.2}$ = 157 MPa, Vickers hardness (average of 8 measurements) = 146.125 HV0.5, breaking elongation A5 = 9 %, coefficient of longitudinal elasticity E = 97 GPa, density ρ = 8.77 g/cm^3.

The two-phased structure made up of α-phase solid solution and eutectoid grains (α + δ) [2], figure 1b.

3. Method and equipment used for the experimental tests

The equipment used to generate cavitation conditions is a standard piezoelectric crystal plates equipment, shown in figure 2, from the Cavitation Laboratory [3-10] within the Polytechnic

University from Timisoara, whose operational parameters are constantly monitored and kept within the limits provided for in the ASTM G32-2010 standard [11], as follows:

- Vibration amplitude (double) = 50 μm;
- Vibration frequency = 20 ± 0.02 kHz;
- Power of the electronic ultrasound generator = 500 W;
- Liquid environment = double-distilled water;
- Liquid temperature = 22 ±1° C.

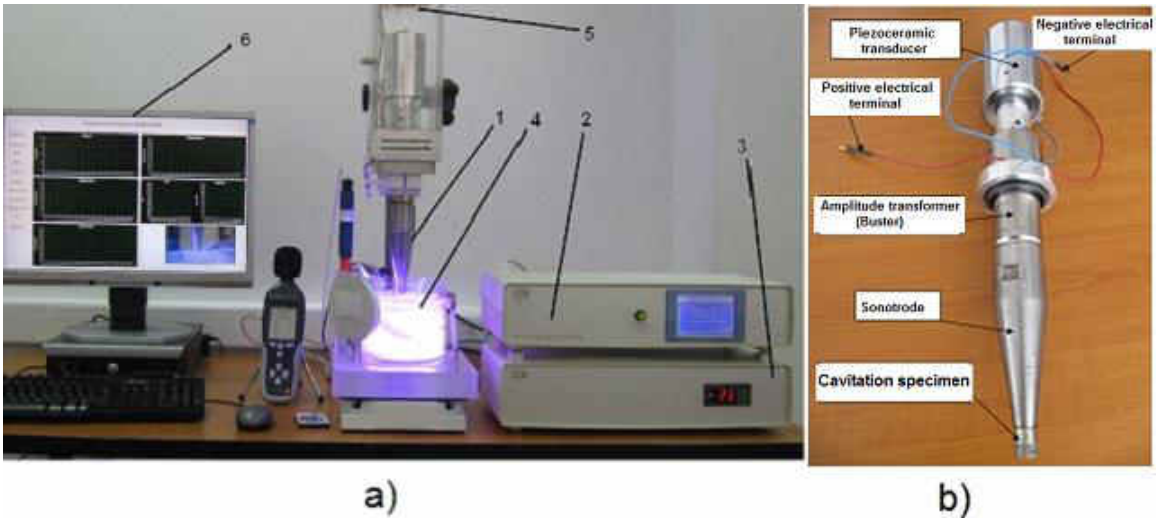

Fig. 2. Vibrating piezoelectric crystal plates

a) Image of the equipment used (1 - sonotrode; 2 - electronic system used to generate the vibration frequency and the power necessary for the 20 KHz/500 W piezoceramic transducer; 3 - water temperature regulator; 4 - container for the liquid, with a serpentine cooler; 5 - piezoceramic transducer ventilation/cooling system; 6 - computer, used to command and control the vibratory equipment parameters).

b) The vibratory mechanical system

Before the cavitation tests were performed, the samples were brought to the shape and dimensions in figure 3, while the surfaces subjected to cavitation attack were polished to a roughness Ra ≅ 0.02 μm. In keeping with the laboratory protocols, at least three samples were tested for each of the states of the materials under research [5, 6], [10], [12].

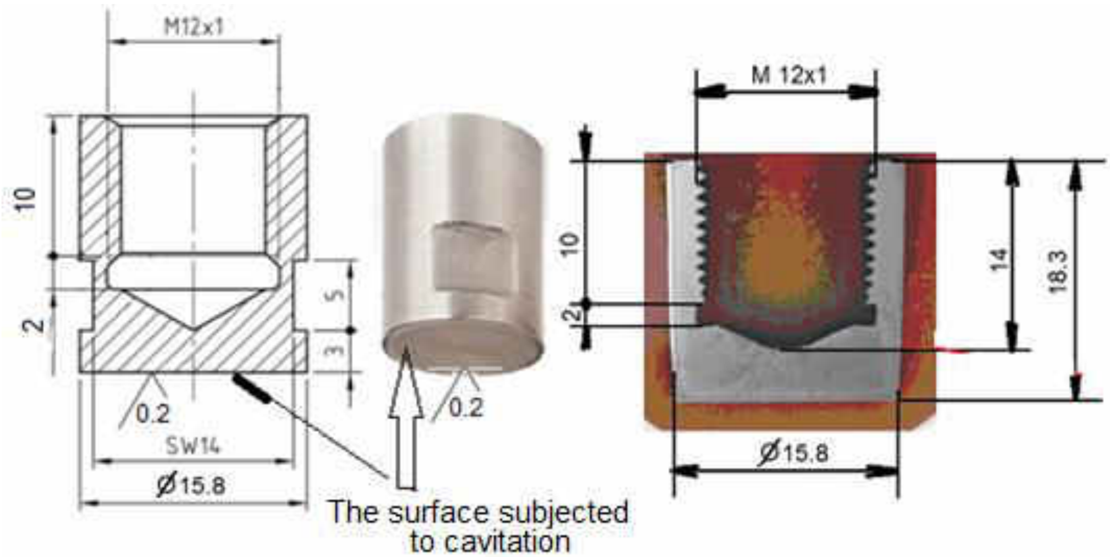

Fig. 3. The sample used for the cavitation test

According to the methodology observed in the Cavitation Research Laboratory, and in compliance with the requirements established by the ASTM G32-2010 standards [9], [11], the total duration of a vibratory cavitation erosion-corrosion test was 165 minutes. This duration was divided in intermediate durations: 5 minutes (one), 10 minutes (one), and 15 minutes (the remaining 10 durations), in order to observe the behavior of the surface subjected to cavitation.

4. Experimental results. Analysis and discussions

4.1. The evolution of the morphological damage in the semi-finished slabs

Figures 4 and 5 show SEM and macro images of the surfaces eroded by vibratory cavitation, after 165 minutes of exposure to the vibratory cavitation erosion-corrosion process. These images show that, at the end of the 165 minutes of exposure to erosion by vibratory cavitation, the crevice sizes increase, while the crack propagation expands both at the surface and in depth, with cracks forming along the grain boundaries.
In the case of brass (figure 4), it can be seen how the β′-grain is removed and how the cracks propagate. The distinct characteristics of the cavitation-eroded sample surface are determined by a number of irregular crevices, resulted from the removal of the Cu-Zn compound (β′ - phase), i.e. increased toughness and brittleness. Also, other crevices are caused by the Pb-inclusions inside solid-state solution α grains, resulted from the substitution of Zn with Cu.

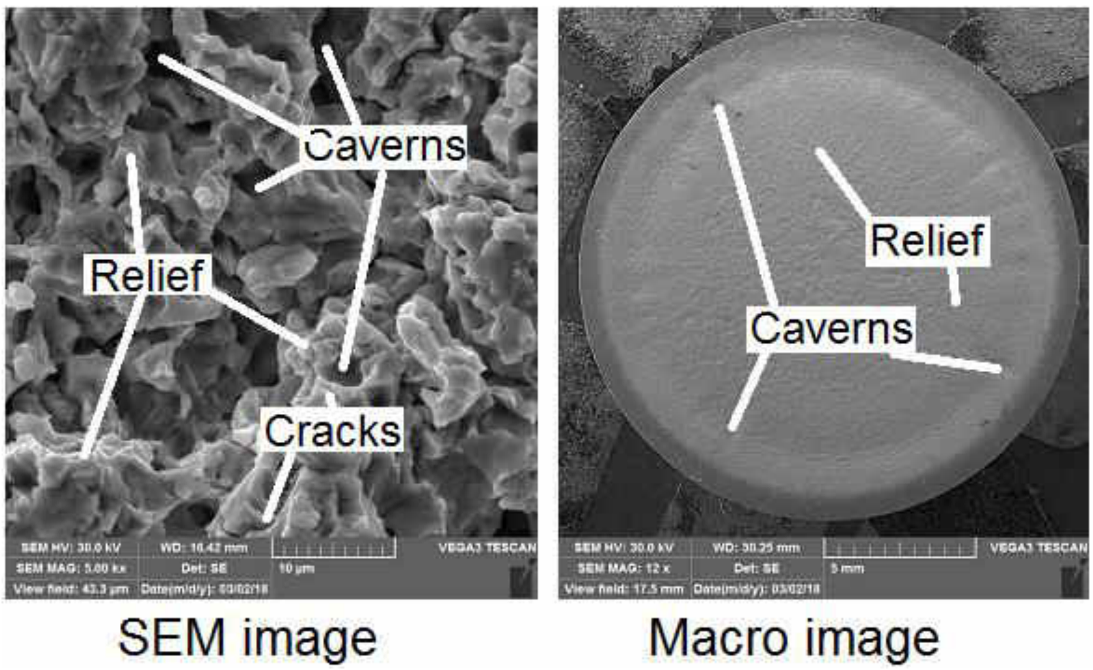

Fig. 4. SEM and macro images of the brass (CuZn39Pb3) sample microstructures, in the semi-finished state, after 165 minutes of exposure to cavitation erosion-corrosion

The SEM and macro images of the bronze (CuSn-12C) sample from figure 7 show the propagation of cracks and the formation of indentations and crevices by grain removal and coalescence of such cracks, as a result of the cyclical stress on the sample surface, caused by cavitation microjets and shock waves, specific to the fatigue process, thus resulting in a porous and very rough surface. Also, the SEM investigation reveals the formation of evenly distributed pitting in the matrix of solid solution α, which substitutes SN in Cu, and the occurrence of polyhedral indentations in the former δ-electronic compound areas, characterized by increased brittleness.

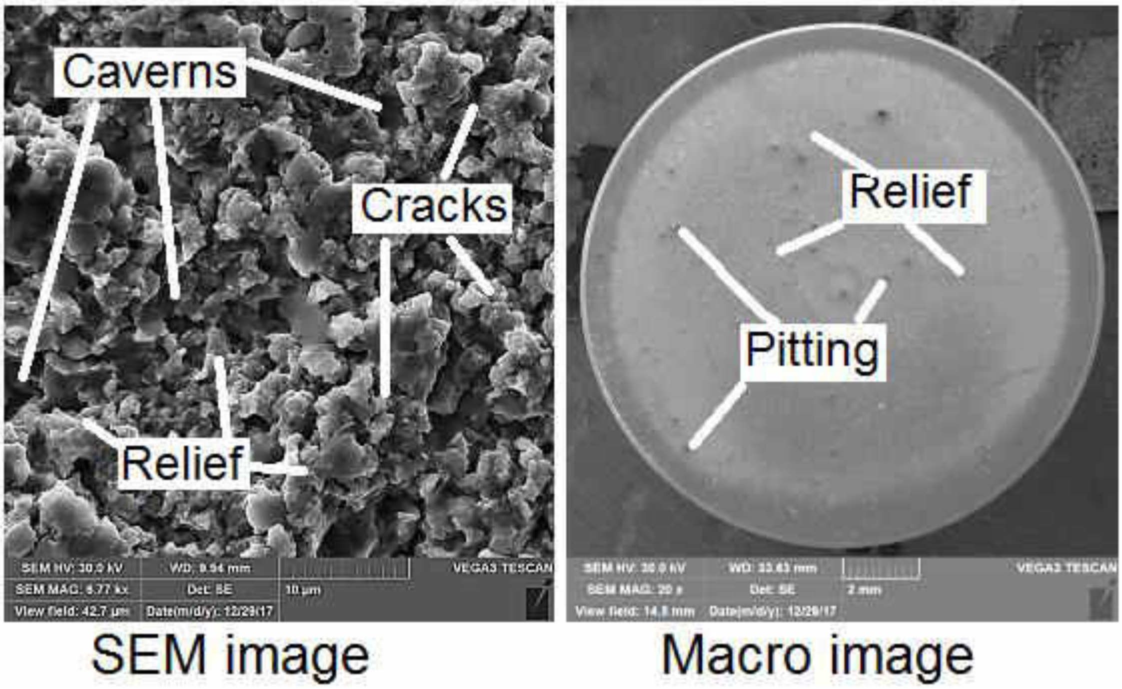

Fig. 5. SEM and macro images of the bronze sample microstructures, in the semi-finished state, after 165 minutes of exposure to cavitation erosion-corrosion

4.2. Comparison of the research results for the semi-finished slabs

The curves and parameter values illustrated in diagrams in figures 6 and 7 show the differences and similarities between the behaviors and resistances to cavitation of the two materials. The points on the diagrams are experimental values, arithmetic average values of the experimental results obtained for the three samples taken from each of the materials, while the curves show an averaging of the experimental and analytical values, with their specific relations, as calculated in the Cavitation Research Laboratory at the Polytechnic University from Timisoara [2, 3], [5],[6], [13].

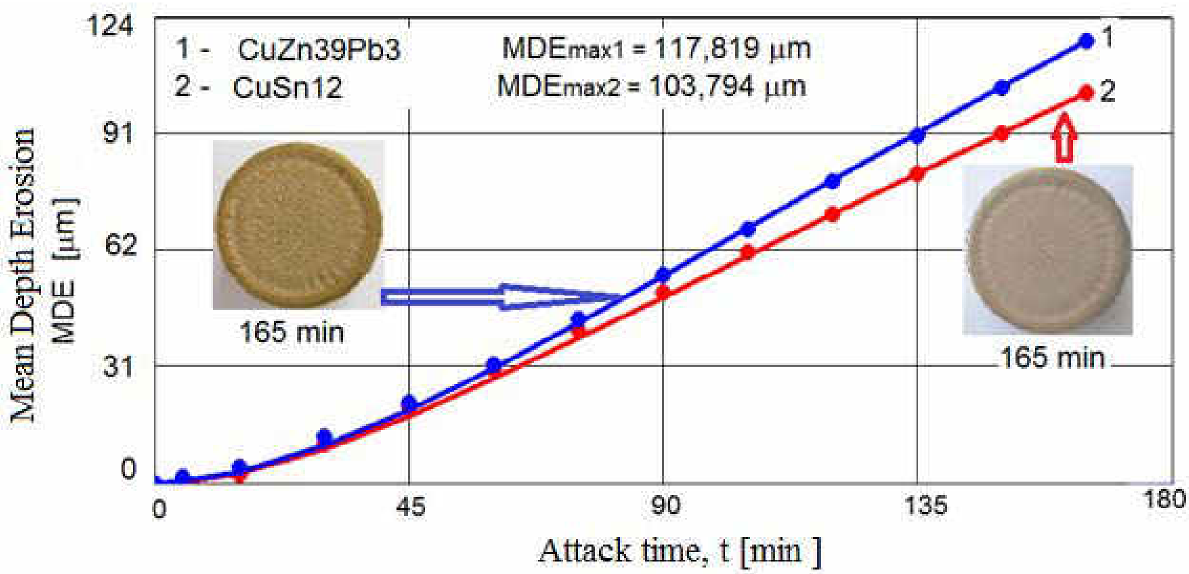

Fig. 6. The variation of the average erosion depth, in relation to the duration of the cavitation test (compared)

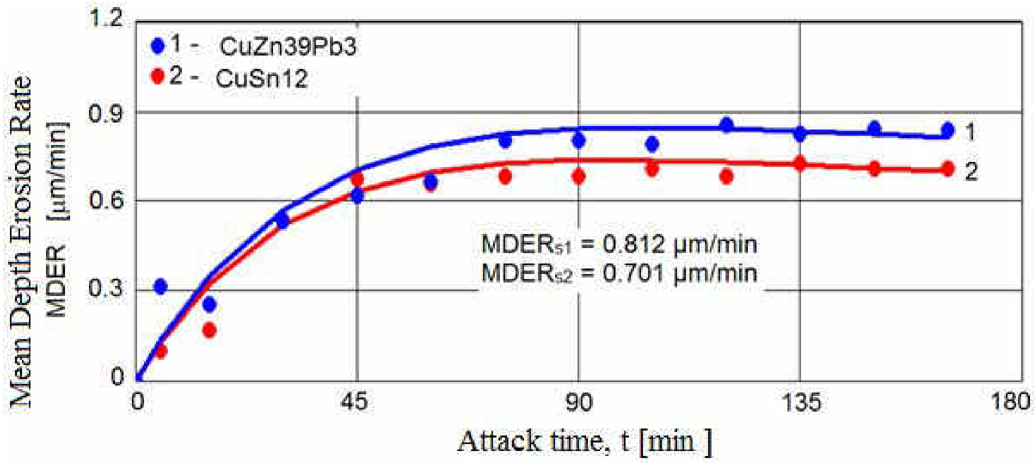

Fig. 7. The variation of the mean depth of penetration rate, in relation to the duration of the cavitation test (compared)

Findings based on the evolution of the curves and the dispersion of experimental points, from figure 6 and 7.

Similarities:

- a similar exponential evolution of the MDE(t) curves, with a plateau starting with minute 45;
- a similar evolution of the MDER(t) curves, which reach maximum values after 90 minutes of cavitation erosion-corrosion attack ($MDER_{max}$ = 0.846 µm/min – for brass, and $MDER_{max}$ = 0.737 µm/min - for bronze), and a slight decrease (4 - 5 %) towards the final, plateau value, indicating a leveling of the erosion rate ($MDER_s$ = 0.812 µm/min – for brass, and $MDER_{max}$ = 0.701 µm/min - for bronze). These similar evolutions result from the identical behavior of the sample surfaces to the cavitation attack, but showing different resistances;
- approximately identical dispersions of the experimental values and their arithmetic averages for the three samples, in comparison with the mediation curves MDER(t), starting with minute 45 of the exposure to cavitation.

Difference: a better behavior of bronze (CuSn12-C), as shown in the bar chart from figure 8, which compares the erosion parameters (cumulated average erosion depth, after 165 minutes of cavitation erosion-corrosion attack, MDE_{max} and the cavitation resistance, R_{cav} = 1/$MDER_s$) and also by comparing the values of the roughness parameter R_Z. It can be seen that any of the brass parameter values are lower than the bronze parameter values.

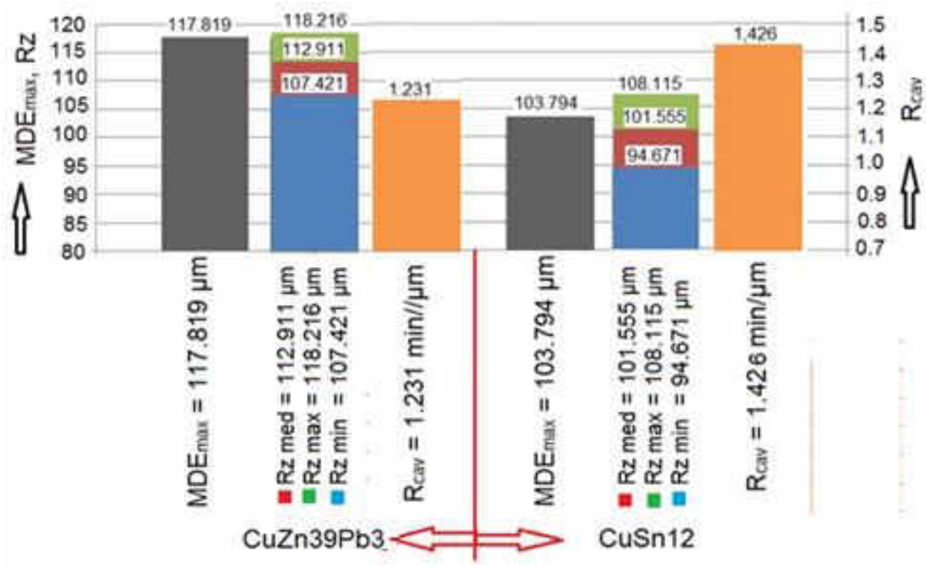

Fig. 8. Bar chart estimating the resistance to cavitation erosion-corrosion, by comparing the values of the specific parameters

Table 1 shows the percentage of decrease in brass (CuZn39Pb3) resistance to cavitation, in comparison with the bronze (CuSn12-C) resistance. It can be noted that this decrease does not differ substantially from one parameter to the other, having variations between 11% and 16%.

Table 1: Comparison of specific parameters

Reference material	Cavitation erosion parameter	Variation in comparison with bronze parameters [%]
		Brass (CuZn39Pb3) as delivered
Bronze (Cu Sn12) as delivered	MDE_{max} [μm]	↑ 13.5
	$R_{cav} = 1/MDER_s$ [min/ μm]	↓ 15.8
	$R_{z\ med}$ [μm]	↑11.2

↓ - decrease ↑ - increase

The research studies that our laboratory has been performing for more than 70 years [7], [13, 14] have shown that the differences under 15% between the erosion parameters may occur not only between different quality materials, but also between samples taken from the same material, being mainly caused by:

- different values for mechanical properties, which are not constant;
- the uneven dispersion of hardness in the structure of the surface exposed to cavitation;
- the degree of smoothness of the surface structure exposed to cavitation, as well as the existence of structural constituents that may decrease the resistance to the pressures created by the impact with the microjets and shock waves.

Therefore, we can conclude that brass (CuZn39Pb3) and bronze (CuSn12-C) have slightly different behaviors and resistances when exposed to erosion by cavitation; they are both materials displaying weak resistance to cavitation when they are not subject to heat treatments, but they can be used for components operating in low-intensity cavitation currents (elbows, manifolds, pressure and flow rate command and control equipment, machinery operating with fluids with viscosities higher than water).

5. Conclusions

1. Brass (CuZn39Pb3) and bronze (CuSn12-C) display the behavior specific to materials with evenly distributed structural components; however, they have low mechanical resistance, therefore the materials in their initial research state (as delivered) can only be used for parts operating in low-cavitation hydrodynamic conditions, i.e. hydraulic equipment (pressure valves, flow regulators, thread valves, etc.), which operate with fluids with viscosities higher than water.
2. The start and advancement of the damage under the impingement of microjets and shock waves developed in the cavitation process, occur at the boundary between the α-solid solution and the β′ electronic component, with a rapid destruction of the β′ phase - in the case of brass - and in the matrix of α-solid solution, replacing Cu with Sn and generating the occurrence of polyhedral indentations in the former δ-electronic compound areas, characterized by increased brittleness.
3. Both materials show similar behaviors to cavitation erosion-corrosion, yet they display slightly different resistances (with an approx. 11% increase for bronze CuSn12-C).
4. In order to use these two materials, i.e. brass (CuZn39Pb3) and bronze (CuSn12-C), for the production of components operating in higher cavitation hydrodynamic environments, such

as ship impellers (hub + blades) and/or hydraulic machine rotors (hydrodynamic power transmission of railway engines), the said components need to be subjected to in-depth and surface heat treatments, leading to significant increases in their mechanical characteristics (R_m, $Rp_{0.2}$ and HV).

References

[1] Lin, Cui, Qing Zhao, Xiaobin Zhao, and Ying Yang. "Cavitation Erosion of Metallic Materials." *International Journal of Georesources and Environment* 4, no. 1 (2018): 1-8.
[2] Lazăr, Iosif. *Techniques for the optimization of the resistance to cavitation erosion of certain Cu-Zn and Cu-Sn alloys / Tehnici de optimizare a rezistenței la eroziune prin cavitație a unor aliaje Cu-Zn și Cu-Sn*. Doctoral Thesis. Timisoara, 2020.
[3] Bordeașu, Ilare, Ion Mitelea, Iosif Lazar, Lavinia-Madalina Micu, and Olimpiu Karancsi. "Cavitation Erosion Behaviour of Cooper Base Layers Deposited by HVOF Thermal Spraying." *Reviste de Chimie* (Bucharest) 68, no. 12 (2017): 2914-18.
[4] Bordeasu, Ilare, Ion Mitelea, Laura Salcianu, and Corneliu Marius Crăciunescu. "Cavitation Erosion Mechanisms of Solution Treated X5CrNi18-10 Stainless Steels." *Journal of Tribology-Transactions of the ASME* 138, no. 3 (July 2016): Article no: 031102 (7 pages).
[5] Oanca, Octavian Victor. *Techniques for optimizing the resistance to cavitation erosion of CuAlNiFeMn alloys for the execution of naval propellers / Tehnici de optimizare a rezistenţei la eroziunea prin cavitaţie a unor aliaje CuAlNiFeMn destinate execuţiei elicelor navale*. Doctoral Thesis. Timisoara, 2014.
[6] Salcianu, Cornelia Laura. *The flow by the butterfly valves and the cavitation erosion to components by austenitic stainless steels / Curgerea în vanele fluture și eroziunea prin cavitație a componentelor din oțeluri inoxidabile austenitice*. Doctoral Thesis. Timisoara, 2017.
[7] ***. *Standard method of vibratory cavitation erosion test*. ASTM Standard G32, 2010.
[8] Mitelea, Ion, Lavinia-Madalina Micu, Ilare Bordeasu, and Corneliu Marius Crăciunescu. "Cavitation Erosion of Sensitized UNS S31803 Duplex Stainless Steels." *Journal of Materials Engineering and Performance* 55, no. 2 (2016): 1939-1944.
[9] Karimi, Amir, and J.L. Heuze. "Cavitation Erosion of High Damping Manganese and Copper Based Alloys / Erosion de cavitation d'alliages amortissants a base de magnese et de cuivre." *La Houille Blanche*, no. 7-8 (December 1992): 617-624.
[10] Anton, Ioan. *Cavitation / Cavitația.* Vol. II. Bucharest, R.S.R. Academy Publishing House, 1985.
[11] Bordeasu, Ilare. *Cavitation erosion of materials / Eroziunea cavitațională a materialelor*. Timişoara, Politehnica Publishing House, 2006.
[12] Bordeaşu, Ilare. *Cavitation erosion on materials used in the construction of hydraulic machines and naval propellers. Scale effects / Eroziunea cavitațională asupra materialelor utilizate în construcția mașinilor hidraulice și elicelor navale. Efecte de scară*. Doctoral Thesis. Timişoara, 1997.
[13] Mitelea, Ion, Cristian Ghera, Ilare Bordeaşu, and Corneliu-Marius Crăciunescu. "Ultrasonic cavitation erosion of a duplex treated 16MnCr5 steel." *International Journal of Materials Research* 106, no. 4 (2015): 391-397.
[14] Mitelea, Ion, and Ilare Bordeasu. "Cavitation Erosion Behaviour of Stainless Steels with Constant Nickel and Variable Chromium Content." *Materials Testing* 54, no. 1 (2012): 53-58.

Researches on the Development of a Nanobubbles Generator Used to Waters Aeration

PhD. Student **Marilena Monica BOLTINESCU (ROZA)**[1], Prof. Dr. Eng. **Nicolae BĂRAN**[1], ŞL. Dr. Eng. **Mihaela CONSTANTIN**[1*]

[1] Politehnica University of Bucharest

* i.mihaelaconstantin@gmail.com

Abstract: *The paper presents a new type of air bubble generator that uses a plate with 900 nm orifices. Previous research has worked with fine bubble generators with orifices of 0.1 mm order. It is known that the smaller the orifices diameter, the smaller the bubbles immersed in water, so the water aeration will be more efficient.*
Obviously, the constructive solution of the nanobubbles generator presented in the paper is clearly superior to the other bubble generators built in the laboratories of POLITEHNICA University of Bucharest.
At the end of the paper, the framing of the nanobubbles generator within an experimental installation is presented.

Keywords: *Nanobubbles generator, nanotechnologies, water aeration.*

1. Introduction

By water aeration is meant the transfer of oxygen from atmospheric air to water; this phenomenon is a process of mass transfer of a gas to a liquid.
In the paper [1], the authors propose to make a distinction between water aeration and water oxygenation of in the following sense:
- In aeration processes, atmospheric air has a content of 21% O_2;
- In the processes of oxygenation, oxygen is added to the atmospheric air and later this mixture is introduced in the water; as a result, the volume of oxygen in the mixture is higher than 21%;

The supplemental oxygen introduced can be obtained by one of the following methods:
a) From a cylinder containing liquid oxygen;
b) From devices called oxygen concentrators that deliver a gas with a concentration of 95% O_2 and 5% N_2;
c) With the help of ozone generators by mixing atmospheric air with ozone;
All three solutions (a, b, c) lead to a faster increase in the concentration of dissolved oxygen in the water.
Figure 1 shows the following:
- Each water molecule consists of an oxygen atom bonded to two hydrogen atoms (H_2O);
- Oxygen dissolved in water can be found, among water molecules, in the form of two oxygen atoms (O_2);

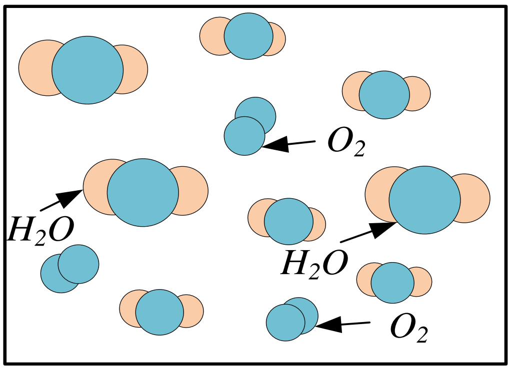

Fig. 1. The presence of dissolved oxygen in water; water molecules (H_2O) and dissolved oxygen molecules (O_2)

Both water aeration and water oxygenation increase the concentration of dissolved oxygen in the water.
This ensures good water quality, avoids the occurrence of a dissolved oxygen deficiency that would endanger living things in the water. For example, fish need about 5 mg / dm^3 of dissolved oxygen in water to survive [2].
By introducing gaseous oxygen into wastewater, organic impurities are removed under the action of aerobic bacteria.

2. Characteristics of fine bubble generators

Pneumatic aeration systems that generate fine bubbles (ø <1 mm) are the most efficient.
Fine bubble generators (FBG) are divided into five classes according to their construction, namely [3][4]:
I. FBG constructed of perforated membranes;
II. FBG made of porous plastics;
III. FBG constructed of ceramic (ceramic FBG);
IV. FBG constructed by micro-drilling or spark-erosion;
V. FBG built using nanotechnologies;
The parameters that influence the performance of a water aeration process are [5]:
a) The constructive characteristics of the fine bubble generators which mainly refer to:
- the orifices diameter in the perforated plate of the FBG;
- the orifices distribution in the perforated plate to avoid bubbles coalescence;
- the shape of the orifices plate and the construction of the fine bubble generator;
b) The characteristics regarding the architecture of the fine bubble generators that are mounted in the aeration tanks.
These characteristics refer to the distribution of FBG in the aeration tank, to the constructive solution of compressed air supply.
- The following conditions must be observed when constructing an FBG:

$$\frac{s}{d_0} > 3 \tag{1}$$

$$\frac{d}{d_0} > 8 \tag{2}$$

where: s - thickness of the perforated plate [m];
d_0 - the orifices diameter [m];
d - the distance between two successive orifices [m];
- At the location of the FBG in the aeration tank depending on the water layer height, a distance between two side by side FBG is calculated so as to avoid of the bubble columns coalescence formed by the two fine bubble generators.

3. Presentation of the nanobubbles generator

The main element of the nanobubbles generator (figure 2) is the plate (3) which ensures the uniform dispersion of the compressed air in a certain volume of stationary water.
In the plate (3), 290 orifices with diameter ø = 900 nm are performed with a step between them equal to 5 mm.

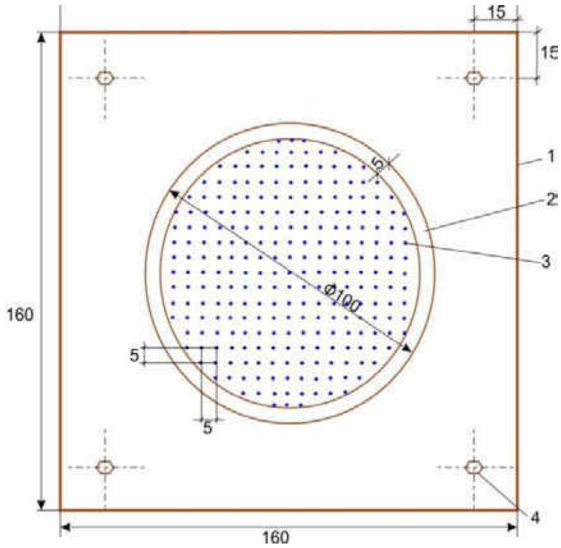

Fig. 2. Plan view of the nanobubbles generator.
1 - support plate 160 x 160 x 8; 2 - fixing ring of the orifices plate;
3 - plate with 290 orifices ø = 900 nm; 4 - plate fixing screws.

The plate (3) is made of silicon and has the following characteristics:
Diameter: 100 ± 0.3 mm
Resistivity: 1 ÷ 5 ohm cm
Thickness: 525 ± 20 µm
The orifices were made by anisotropic corrosion of silicon, applying the BOSCH process.
The plate is manufactured in Germany by SIEGERT WAFER GmbH. The plate was processed by the collaboration between the University POLITEHNICA of Bucharest and the National Institute for Research and Development in Micro technology Bucharest.

Figure 3 shows a view of the nanobubbles generator (NBG) in a vertical position. The plate with the 290 orifices (6) is fixed to the cylinder body (4) by the annular angle (5).

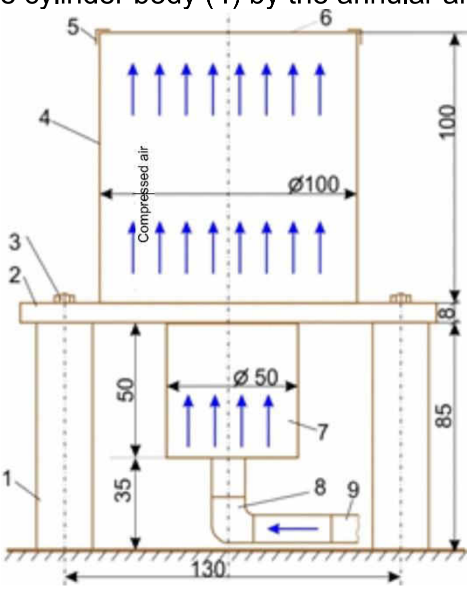

Fig. 3. Side view of the nanobubbles generator.
1 –support ø20 x 2; 2 - support plate 160 x 160 x 8; 3 - fixing screw;
4 - cylindrical body ø100 x 4; 5 - fixing ring; 6 - orifices plate; 7 - pipe ø50 x 2;
8 – bend at 90^0, ½ ''; 9 - pipe Dn 15 for compressed air supply.

The compressed air delivered by a compressor through the pipe (9) expands first in the tube (7) and then in the cylinder (4); in this way, a uniformity of the air flow rate through the orifice plate (6) is achieved.

4. Scheme of the experimental installation

Figure 4 shows the scheme of the experimental installation designed to test a set of four nanobubbles generators. The compressed air delivered by the electro compressor (2) is accumulated in the tank (3) and subsequently passes through the pressure reducer (4) to the assembly of four NBG (7); the compressed air pressure must overcome the hydrostatic load (H) i.e. the water layer height in the tank (8) and the loss of air pressure when passing through the orifices [6][7].

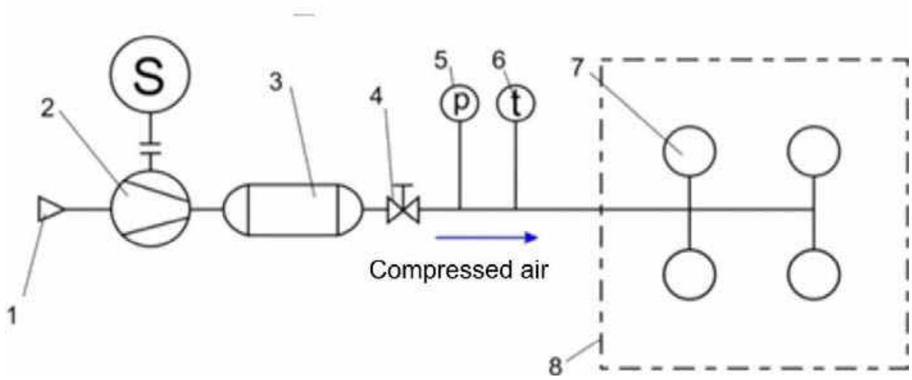

Fig. 4. Scheme of the experimental installation for water aeration with nanobubbles generators.
1 - air filter; 2 - electro compressor; 3 - compressed air tank;
4 - pressure reducer; 5 - pressure measuring device; 6 - temperature measuring device;
7 - set of four nanobubbles generators; 8 - the contour of the water tank.

The air flow rate passing through a NBG will be [8][9]:

$$\dot{V} = A \cdot w \ = \ n \cdot \frac{\pi d^2}{4} \cdot w \ [m^3 / s] \quad (3)$$

where:
A - the area of the air inlet water section;
n - the orifices number;
d - the orifices diameter;
w - air speed when passing through the orifices;.

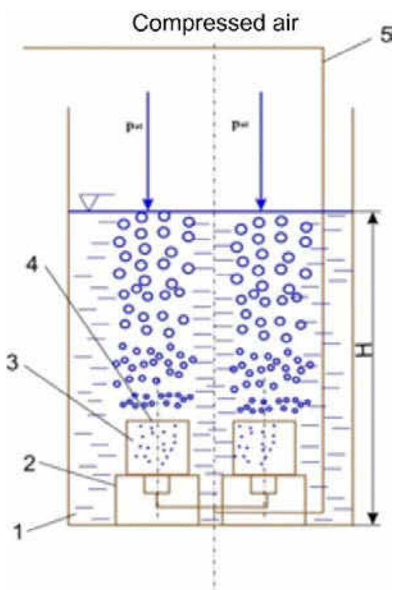

Fig. 5. Placing the NBG inside the water tank.
1 - water tank; 2 - NBG support skeleton; 3 - cylindrical body with compressed air;
4 - silicon plate with orifices ø = 900 nm; 5 - NBG compressed air supply pipe.

The total flow rate of compressed air entering all four NBGs will be:

$$\dot{V}_t = 4 \cdot \dot{V} \ [m^3 / s] \tag{4}$$

The air flow speed (w) depends on the pressure drop that occurs when air passes through an orifice and is to be experimentally determined.

5. Conclusions

* Nanotechnology is a technology whose practical result is of the magnitude order of nanometres; creating a NBG is an original and much better solution for the FBG class.
** Advantages of using FBG when aerating the waters are:
- a low pressure drop compared to other aeration systems;
- a high efficiency;
- ensures a uniform distribution of the air bubble columns in the volume of water subjected to aeration;
- simple from a constructive point of view;
- quick and easy to assemble and disassemble;
- a long service life and do not require permanent supervision;
*** Experimental researches will aim to increase the concentration of dissolved oxygen in water as a function of time C_{O_2} = f (τ); it will be compared with similar data existing in the literature.
**** The results of the experimental researches will be published in a future paper that will appear in this journal.

References

[1] Cusma, Rasha, Nicolae Băran, Nicolae Vlad Sima, Mihaela Petroșel, Remus Voicu, and Mihaela Constantin. "Researches on the delimitation between the water aeration and oxygenation processes." Paper presented at 9th International Conference on Thermal Equipments, Renewable Energy and Rural Development (TE-RE-RD 2020), online, June 26-27, 2020.
[2] Tănase, Elena Beatrice. *Influence of the composition of the gas blown in water on the dissolved oxygen content / Influența compoziției gazului insuflat în apă asupra conținutului de oxigen dizolvat*. PhD Thesis. Politehnica University of Bucharest, Faculty of Mechanical Engineering and Mechatronics, 2017.
[3] Pătulea, Al.S. *Influence of functional parameters and the architecture of fine bubble generators on the efficiency of aeration installations / Influenţa parametrilor funcţionali şi a arhitecturii generatoarelor de bule fine asupra eficienţei instalaţiilor de aerare*. PhD Thesis. Politehnica University of Bucharest, 2012.
[4] Mateescu, G.M. *Hydro-gas-dynamics of fine bubble generators / Hidro-gazo-dinamica generatoarelor de bule fine*. PhD Thesis. Politehnica University of Bucharest, Faculty of Mechanical Engineering and Mechatronics, 2011.
[5] Băran, N., M. Constantin, E. Tănase, and R. Mlisan. "Researches regarding water oxygenation with fine air bubbles." *Buletinul Științific al Universității POLITEHNICA din București, seria D, Inginerie Mecanică*, 78, no. 2 (2016): 167-178.
[6] Constantin, Mihaela, Nicolae Băran, Rareș Păun, and Albertino Giovani Roza. "Theoretical and Experimental Researches about the Pressure Loss of a New Type of Fine Bubble Generator." *International Journal of Emerging Research in Management & Technology* 6, no. 2 (February 2017): 115 – 120.
[7] Tsuge, H. *Micro- and Nanobubbles: Fundamentals and applications*. University of California – Irwine, Pan Stanford Publishing, 2014.
[8] Tănase, B., M. Constantin, R. Mlisan (Cusma), R. Mechno, and N. Băran. "Water oxygenation using gas mixtures." Paper presented at Huitième edition du COlloque FRancophone en Energie, Environnement, Economie et Thermodynamique (COFRET'16), Bucharest, Romania, June 29 – 30, 2016.
[9] Constantin, M., N. Băran, and B. Tănase. "A New Solution for Water Oxygenation." *International Journal of Innovative Research in Advanced Engineering (IJIRAE)* 2, no. 7 (2015): 49-52.

ISSN 1453 – 7303 "HIDRAULICA" (No. 3/2020)
Magazine *of Hydraulics, Pneumatics, Tribology, Ecology, Sensorics, Mechatronics*

Numerical Modeling of River Embankment Local Failure under Accidental High-Waters Conditions

Assist.prof.dr.eng. **Marie Alice GHIȚESCU**[1], Assoc.prof.dr.eng. **Gheorghe I. LAZĂR**[2], Assoc.prof.dr.eng. **Albert Titus CONSTANTIN**[3], Lect.dr.eng. **Şerban-Vlad NICOARĂ**[4]

[1] POLITEHNICA University Timişoara, alice.ghitescu@upt.ro

[2,3,4] POLITEHNICA University Timişoara

Abstract: *Exploitation in safety condition of flood protection hydraulic structures along watercourses is still an important problem, from economic and social point of view. The complex phenomenon of failure, an event of big importance for riparian areas, must be studied both in terms of genesis and development. In addition to exceeding the filling shear strength, the local failures of the river embankments are most often due to infiltrations through the body of the building, generating suffusions and leaks, respectively discharges over the canopy, generating progressive washing of the downstream facing of the filling. This paper presents a discrete 1D / 2D combined numerical modelling made with the help of the HEC-RAS v.5.07 package that simulates the hydraulic event on the Crasna River in the area of Craidorolț village, Satu Mare county, Romania, under the conditions of forming a breach in the shore defence dam left at the appearance of an accidental flood wave. The configuration of the adopted hydrograph is given by the actual recording during the flood event that took place between 26 and 30 May 2015. The uncertainty parameters at the breach formation through the defence dam were analysed using a probabilistic sampling application of predefined statistical distributions. Specifically, the statistical analysis was performed using the additional McBreach control facility, using the Monte Carlo method. The numerical simulation has as distinct purpose the highlighting of possible breach propagation on the left bank of the flood defence; as well as the estimation of the flood extent and the establishment of the transient (non-permanent) hydraulic parameters. Consequently, some constructive aspects of flood protection of a specific economic objective located nearby are under discussion.*

Keywords: *River engineering, highwaters flow, flood defence structures, crest overtopping, dam breach, hydraulic model.*

1. Introduction

HEC-RAS version 5.07 [4] is a hydrodynamic software which can simulate a structure breach (dam, lateral embankment, flood defence structure or connection type SA/2D structure) with 1D and 2D numerical equations. McBreach © version 5.07 [5] is an external control software application that facilitates the probabilistic modelling of yielding a structure by sampling the yield parameters of predefined statistical distributions and automatic running with HEC-RAS version 5.07 thousand times, using the well-known Monte Carlo method. The probabilistic analysis of a structure failure will thus contribute to the quantification of the uncertainties associated with flood mapping and the associated potential risk attributed to the probabilities of exceeding the peak flood flows.

McBreach © version 5.07 could randomly test predefined statistical distributions for all parameters of yield of frontal (dams) or side hydrotechnical structures, respectively of SA / 2D connections. In addition to the yield parameters, the user may include the flow hydrographs of the numerical model in the probabilistic analysis.

A Monte Carlo simulation with McBreach © version 5.07 produces peak flows with different probability of exceeding flood events, respectively, determines all the parameters of the sampled failure that can be further used to produce flood maps for different annual exceeding probability (A.E.P.) flood events.

McBreach © version 5.07 satisfies the need for hydraulic structures' safety in the modelling of cession as an overly conservative deterministic approach, with the probabilistic approach quantifying the uncertainty in the analysis. McBreach © version 5.07 therefore allows decision-making based on risk and uncertainty and compliments the safety desires of structures, leads to informed about risks and uncertainties in decision-making. Execution in HEC-RAS version 5.07 in an uncertainty exercise in Monte Carlo requires many hundreds or even thousands of simulations to achieve statistical convergence of the mean and standard deviation.

After McBreach © version 5.07 simulation, the user reproduces sets of predefined failure parameters for peak flows, includes them in the fully discretized numerical model, and then maps the flood extension maps. This will usually be done automatically in the eight sets of failure parameters (A.E.P.: 0.2%, 1%, 5%, 10%, 50%, 90%, 95%, 99%).

Fig. 1. Plan view of the private development establishment and a Crasna River reach *–2019*

The numerical modelling is based on a flooding study on Crasna River, in order to establish constructive aspects of flood protection of the technological platform on the left bank of a private development [1]. For the numeric modelling HEC-RAS vers.4.1 [2], 5.07 [5] software package was used, and is based on two discretization numerical systems: one dimensional (1D) system and one-two dimensional (1D-2D) system.

The technological platform of the private development is located at approx. 1 km from the riverbed of river Crasna (approx. distance from the left bank side flood defence embankment).

The natural terrain from the area is agricultural and rural, with an average elevation of 125.50 maSL and covers a total area of 60,000 m^2 (Fig.1).

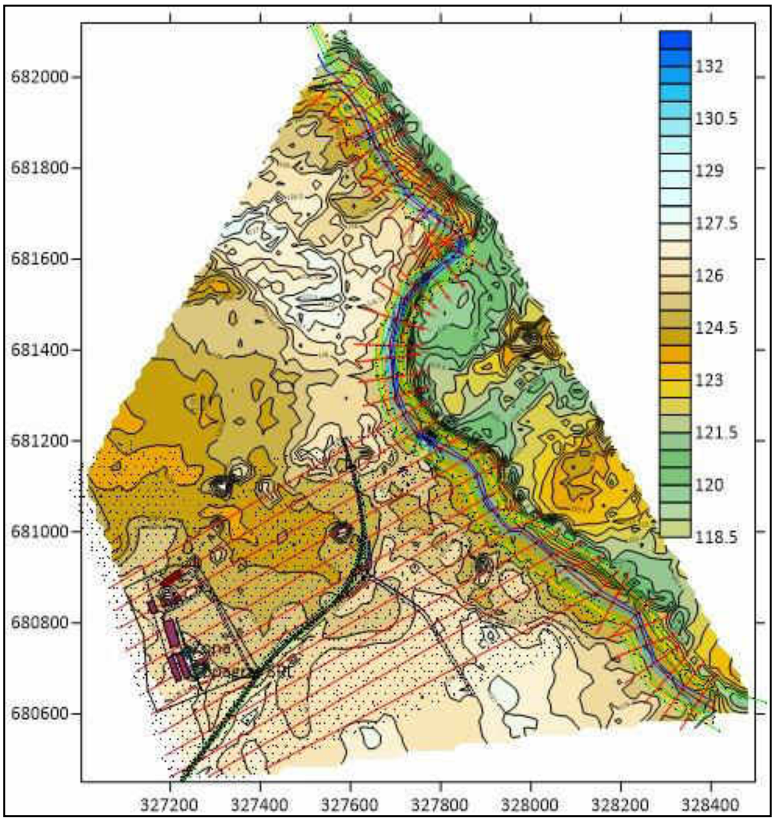

Fig. 2. 3D terrain surface representation

When modelling the geometry of the Crasna riverbed in 1D, a section with a length of approx. 1872 m was considered. On this river reach a database was created with a general plan (topographic survey in Stereo 70), 49 transversal profiles (out of which 37 short profiles framed by the flood defence embankment and respectively, 12 longitudinal profiles that also include the location of the private development, visible in (Fig. 2).

The analysis section of the Crasna River was divided into profiles (49 segments) limited at the ends by 50 cross sections obtained in accordance with the actual topographic surveys, of which a section of automatic linear interpolation (1 segment), respectively, 2 sections upstream and downstream from the road bridge on DJ195B (geometric features are known from the Craidorolț hydrometric station).

Between the two cross-sections was introduced a structure bridge type. The surveyed cross-sections are highlighted in red in the 3D terrain surface representation (Fig. 2). From the current configuration of the natural terrain, originating the spatial points (x, y coordinates, terrain elevation) resulting from the topographic survey - Stereo 70 [1] and the graphic processing of the geometric surface in 3D (analysing different types of procedures in numerical modelling can be seen in detail in the numerical models [7], [8], [10] and [11], respectively, in the technical documentation [13] and [14]), the spatial configuration of the flow range presented in (Fig. 3). The maximum flows for different AEP flood events on the Crasna river, Craidorolț area, at the road crossing bridge location (Craidorolț hydrometric station) are known and have values of: $Q_{5\%}$ = 322 m^3/s and $Q_{1\%}$ = 570 m^3/s.

2. General elements of numerical modelling

2.1 General consideration

The 3D terrain representation is given by satellite graphics of Earth Explorer. This accessible graphic representation is rough, limited to a discrete network of points, most often 30mx30m and at the same time, very difficult to access. A very useful method for graphically processing discrete topographic data known from topographic surveys is presented in documentation [7], [8], [10] and [11]. The method uses a 2D graphical interpolation topographic program, from which a 3D shape surface (shx extension) can then be generated. This surface is then loaded into ArcMAP 9.3 [3], divided by discrete triangular elementary surfaces and resulting in a final 3D spatial shape type TIN (Triangulated Irregular Network).

In order for this spatial form to be recognized by RAS Mapper module (graphics processing or post-processing module in the HEC – RAS 5.07 program [5]), it must be converted into a file with an accessible grid loading form - DTM (Digital Terrain Model).

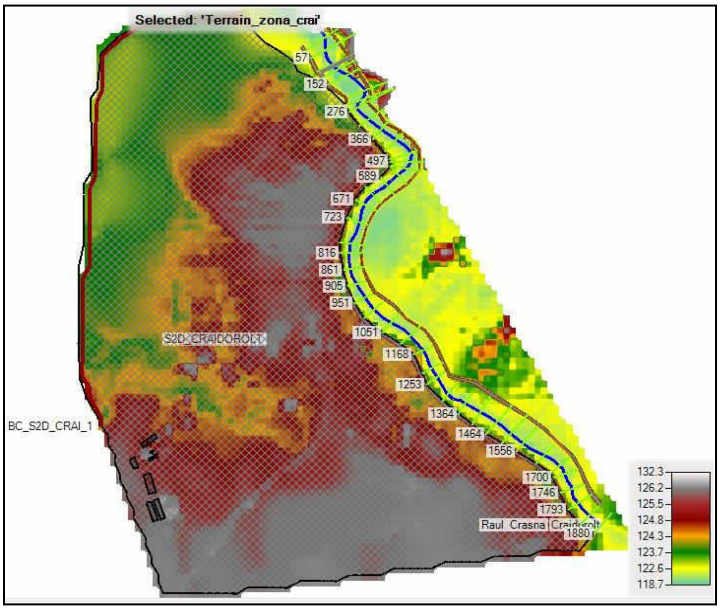

Fig. 3. Numerical model 1D/2D representation: *1D* (*Crasna River*), respectively, *2D* (*2D discretization and lateral structure on left bank* – "*1836*" representation)

A satellite representation example is shown in Fig.3 and was obtained for this paper.

Although these spatial representations are usually based on a small number of points in the topographic survey, they reproduce a real 3D surface quite well.

And yet, this type of model does not faithfully generate the configuration of flood defence embankments, respectively, the configuration of the land below the water level for low return period flood events.

To solve these special issues, within the HEC-RAS program version 5.07, introduced a facility to add a fictitious route through which various corrections can be made to the 3D spatial surface [14]. This route can be a defensive embankment or a watercourse (where successive changes can be introduced on the discrete mode), so that the cross sections below the hydrostatic water level can be updated. In this discrete numerical model these two options were used, and the final discrete surface resulting in the 3D domain has the graphic and visible representation in Fig.3.

2.2 Numerical model 1D/2D build

Documentation "Flood study" [1] includes in the first phase a discrete 1D numerical model where the floodplain area was discretized as a "Polder" with the real contour, which was obtained using the topographic map of Romania (Craidorolț area, Satu Mare county, scale 1 : 25000), and by planning and processing the surfaces given by the elevation curves. Therefore, the correlation between the water level in the polder and the possible cumulated water volume was determined (*Table1*).

The flow transition through 1D domain was done in three stages, as follows:

Stage 1 - Model calibration with 26 May 2015 flood event hydrograph, with peak flow Q_{max}= 146 m^3/s

Stage 2 – Flood event for 5% A.E.P., with a peak flow value of $Q_{5\%}$= 322 m^3/s.

Stage 3 – Flood event for 1% A.E.P., with a peak flow value of $Q_{1\%}$= 570 m^3/s.

Table 1

Nr.crt.	Cotă [mdM]	Suprafața planimetrată [m²]	Suprafața mediată [m²]	Volum acumulat [x10³ m³]
0	**122.25**	1075791.00	–	**0.000**
1	**123.75**	9202968.40	5139380.00	**7709.070**
2	**125.00**	17639613.88	13421291.22	**24485.683**
3	**126.25**	22759503.43	20199558.63	**42026.062**
4	**127.20**	–	–	–

To monitor the discharged flows over the left bank embankment's crest, respectively on the right bank of Crasna River, two lateral artificial structures were considered. The structures are broad crested weir type structures, with a weir flow coefficient md=0.248. The crest configuration of the two artificial structures was determined by topographic surveyed points.

While monitoring the transition flow water volume over the artificial lateral structure on the left bank, (worst case scenario flow $Q_{1\%}$), and the real polder is marked with "Polder at_ 125.00"; the minimum contour of real representation was chosen to visualize the inner water level contour (at approx. elevation level of 125.00 maSL, for the maximum peak flow of $Q_{1\%}$=570 m^3/s). Therefore, graphical characteristic elements were obtained for the maximum water volume reached.

At an additional analysis of the area at the location of the private development, regarding the natural terrain elevation, it was found the existence of a clogged irrigation canal with an elevation level below 124.50 maSL. For this reason, it was chosen a 1D/2D numerical model to replace the polder from stage 3 with a discrete spatial surface. Thus the floodable area of the natural terrain associated with the lateral artificial structure was replaced with a discrete natural surface limited in 2D and marked as "S2D CRAIDOROLT", in HEC-RAS 5.07, illustrated in graphic representation from Fig.3.

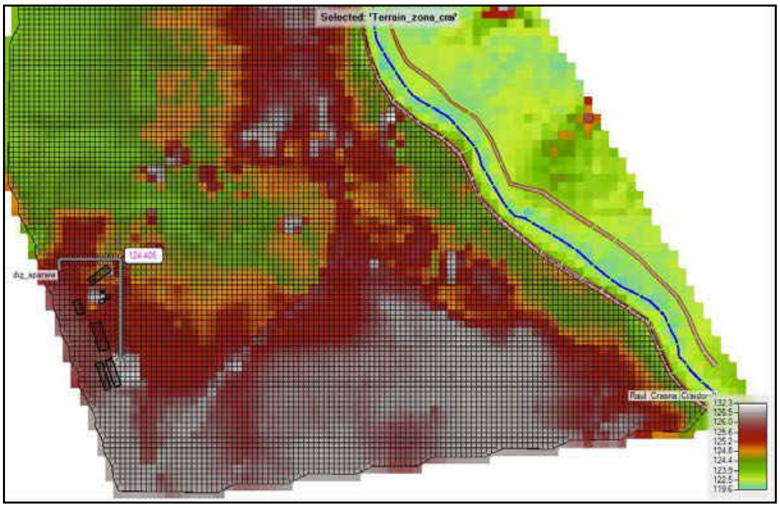

Fig. 4. Detail representation of the additional discretization at the introduced connexion structure (defence embankment) at the northern vicinity of technological platform

Following the actual simulation of this new discrete model and following the graphic processing of the post-processing, the flooding of the platform in the northern area was identified and for protection, additional improvements were made regarding the numerical model described above. Thus, a connection structure was introduced on the northern contour of the technological platform (referred as: dig_aparare) inside the discrete surface" S2D CRAIDOROLT", shown in the graphic representation from Fig.4, as well the development of a breach in the left bank embankment of Crasna River.

The truncated version of the 1D/2D numerical model, required only during McBreach© version 5.07 simulation (used as an external control application), facilitates the probabilistic failure/breach modelling of the embankment through sampling the yield parameters of the predefined statistical distributions and used in the automatic running with HEC-RAS version 5.07 hundreds times using

the Monte Carlo method. Launch of McBreach © version 5.07 [5] mode and automatic coupling with HEC-RAS version 5.07 is illustrated in Fig.5.
The use of probabilistic modelling of the failure of the defense embankment by sampling the parameters of failure of the predefined statistical distributions and associated in automatic running with HEC-RAS version 5.07, can be observed in the representations from the below figures Fig.5 and Fig.6.

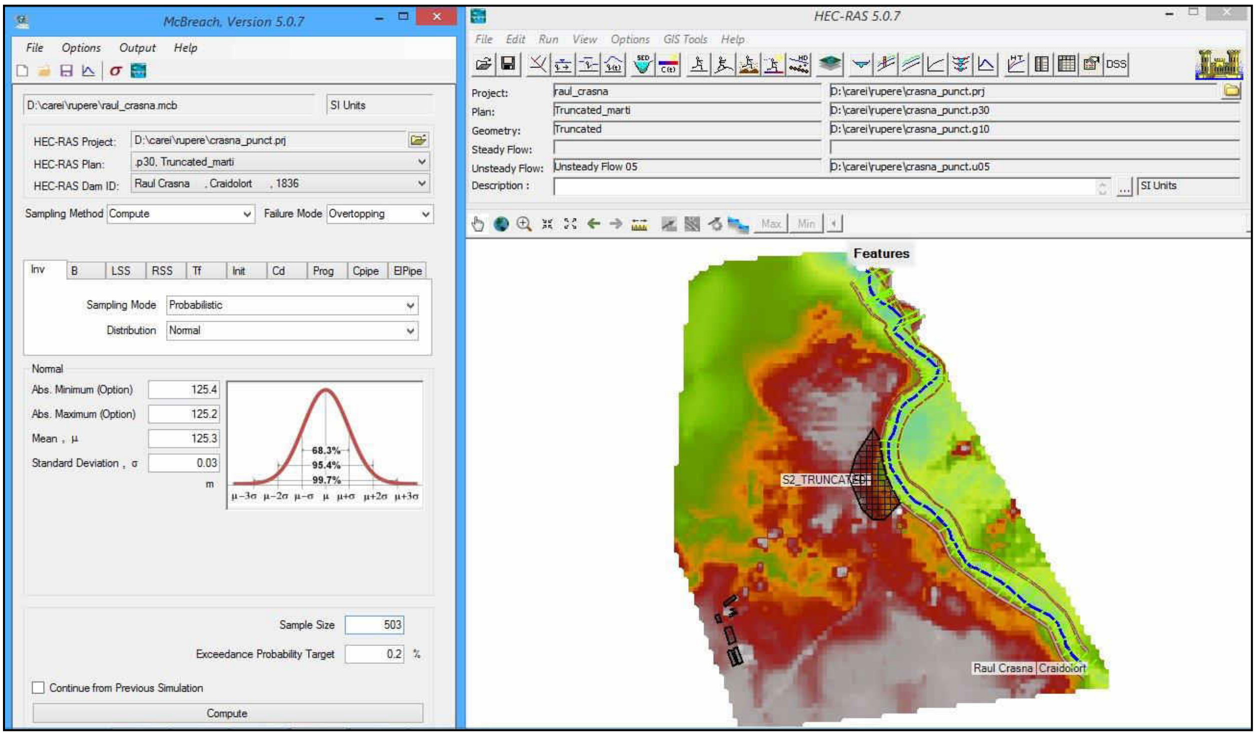

Fig. 5. Numerical model in truncated version of 2D surface and associated with *McBreach © version 5.07*

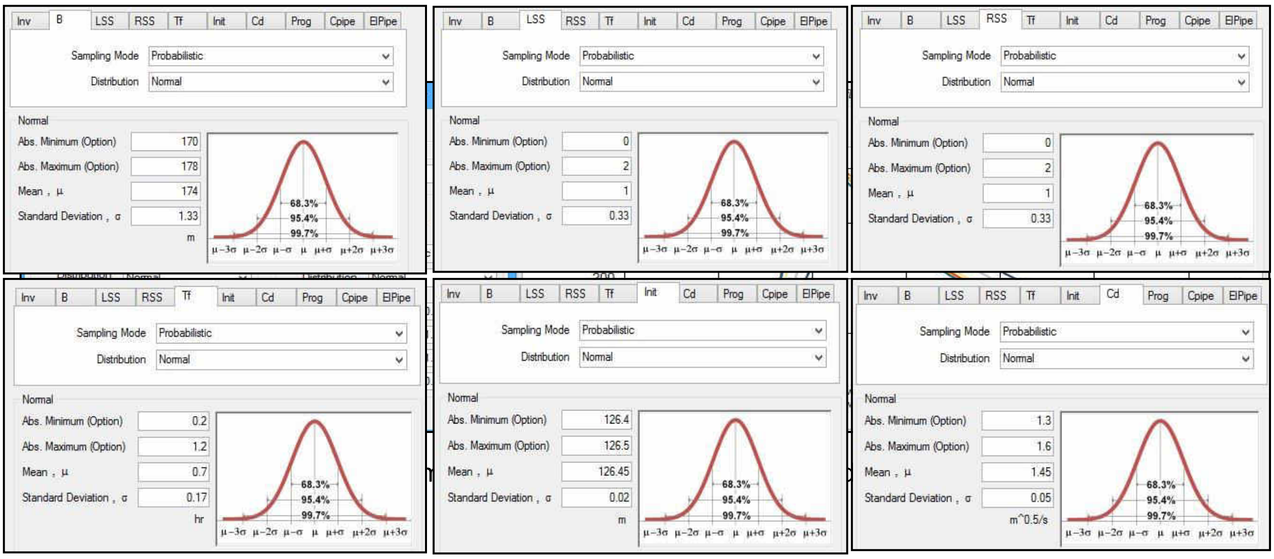

Fig. 6. Sampling elements of predefined statistical distribution failure parameters

In addition to the yield parameters, the user can include the flow hydrograph of the model in the probabilistic analysis by random sampling of the flow hydrograph and scaling factors as seen in the graphical representation shown in Fig.7.

After simulation, the final elements were obtained from sampling the yielding parameters of the statistical distribution (*approx. 11hours*) and are illustrated in the figure below (Fig.8).

Exceedance Probability Breach Parameters

	0.2% User	1%	5%	10%	50%	90%	95%	99%
Realization #	503	503	503	503	501	504	504	504
Peak Discharge, m^3/s	503.39	503.39	503.39	503.39	479.47	80.24	80.24	80.24
Invert El., m	125.4	125.4	125.4	125.4	125.4	125.4	125.4	125.4
Bottom Width, m	172.05	172.05	172.05	172.05	174.11	173.13	173.13	173.13
Left Side Slope, m/m	1.08	1.08	1.08	1.08	1.05	1.03	1.03	1.03
Right Side Slope, m/m	0.71	0.71	0.71	0.71	0.49	0.9	0.9	0.9
Formation Time, hr	0.66	0.66	0.66	0.66	0.75	0.75	0.75	0.75
Initiation, m	126.45	126.45	126.45	126.45	126.47	126.43	126.43	126.43
Discharge Coeff.	1.5	1.5	1.5	1.5	1.5	1.5	1.5	1.5
Progression	Sine	Sine	Sine	Sine	Sine	Sine	Sine	Sine
Failure Mode	Overtopping	Overtopping	Overtopping	Overtopping	Overtopping	Overtopping	Overtopping	Overtopping
Piping Coeff.	1.49907609616348E+76	1.49907609616348E+76	1.49907609616348E+76	1.49907609616348E+76	-3.01200118148214E+76	1.78020108949793E+77	1.78020108949793E+77	1.78020108949793E+77
Initial Piping El., m	6.57040973605107E+76	6.57040973605107E+76	6.57040973605107E+76	6.57040973605107E+76	1.1417227993801E+77	1.69584024369851E+77	1.69584024369851E+77	1.69584024369851E+77
Flow Multiplier	1.01	1.01	1.01	1.01	1.01	1.02	1.02	1.02
Flow Duration Multiplier	1.07	1.07	1.07	1.07	1.06	1.01	1.01	1.01
Peak Inflow Value, m^3/s	573	573	573	573	578	583	583	583

Fig. 8. The yielding parameters of the statistical distribution

2.3 Initial and boundary conditions

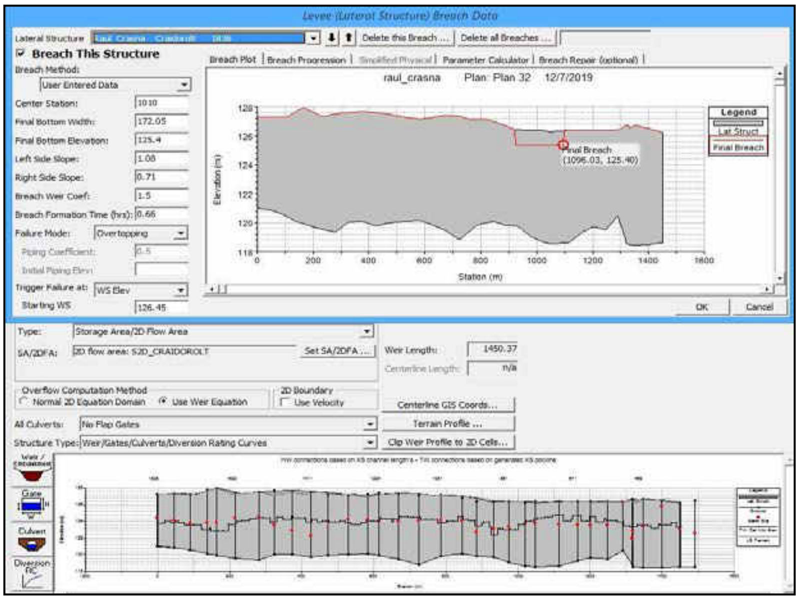

Fig. 9. Uncertainty parameters for left bank breach embankment

From Fig.8 are chosen the parameters with the probability of exceeding of 1 in 100 year (1%), which define the breach from defence embankment on the left bank of the Crasna River, and are then introduced in the discrete numerical model as shown in Fig.9.

Currently, the boundary conditions in the 1D path are given by: the transit flow with a certain probability of exceeding set as an initial flood hydrograph, values that are entered in the upstream section at “1880”, hydrodynamic slope (i=0.0695‰) in the last cross section of the numerical model or rating curve in cross section at “21”, and for the initial conditions the initial inflow values were set in section “1880” (Q=65.98 m^3/s).

For the initial conditions in 2D, the 2D discrete surface (“S2D_CRAIDOROLT”) is associated with the artificial lateral structure from the left bank (1836), respectively setting-up the hydrodynamic slope (i=0.0695‰) as a boundary condition of the 2D discrete surface (“BC_S2D_CRAI_1”). It was chosen the flood flow hydrograph configuration recorded on Crasna River gauge station; and scaled by a numerical coefficient (3.90411) in order to reach the target peak flow value of 570 m^3/s. The numerical simulation of flow transition was set to start from 26th of May 2015 at 6:00 o’clock, and end at 30 of May 2015, hour 18:00. The run simulation has a time step of Δt = 5 seconds, and the output results interval is setup to 5 minutes.

3. Numerical model simulation and results

Following the execution of the actual numerical simulations, all constant or time de-depending parameters were obtained regarding: levels, flow rates and velocities, in all cross sections of the 1D numerical model and on the whole 2D domain (discrete surface referred as “S2D CRAIDOROLT”). Further the 2D domain associated with Crasna river was connected with the artificial lateral structure from the left bank, marked in the new model as "1836"’. The results representation after post-processing in final graphic form on the 1D/2D model in RastMapper, is shown below.

• Plotting the trajectories of the overlapping particles over the level surface (in maSL) – graphical representation at different time steps and with corresponding peak flows values: 27 May 2015, time 15.26.00 → Q=224.97m^3/s; 27 May 2015, time 15.50.00 → Q=258.65m^3/s; 28 May 2015 time 01.57.00 → Q=570.00m^3/s and 29 May 2015, time 09.00.00 → Q=167.75m^3/s – Fig.10;

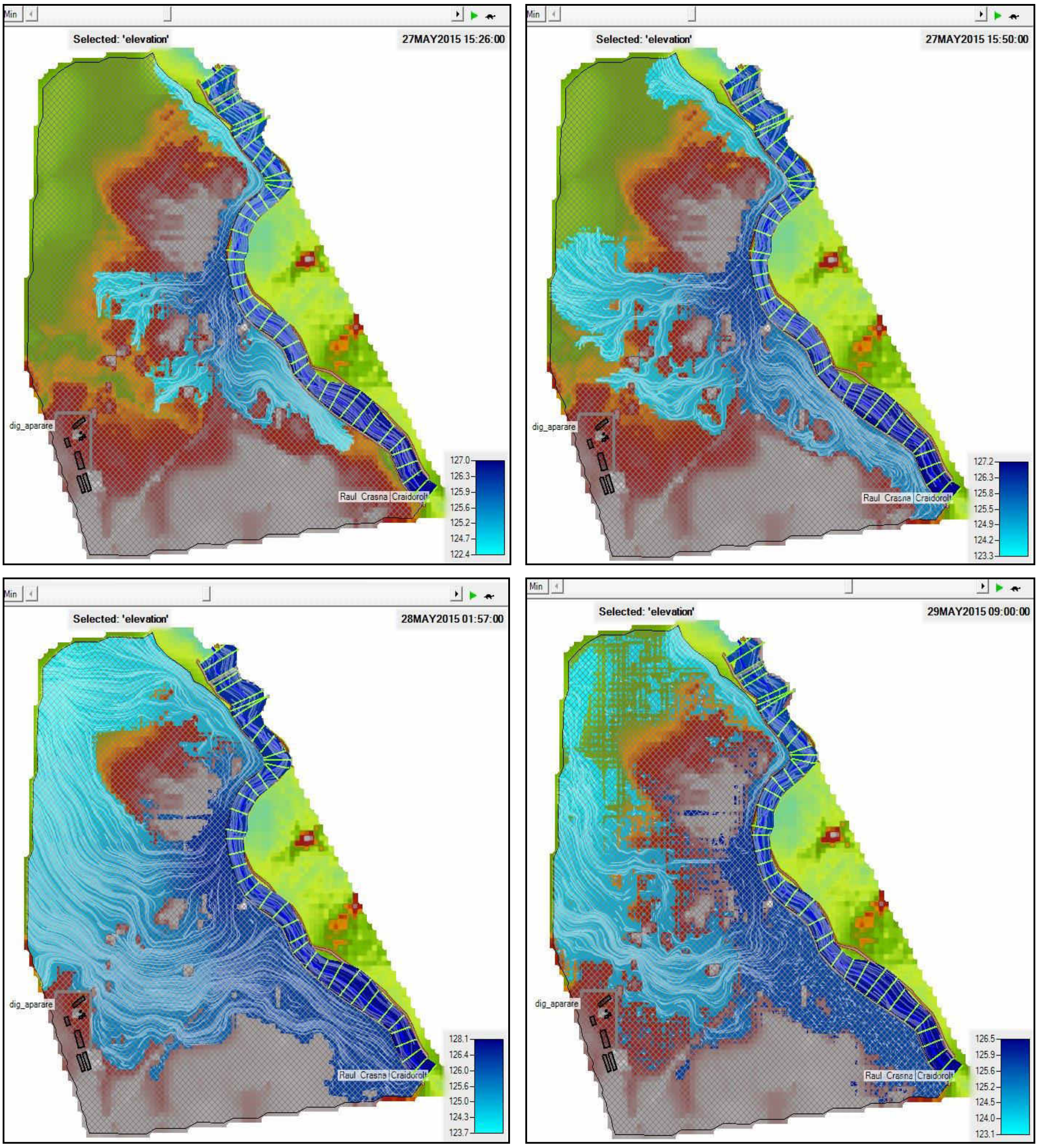

Fig. 10. Surface path draw in 1D/2D model (*maSL*), represented graphic at different time steps 27 of May 2015, time *15.26.00; 27 May 2015 time 15.50.00; 28 May 2015 time 01.57.00 and 29 May 2015 time 09.00.00*

• Water depth variation (m) in 1D/2D model at time step: 28 of May 2015 time 01.00.00, and peak inflow at the entrance Q = 570 m^3/s, respectively, velocity distribution (m/s) from numerical model 1D/2D at time step: 28 May 2015 time 01.01.00 and transitory peak flow at the entrance with a value of Q = 570 m^3/s – Fig.11.

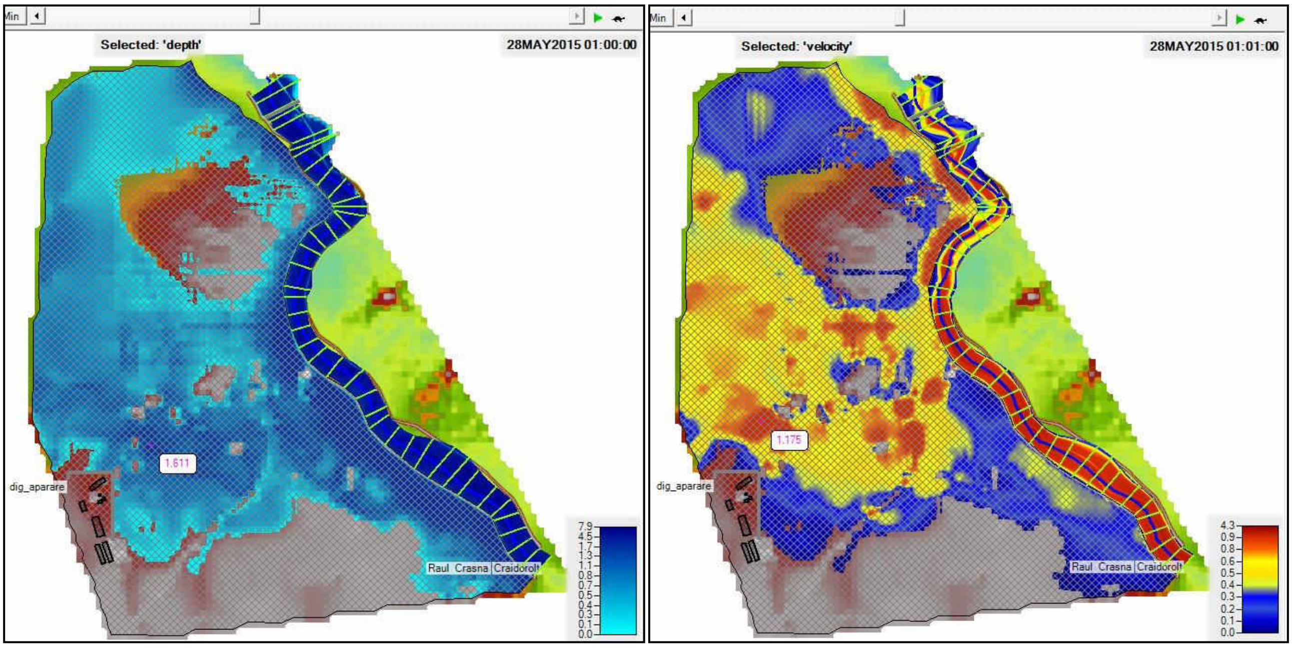

Fig. 11. Water depth variation (*m*), respectively, velocities (*m/s*) – graphic representation in 1D/2D model at time step: *28 Mat 2015 time 01.00.00* and peak flow of *Q = 570 m^3/s*

• Plotting the trajectories of overlapping particles over the level surface (maSL), respectively, the variation of water level in the longitudinal profile by the discrete model 1D and 2D, referred as: "*profil_longitudinal 1D_2D*" (maSL) – graphical representation at time step: *28 of May 2015 at time 1.00 – Fig.12*.

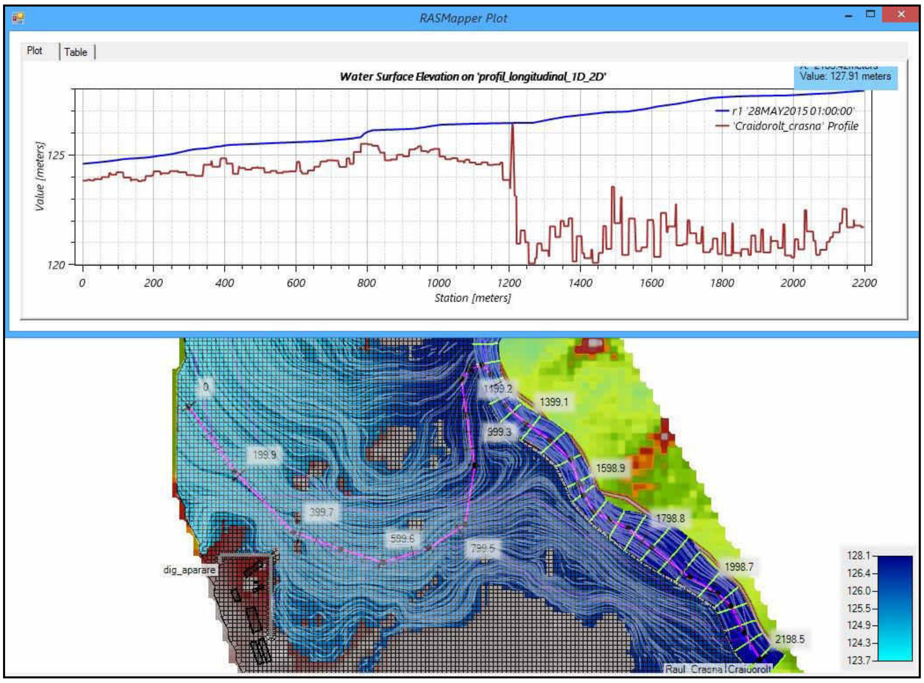

Fig. 12. Surface trajectories draw over the level surface (maSL) and longitudinal section through 1D/2D model – graphic representation at time step: *28 of May 2015 time 01.00.00* and inflow *Q = 570 m^3/s*

• Piezometric line variation (maSL) in longitudinal profile in 1D at time step: 28 May 2015 hour 01.00 and at peak flow value at the entrance section of Q = 570 m^3/s, respectively, the location of the beach in the left bank defence embankment, obtained from sampling the yielding parameters of the statistical distribution (Fig. 13).

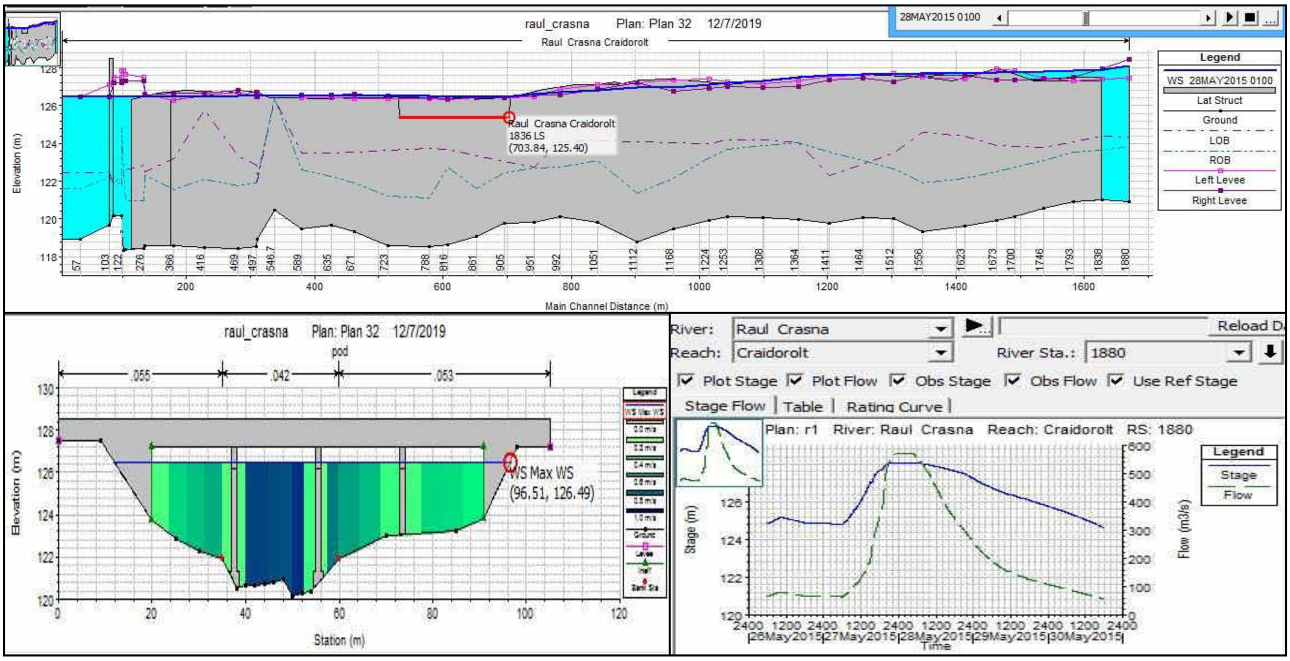

Fig. 13. Piezometric line (maSL) in 1D longitudinal profile – at time: *28 May 2015 hour 01.00*, and graphical breach location in the defence embankment; Maximum water level in section "106.50"; Level and flow hydrographs in the entrance section

Fig.14 illustrates geometric characteristic of the contour flood defence embankment, and the maximum water level reached in the accidental flow transit scenario (125.50 maSL), for the worst case scenario, 1% A.E.P on Crasna River with a peak flow value of $Q_{1\%}$ =570 m^3/s (safety embankment level at 125.60 maSL).

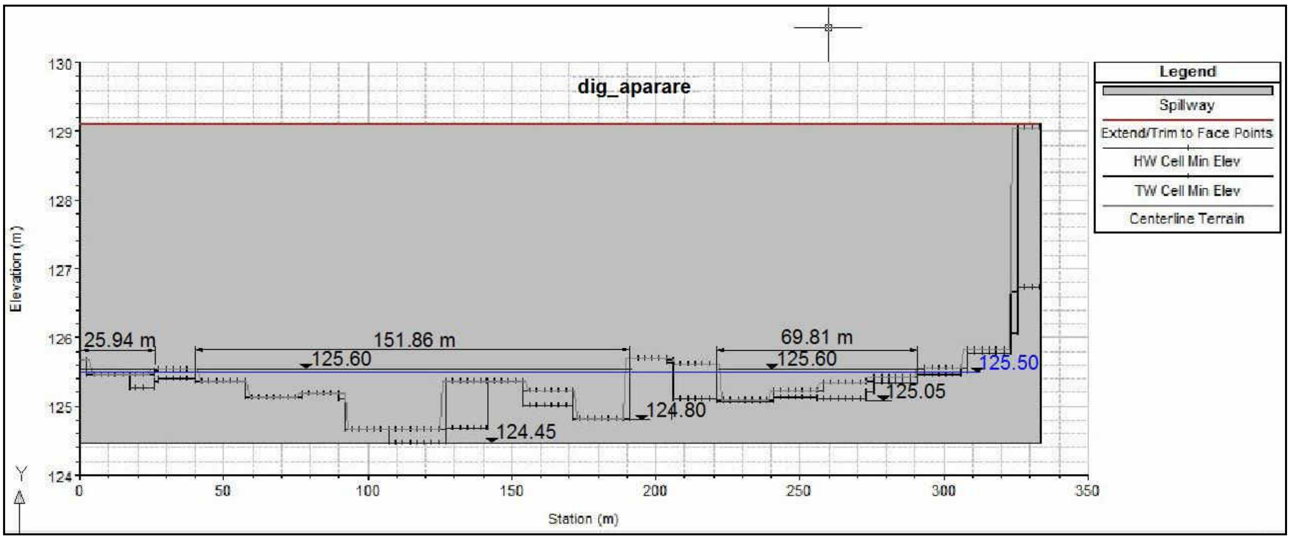

Fig. 14. Contour defence embankment - Longitudinal profile

4. Conclusions

It is observed in this discrete numerical modelling that the water transits through the minor floodplain, the major floodplain and over the defence embankments on the two banks of Crasna river, as well as through the breach developed at the left bank defence embankment. The flow transition starts when the possible transit flow reaches the maximum value for the verification flow with the probability of exceeding 1% (ex. the value $Q_{1\%}$ = 570 m^3/s), on the other hand flooding is not occurring in the private development establishment, at this accidental transition.

In conclusion, in the case in which the embankment on the left bank fails and a breach occurs with a base length of approx. 172.05 m, and in the floodplain a flood protection of the technological enclosure is made by placing a contour defence embankment, it can be said that the platform chosen for the private development is not at risk of flooding when the accidental flood flow transits.

Therefore, the variation of water levels reached in the floodplain area, highlighted and obtained by non-permanent hydraulic calculations (with the HEC-RAS software package version 5.07 in dynamic flow regime, respectively, with the McBreach © version 5.07 program, used as an external control system application that quantifies the uncertainty), reflects the existing situation at the terrain's ground level at the moment of the topographic surveys.

References

[1] ***. *Hydraulic flow modeling on the Crasna watercourse, in the area of the objective - TOPAGRAR farm - Craidolorț locality / Modelarea curgerii hidraulice pe cursul de apă Crasna, în zona obiectivului – ferma TOPAGRAR – localitatea Craidolorț*. Contract no. BC 77/22.07.2019 (UPT).

[2] Brunner, Gary W. *HEC–RAS 4.1, River Analysis System Hydraulic Reference Manual*. US Army Corps of Engineers, November 2002.

[3] ***. *HEC–GeoRAS. GIS Tools for Support of HEC-RAS using ArcGIS*. User's Manual, Version 4.3.93. February 2011, US Army Corps of Engineers Institute for Water Resources Hydrologic Engineering Center.

[4] Brunner, Gary W. *HEC–RAS 5.07 March 2019*. US Army Corps of Engineers.

[5] ***. *Mc Breach by Kleinschmidt, Probabilistic Dam Breach Modeling*. User's Manual, Version 5.07. June 2019, Portland, Oregon.

[6] Brunner, Gary W. *Combined 1D and 2D Modeling with HEC–RAS*, *October, vers.5 2016*. US Army Corps of Engineers.

[7] Ghiţescu, M.A., Gh.I. Lazăr, A.I. Popescu-Buşan, A.T. Constantin, and Ş.V. Nicoară. "Numerical modelling of high water flow transit for a specific river reach." *Scientific Journal of Politehnica University Timişoara, Transactions on Hydrotechnics* 60 (74), no. 2 (2015): 29-36.

[8] Ghițescu, M.A., Gh.I. Lazăr, A.T. Constantin, and Ș.V. Nicoară. "Numerical Model of Transitory Flood Flow in 2005 on River Timiș." Paper presented at World Multidisciplinary Civil Engineering – Architecture – Urban Planning Symposium (WMCAUS), Eco-Friendly Symposium, Prague, Czech Republic, June 12–16, 2017.

[9] Lazăr, Gh.I., Ş.V. Nicoară, A.T. Constantin, and A.I. Popescu-Bușan. "Accidental Overflow Modelling for the Timiş River on Section Şag-Grăniceri - Serbian Border, APRIL 11 – MAY 5." *Scientific Bulletin of "Politehnica" University of Timişoara, Romania, Transactions on Hydrotehnics* 54 (68), no. 2 (2009): 3-12.

[10] Nicoară, Ş.V., Gh.I. Lazăr, and A.T. Constantin. "Computer analysis of water flow transition under existing conditions on a river sector in the range of a bridge structure." *Hidraulica - Magazine of Hydraulics, Pneumatics, Tribology, Ecology, Sensorics, Mechatronics*, no.1 (March 2019): 98-106.

[11] Nicoară, Ş.V., Gh.I. Lazăr, and A.T. Constantin. "Comparative study of a 1D and 2D numerical analysis modelling a water flow at a river confluence under accidental high waters." *Hidraulica - Magazine of Hydraulics, Pneumatics, Tribology, Ecology, Sensorics, Mechatronics,* no. 4 (December 2018): 90-97.

[12] Constantin, A.T., Gh.I. Lazăr, and Ş.V. Nicoară. "2D numerical model of a river sector flow in case of hypothetical side flooding due to embankment failure." *Hidraulica - Magazine of Hydraulics, Pneumatics, Tribology, Ecology, Sensorics, Mechatronics,* no. 1 (March 2019): 57-63.

[13] ***. *HEC-RAS River Analysis System*. Supplemental to HEC- RAS Version 5.0. User's Manual. Version 5.0.4. April 2018. US Army Corps of Engineers.

[14] Kiers, Gerrit. *Lifting Terrain in HEC-RAS 5.0*. VIZITERV Consult Kft., Hungary, Copyright © The RAS Solution and Gerrit Kiers, 2015.

Examining Centrifugal Pump BKS300 on Cavitation

Assist. Prof. **Nikolett FECSER[1],** Senior Lecturer in Fluid Mechanics and Computational Eng. **Könözsy LÁSZLÓ[2],** Graduate Student **Nicolas LEDOS[3],** Senior Seal System Project and Standardization Eng. **Balázs SÁRA[4]**

[1] Széchenyi István University, Department of Automation, H-9026 1 Egyetem tér, Győr, fecser.nikolett@sze.hu

[2] Centre for Computational Engineering Sciences, Cranfield University, Cranfield, Bedfordshire, MK43 0AL, United Kingdom, laszlo.konozsy@cranfield.ac.uk

[3] Centre for Computational Engineering Sciences, Cranfield University, Cranfield, Bedfordshire, MK43 0AL, United Kingdom, nicolas.ledos@cranfield.ac.uk

[4] FLOWSERVE HUNGARY SERVICE, H-1097 6/b Gubacsi út, Budapest, bsara@flowserve.com

* fecser.nikolett@szehu

Abstract: *Pumps influence all our lives directly or indirectly. Pumps are one of the most widespread types of turbomachines. Their task is to pump fluid from one place to another and engineers who are experts in pump technologies are familiar with the phenomenon of cavitation. The present work focuses on the cavitation from an experimental point-of-view. Measurements have been carried out on the type of a centrifugal pump. A polynomial fitting method has been developed and a semi-empirical formula has been proposed. Furthermore, numerical simulations have been performed for modelling two-phase cavitating turbulent flows in the investigated centrifugal pump. The objective of this study is to bring attention to cavitation and contribute to the knowledge in terms of its harmful effects.*

Keywords: *Pumps, fluid, cavitation, measurement, centrifugal pump*

1. Introduction

The advantages of measuring the noise and oscillation levels in cavitation is that during noise measurement no modification is required on the hydro-plant, and it also provides information about cavitation developed in places hardly or not available at all for visual observations. By measuring noise, the type of cavitation and whether its effect is damaging or not can be identified [1].
Hungarian researchers have dealt with the phenomenon of cavitation in-depth since the 1960s. Sebestyén and Varga carried out cavitation measurements with hydrofoils of variable pitch angles. They determined the Strouhal number of the cyclical cavitation flow behind the cylinder over critical Reynolds numbers [2].
A measuring technological method was developed to examine cavitation noises at discrete frequency. Sebestyén and Varga have also carried out experiments on the cavitation erosion rates. They concluded that the cavitation number at noise peak equals to the cavitation number at the erosion peak. The research results of Fáy in cavitation scale effect were employed in the standardisation process by the International Electrotechnical Commission. The value of noise level was measured at a given frequency, they were illustrated along with the cavitation number, then from the curves presenting noise levels he concluded the different phases of the development of cavitation [3].
Sebestyén and Varga (1970) recorded their results of the experiments related to the cavitation bubbles formed behind cylinders of various diameters, wedges of different pitch angles and the hydrofoils of variable pitch angles and cavitation erosion on films. The video film recorded by Sebestyén and Varga was digitalised by Könözsy, 1999 [4].

2. Several types of cavitation

Transient cavitation bubble (travelling) are: those bubbles which are taken away by the flow. Quasi-stationary cavitation bubbles (fix): appear adhered to a solid object - for example at a fix place of a pump impeller.
Layer cavitation: is the thin headspace - independent from the concentration of the cavitation nuclei - of a quite uniform thickness created from the mass of the bubbles and adhered to the surface.
Cloud cavitation: a special type of bubble cavitation. It is the cloud of small, spherical bubbles with higher vapour concentration of nuclei, which depends on the viscosity of the flowing medium and the effects of turbulence.
Physical cavitation: a smaller type of cavitation occurs under normal operational conditions in holes or due to detachments caused by collision. Its effects can be tracked down by noise and smaller erosive dissolutions. The effects are undetectable in the pump characteristic curves and do not cause reduction in transfer or a decline in efficiency.
Mechanical cavitation: causes "detachments" in the pump characteristic curves and the operation of the pump becomes chaotic.
Supercavitation (blocking state): supercavitation is a long stable cavitation bubble in the measurement area of the cavitation channel developing when a small number of cavitation occur and the implosion of cavitation bubbles fails in the flow [5].

3. The venue of the measuring process

Ganz Works have a long history in producing pumps. Their results in the field are both well-known and internationally recognised. It should be noted here that among the authors of the related literature there is István Józsa, who was one of the key technical experts at Ganz. In order to meet the strict international requirements and the specific needs - like pumps for nuclear power plants, it was necessary to use appropriate methods for measuring the characteristics and quality of their products. The first author of this work had the opportunity to join a cavitation measurement led by Balázs Sára, who is the designer of the system carrying out cavitation measurements.
The hydro-plants of Ganz Works have studs with 200-2500 mm in diameter and fully exploit the potentials of the revolution range. Mostly irrigation pumps, heat pumps used in power plants and smaller/medium turbines are manufactured. Over the years the performance of the units has increased. The market has also had a demand for machines with higher and higher revolution. Without running trial tests, the delivery of large size machines or the ones transported into remote countries posed a serious risk. To avoid such problems, the first hydro-plant test stations were created and later on constantly developed. The problem of enhancing performance was solved with building a new test station in 1990. To measure cavitation, you can use open and closed test loops. The open test loop of Ganz' trial station is marked among the largest ones in Central Europe.
Before delivery, all the machines not exceeding the measurement thresholds of the trial station are tested. Whereas the types of tests that can be carried out in the trial station are limited since, due to the size of the machine, some equipment cannot be built at the trial station, they are normally assembled on site. The model test method was created to be able to carry out tests on such large-sized machines. In such cases a smaller replica of the original large-sized machine is built with the same rheorological and geometric features. This model serves the basis for analysing the characteristic curves; and the results obtained are used at the process of designing the product, handing it over to the costumer and verifying warranty information of the final life-size machine.
The full range of the characteristic curve can be measured on the model built into the test loop in the hydro-plant laboratory. The model machine itself cannot be too small - with usually a power of 50-100 kW; its minimum size and the method of the measurement are determined by international standards. Although flow sections play an important role, the most important factor is the proportional reduction of the elements essential in energy conversion (impeller, spiral case, guide vanes, stay vanes, suction tube). The diameters of the model's impellers on suction side are normally between 150 - 400 mm, while the range of reduction - depending on the size of the real machine to be built - is between 1:2 – 1:8.

Over the recent years, the types of devices applied for examining models have been further enriched due to the development of computer aided modelling and simulation, which allows a wide scope of flexible and quick tests to be done. They are used for comparing the various versions, in particular during the preliminary phase carrying out approximation tests. For the delivery of largemachines and accurate efficiency and cavitation tests small sample tests and the conventional model measurement technique are used [6].

3.1 The main measurement devices of the hydro-plant laboratory

In the Ganz hydro-plant laboratory there is a closed test loop.
The main elements of closed test loops:

- Model pump
- Circulator
- Choke valve
- Devices for basic quantities
- Variable frequency drives
- Pressure-suction control

1. Measurement of the Amount of Delivered Water
Figure 1 shows the measurement pattern of the induction flow meter.

Fig. 1. Measurement of the Amount of Delivered Water

The principle of the measurement is that a winding creates strong and homogenous magnetic field in the transverse direction to the flowing. Meanwhile, in the water as an electric conductor, voltage evokes perpendicular to it. On the inner surface two electrodes are positioned and the evoked voltage between them is the measurement signal. This electrical signal is used for measuring flow rate. The flow must be homogeneous and vortex free, which can be achieved by applying a prolonged straight pipe, a rectifying grid and a confusor built into the initial part of the pipe.

2. Measuring shaft torque
A so called torque disk is used to measure the performance going through the shaft in a closed test loop. Its measurement principle is that under the influence of the torque, the measuring device in the disc is deformed flexibly and under the principle of strain gauge it is transformed into change of resistance. Finally, the change of resistance is transformed into a bridge voltage signal. The bridge on the revolving disc has to have supply voltage and the output signals to be received. This was implemented through using contactless signal transmission. The photo illustrates the measurement disc. The outer black ring contains the antenna and the receiver, which receives the measurement signals transmitted by the revolving part. The measurement limit of the torque disk is 1 kNm. To avoid measuring false torques, they are connected to the motor with a flexible coupling.
Figure 2 shows the torque disk.

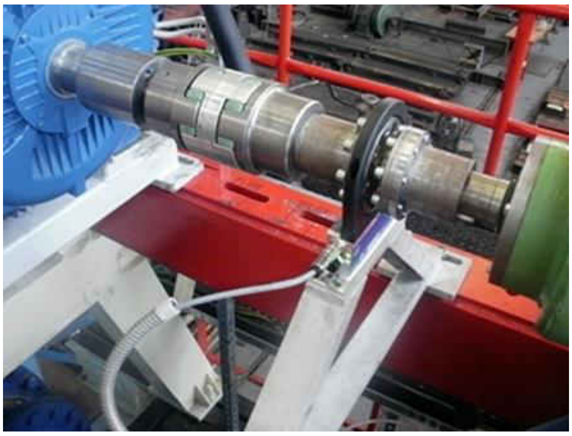

Fig. 2. The torque disk

3. Measuring pressure
Pressure is measured at three positions:
- Intake pressure
- Differential pressure:
- Atmospheric pressure

The measurement principle of the different types of pressure is similar to the one measuring the torque. The pressure deforms a flexible element, such as a membrane or an object made of silicon, and this deformation is converted into a resistance signal, which is accurately measurable under the principle of bridge-measurement. The picture shows that Psz pressure on the suction side affects on the pipe on the right, while Pny pressure on the discharge sideaffects on the pipe on the left. The differential pressure gauge is their difference and the head is gained from its signal. The absolute pressure gauge placed into the middle measures the pressure on the suction side, and the pressure needed for calculating the cavitation coefficient (NPSH) is gained from it. The pressure gauge on the left is especially designed to be able to carry out the accurate measurement of the atmospheric pressure. The measured value is also needed for calculating NPSH.

4. Revolution gauge
Measuring revolution means the counting of impulses per time unit. In the closed apparatus an incremental encoder made by Baumer is attached to the end of the motor shaft and it emits 4096 signals per revolution. The signals are counted by the computer and analyzes the revolution per minute. This signaller is positioned under the case of the motor; therefore it is invisible from outside. In the open system, mainly the optical revolution counter is the best device. The pump units measured here are varied. Generally, there is a revolving element (coupling, axle stud) the reflective markings can be sticked to or painted on. The sign is lit by the trip meter; the counter counts the reflected impulses or the period time and displays the revolution per minute.

5. Pressure regulation and cavitation measurement
In the illustration the opened scheme of the closed test loop and its pressure line can be seen. The pressure line is determined by defining one of its points. A tank including an air cushion is attached at point „A”. The pressure of the air cushion is kept constant by a controller. Decreasing the pressure of the air cushion step-by-step makes the pressure line sink accordingly. The operating point of the pump is unchanged until the pressure on the suction side (more precisely NPSH, net positive suction head) approaches the critical value. Then the pump cavitates and its head decreases. In general, the pressure is decreased in 8-10 steps to find the breakdown point. This is called cavitation measurement.

6. Pressure regulator
The figure below illustrates the conceptual operational model of the pressure regulator. The regulator has a strong and moderate function. The strong one is for carrying out large pressure changes rapidly. The moderate one is used after finishing the strong phase and only some refining is needed. Both moderate and strong functions control between 0.2 bar abs vacuum and 2 bar abs compressed air pressure. The strong function actuates valves with ON/OFF switches. The moderate function alters the opening of small size valves. The vacuum is provided by a water ring air pump, while the compressed air comes from the air network of the factory. The regulator system is assembled from FESTO elements. When filling up the system, special attention is needed in order to keep the air cushion up and water not to get into the FESTO system. Thus, it is equipped with a diaphragm valve on the top of the tank on the suction side.

3.2 Presenting measurement results

Table 1 shows readings.

Table 1: Readings [7]

No.	Readings									
	t	n	Q_m	Z_m	p_{m1}	p_{m1}	P_e	Tw	Ta	η_m
	h/min	rpm	m^3/h	m	kPa	kPa	kW	° C	° C	%
1	10:03	1491	1300	-0.095	138.9	584.4	207.9	21.9	24.1	93.0
2	10:12	1491	1300	-0.095	46.9	494.1	207.5	21.9	24.1	93.0
3	10:17	1492	1303	-0.095	5.6	452.7	207.9	21.9	24.1	93.0
4	10:21	1491	1301	-0.095	-35.0	412.2	207.8	21.9	24.1	93.0
5	10:27	1492	1300	-0.095	-39.8	406.8	207.8	21.9	24.1	93.0
6	10:32	1492	1300	-0.095	-47.8	392.3	207.8	21.9	24.1	93.0
7	10:40	1491	1300	-0.095	-53.7	382.5	206.7	21.9	24.1	93.0
8	10:51	1491	1300	-0.095	-57.7	365.6	205.7	21.9	24.1	93.0
9	11:04	1491	1300	-0.095	-61.7	333.2	201.8	21.9	24.1	93.0
10	11:10	1491	1302	-0.095	-62.5	262.3	188.4	21.9	24.1	93.0

Table 2 shows calculated values.

Table 2: Calculated values [7]

No.	Calculated values									
	ϱ_w	p_s	Q_c	v_{m1}	v_{m2}	H_c	Δh_c	P_m	P_{agg}	η_p
	kg/m^3	Pa	m^3/s	m/s	m/s	[m]	[m]	[kW]	[kW]	[%]
1	997.7	2642	0.3611	5.1087	5.1087	44.5	23.4	193.3	207.9	81.4
2	997.7	2642	0.3611	5.1087	5.1087	44.7	14.0	193.0	207.5	81.9
3	997.7	2642	0.3619	5.1205	5.1205	44.7	9.7	193.3	207.9	81.9
4	997.7	2642	0.3614	5.1126	5.1126	44.7	5.6	193.3	207.8	819
5	997.7	2642	0.3611	5.1087	5.1087	44.7	5.1	193.3	207.8	81.7
6	997.7	2642	0.3611	5.1087	5.1087	44.0	4.3	193.3	207.8	80.5
7	997.7	2642	0.3611	5.1087	5.1087	43.6	3.7	192.2	206.7	80.2
8	997.7	2642	0.3611	5.1087	5.1087	42.3	3.3	191.3	205.7	78.1
9	997.7	2642	0.3611	5.1087	5.1087	39.4	2.9	187.7	201.8	74.2
10	997.7	2642	0.3617	5.1165	5.1165	32.2	2.8	175.2	188.4	65.1

Table 3 shows converted values.

Table 3: Converted values [7]

No.	Converted values			
	H	**Δh**	**Q**	**P**
1	44.2	23.2	1294.8	191.0
2	44.4	13.8	1294.8	190.7
3	44.3	9.6	1269.9	190.6
4	44.4	5.5	1295.8	190.9
5	44.2	5.0	1293.9	190.5
6	43.6	4.2	1293.9	190.5
7	43.2	3.6	1294.8	189.9
8	41.9	3.2	1294.8	189.0
9	39.1	2.8	1294.8	185.4
10	32.0	2.8	1296.8	173.1

4. Determination of polynomial equation for centrifugal pump

Most of the semi-empirical formulas required for NPSH diagrams are not available in the literature on processed cavitation. First, we developed a polynomial fitting method and after we proposed a semi-empirical formula that can be used in engineering practice. Semi-empirical formulas are polynomials that are generated by fitting a polynomial to a measured dataset which can easily be employed in engineering practice, because the polynomial can produce an accurate agreement with the measured dataset. Semi-empirical formula provides a more accurate analytical representation of the H-NPSH curve based on measurement points. A MATLAB code has been developed for polynomial fitting to produce a semi-empirical formula relying on the experimental data as

$$y(x) = a_0 - a_1 \cdot x + a_2 \cdot x^2 - a_3 \cdot x^3 + a_4 \cdot x^4 - a_5 \cdot x^5 + a_6 \cdot x^6 - a_7 \cdot x^7 \quad (1)$$

Table 4 shows the coefficients of the proposed semi-empirical equation.

Table 4: The coefficients of the proposed semi-empirical equation

The sign of a coefficient	Value of Coefficient
a_0	0.000001
a_1	0.000071
a_2	0.001786
a_3	0.022991
a_4	0.164923
a_5	0.666180
a_6	1.416480
a_7	1.189720

Figure 3 shows the fitting of a seventh-degree polynomial on the measured dataset.

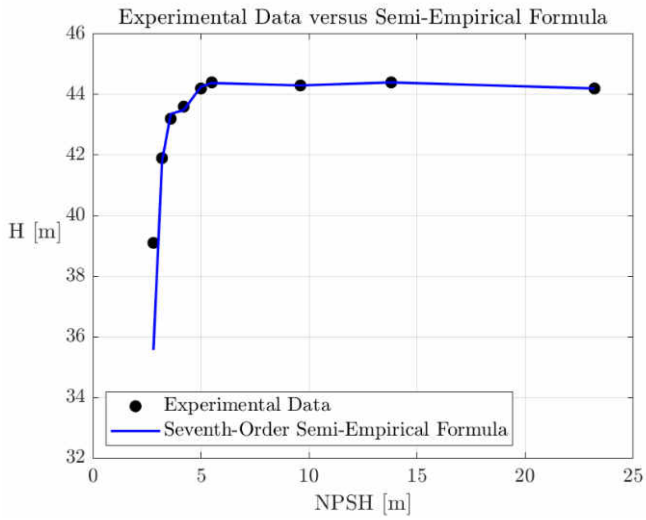

Fig. 3. Fitting of a seventh-degree polynomial on the measured dataset

Third, quarter, etc. degree polynomials can also be fitted to our data. I fitted a seventh-degree polynomial to the data of my measurement. However, for higher polynomials we need to be careful because our shape matrix will be poorly conditioned, and our solution will be uncertain. The polynomial fit perfectly to my measurement points, but oscillation occurred between the measurement points.

5. A computational model for modelling cavitation

The simulation of the two-phase cavitation turbulent flow was performed on the given geometry using 17,810,808 computational cells using a finite volume discretization method using the ANSYS-FLUENT v19.1 software package. The two-phase turbulent flow has been simulated by using the k-epsilon Realizable turbulence model and taking into account a standard wall function. In the two-phase flow, the primary phase was the liquid phase (density: 1000kg/m3, dynamic viscosity factor: 0.001 Pas) and the secondary phase was the vapor phase (density: 0.02558 kg /m3, dynamic viscosity factor: 1.26 * 10e-6 Pas).The resistance factor was calculated with the Schiller-Naumann relationship and the cavitation flow was simulated with the Schnerr-Sauer model. The reference pressure was determined from the measurements, which was 115,500 Pa. The resistance factor was calculated with the Schiller-Naumann relationship and the cavitation flow was simulated with the Schnerr-Sauer model. The reference pressure was determined from the measurements, which was 115,500 Pa. The computational time was two days using 64 processors (CPUs) and the simulations have been performed by using the High-Performance Computing (HPC) facility at Cranfield University, in the UK. These simulation conditions were taken into account in the construction of the data system for the final results during the simulation of the two-phase turbulent cavitation flow. The results were evaluated using the CFD-Post software package. Figure 4 shows the value of fluid velocity on impeller.

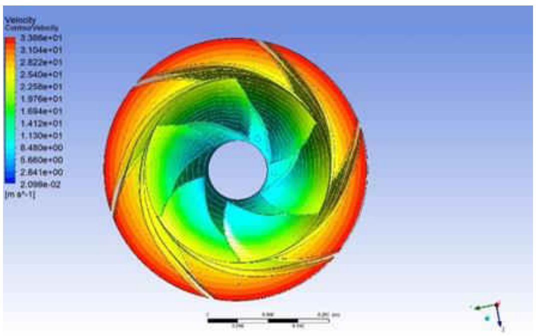

Fig. 4. The value of fluid velocity on impeller

Figure 5 shows the value of fluid velocity on impeller.

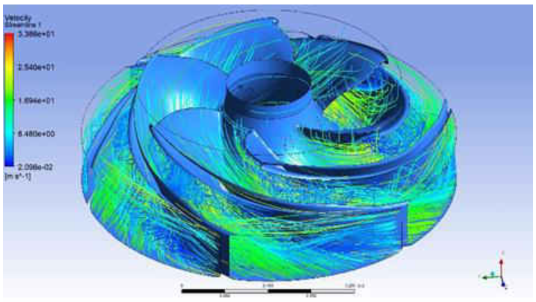

Fig. 5. The value of fluid velocity on impeller

Figure 6 shows the value of the fluid pressure on the impeller

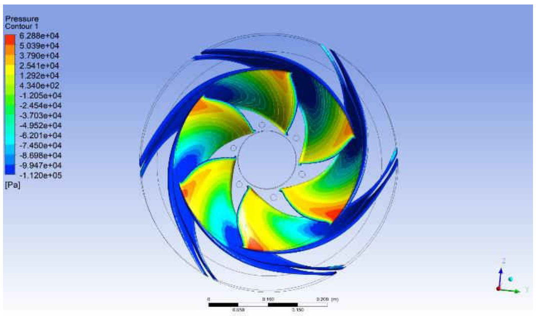

Fig. 6. The value of the fluid pressure on the impeller

The fluid velocity is 2.25 m/s at the inlet edge of the impeller, 5.66 m/s on the suction side of the impeller and 8.48 m/s onthe impeller side. On the suction and discharge sides the measured values were around 5.12 m/s, which shows that the simulation is close to the measured values. The pressure at the impeller leading edge is 25.41 kPa, the suction side suction side is -62.01 kPa and the impeller pressure is 112 kPa. On the suction side -61.7 kPa, on the suction side 333.2 kPa the measured value shows that the simulation is close to the measured value.

6. Conclusions

For the sake of safe operation of pumps, it is essential to investigate the operation parameters, because cavitation could lead to a pump failure. The present work was intended to contribute to the establishment of safe operation of pumps.
In the laboratory of Ganz, the most important parameters of a centrifugal pump have been experimentally studied. A MATLAB code has been developed within a research collaboration with Cranfield University to be able to generate a semi-empirical relationship for the characteristics curves of the pump studied at Ganz. With some modifications to the coefficients of the proposed semi-empirical equation, the contribution of the present work can also be used for other types of centrifugal pumps. Considering the constraints of polynomial fitting, we defined an exponential function to obtain the curve of the measured data. Relying on the measurements conducted, numerical simulations have been performed considering a two-phase turbulent flow which can be used to determine the cavitation processes and their effects on the investigated pump.
Within the research work presented here, we approached several companies and received information that simulation is only used in practice in the case of a machine failure. Therefore, it would be recommended to use simulation techniques in conjunction with measurements at the end of the production. As a consequence of that, it would be beneficial for the future development and for filtering out the dangerous structural elements of an already manufactured pump.

References

[1] Sebestyén, Gy. *Investigation of cavitation flows* / *A kavitációs áramlások vizsgálata*. Manuscript. Budapest University of Technology, Department of Water Machines, 1993, pp.1-23.
[2] Varga, J., and Gy. Sebestyén. Cavitation-film. ASME Cav. Forum, ASME Film Library, shown also in Fluid Machinery Conferences Budapest, 1970.
[3] Varga, J., Gy. Sebestyén, and Á. Fáy. *Some practical applications of cavitation noise testing* / *A kavitáció zajvizsgálatának néhány gyakorlati alkalmazása*. 1969.
[4] Könözsy, L. Cavitation-film (mpg), digital format CD-ROM. University of Miskolc, Department of Flow and Thermal Engineering / Miskolci Egyetem, Áramlás- és Hőtechnikai Gépek Tanszéke. Budapest University of Technology, Department of Water Machines, 1999.
[5] Józsa, I. *Vortex pumps in practice* / *Örvényszivattyúk a gyakorlatban*. Budapest, Invest-Marketing Bt., 2013, pp. 10-128.
[6] Zombor, Cs., and M. Gózon. *New measuring equipment for the development of Ganz water machines* / *Új mérőberendezés a Ganz vízgépeinek fejlesztésére*. Budapest, Technical Publications Editorial Office / Műszaki Kiadványok Szerkesztősége, 2013.
[7] Fecser, N., B. Sára, and R. Kuti. “Examining Centrifugal Pump on Cavitation.” *Magazine of Hydraulics, Pneumatics, Tribology, Ecology, Sensorics, Mechatronics*, no. 4 (December 2019): 6-12.

ISSN 1453 – 7303 **"HIDRAULICA" (No. 3/2020)**
Magazine *of Hydraulics, Pneumatics, Tribology, Ecology, Sensorics, Mechatronics*

About the Contribution of Forest and Aquatic Ecosystems within Protected Areas to the Sustainable Development of Local Communities

PhD. eng. inf. **Bogdan-Vasile CIORUȚA**[1,2*], Lecturer dr. eng. habil. **Mirela COMAN**[3,4], MA eng. **Andrei Nicolae HELINDIAN**[3,5]

[1] Office of Informatics, Technical University of Cluj-Napoca - North University Centre of Baia Mare, 62A Victor Babeș Str., 430083, Baia Mare, Romania

[2] Faculty of Applied Sciences from Bucharest, Politehnica University of Bucharest, 313 Splaiul Independenței, 060042, Bucharest, Romania

[3] Faculty of Engineering, Technical University of Cluj-Napoca - North University Centre of Baia Mare, 62A Victor Babeș Str., 430083, Baia Mare, Romania

[4] Faculty of Agriculture, University of Agricultural Sciences and Veterinary Medicine from Cluj-Napoca, 3-5 Calea Mănăștur, 400372, Cluj-Napoca, Romania

[5] Faculty of Environmental Protection, University of Oradea, 26 Gen. Magheru, Oradea, Romania

* Corresponding author's e-mail address: bogdan.cioruta@staff.utcluj.ro

Abstract: *The EU's vision for 2050 is to properly protect, enhance and restore biodiversity and ecosystem services provided by protected natural areas, considering the intrinsic value of biodiversity and the essential contribution of ecosystem services to human well-being and economic prosperity of the local community. Starting from this desideratum, through this paper we aimed to show that forest ecosystems, as well as aquatic ones, have an important role in the sustainable development of local communities if their contribution is properly assessed. We also want to emphasize that a 'beneficiary pays' policy is much better perceived and adopted among local communities, as opposed to a 'polluter pays' policy, moving from environmentally friendly to protective actions making it much easier.*

Keywords: *Biodiversity, community development, ecosystem services, natural heritage, sustainability.*

1. Introduction

Protected areas in Romania offer a wide range of ecosystem services, such as regulation and support services (water quality control, flood control, erosion control, regulation of nutrient and toxic substances content, maintaining biodiversity), cultural services (leisure activities, tourism, provision of aesthetic, educational and scientific resources), as well as production services (wood resources, non-wood resources, drinking water resources) [1,2]. They can be particularly important for local economic development, thus helping to attract investment funds and providing an important direct or indirect source of employment, both locally and regionally.
This paper aims to present some of the benefits of two groups of ecosystem services in a protected area in Romania - Maramureș Mountains Natural Park (MMNP), as well as the mechanisms that can support their provision. The results of the studies can be replicated nationally and internationally and used to raise awareness among decision-makers about the importance of protected areas for the economy and well-being of local communities.

2. Methodology

The documentation for this paper was based on the authors' concerns for ecological education and environmental protection [3,4], and the idea that a community can only develop harmoniously through care for protected areas and the biodiversity that populates them [5,6]. With a range of highly relevant studies at the national level, both in terms of protected area management [2,7-10] and some reports on the potential and benefits of forest and aquatic ecosystems, the authors decided to extrapolate the respective approaches on the relatively limited space of the protected natural areas, presenting as a case study the situation regarding the ecosystem in the Maramureș Mountains Natural Park.

3. Results and discussion

3.1 Ecosystems in protected natural areas and associated ecosystem services

Ecosystem services are flows of materials, energy, and information from natural capital stocks that combine with the services of manufactured and human capital to produce human well-being [1]. There are of course three perceptual perspectives on what ecosystem services involve, namely:

- processes by which the environment produces resources that are considered free by humans, such as clean water, timber, pollination, etc.
- the benefits that people get from nature.
- components of nature consumed or used directly to produce human well-being.

According to the literature [1,11], ecosystem services are divided, as follows, into the following categories, namely:

- production services are provided by the ability of ecosystems to provide various resources, such as food, wood, fuel, drinking water, etc.
- regulation and maintenance services are determined by the ability of ecosystems to control natural processes - regulation of climate, water quality and quantity, soil formation, control of diseases and pests, habitat maintenance, etc.
- cultural services result from physical, intellectual, spiritual, and symbolic interactions with the components of natural capital, in which case we discuss the aesthetic value of the landscape as a space for recreation.

In this sense, the provision of ecosystem services is achieved by combining natural capital with anthropogenic, but taking into account the Management Plan of protected areas, as well as the specific activities allowed in the three areas related to them, namely:

- Integral Protection Zone (IPZ) - human activities are prohibited, except for traditional grazing activities, research activities, education, and ecotourism;
- Buffer Zone or Sustainable Management Zone (SMZ) - which is the transition zone between the Integral Protection Zone and the Sustainable Development Zone;
- Sustainable Development Zone (SDZ) - which includes the built-up areas of the localities in the park, the areas occupied by permanent communication routes, mountain pastures outside the integral protection area, as well as areas outside the built-up areas of localities that have undergone anthropogenic changes.

3.2 Maramureș Mountains Natural Park from an ecosystem perspective

Maramureş Mountains Natural Park (MMNP) is a delimited territory in which the natural, historical, and cultural attributes are protected based on regulation, for conservation and sustainable development. The surface of the park is 133,621 ha. MMNP was declared a protected area of national interest in the category of natural parks (IUCN category V - Protected landscape: protected area managed mainly for landscape conservation and recreation) in 2005 [12-15]. It was created primarily for the conservation of the local landscape and traditions, for the protection of the zonal natural, spiritual and cultural heritage, for the sustainable management of forests and the encouragement of sustainable tourism based on these values [16]. Moreover, due to the presence of priority habitats and species, it was designated as a site NATURA 2000 - ROSCI0124 and ROSPA0131 Maramureş Mountains (see Fig. 1) [17,18].

The region is one of the richest biologically in the Northern Hemisphere, ensuring connectivity with Ukraine. In this area, there are species of wildlife such as lynx (*Lynx lynx*), wolf (*Canis lupus*), brown bear (*Ursus arctos*), European mink (*Mustela lutreola*), otter (*Lutra lutra*), as well as special species of mountain flora [12 13]. The main economic activity of the region is the exploitation of wood (with a very limited added value for the local economy), animal husbandry, and, not recently, tourism. The main tourist attractions are Mocăniţa - the steam train on the Vaser Valley, the traditional wooden architecture, the local traditions, and the special landscape. The local communities in the Maramureş Mountains Natural Park are located in the north and east, along the national road and rivers. There are two cities - Vişeul de Sus and Borşa, and 8 communes - Bistra, Leordina, Moisei, Petrova, Poienile de Sub Munte, Ruscova, Repedea, and Vişeu de Jos. The total population within MMNP being 87,580 inhabitants (according to the 2012 census).

Within the MMNP, several forest habitats (approx. 26) specific to the hill and mountain area were identified and mapped by specialists, including forest ecosystems of both beech and coniferous mixtures, as well as pure or even rare spruce. The forest vegetation covers approximately 65-68% of the PNMM area. Within the Natura 2000 habitats, the largest share in the area included in the habitat type - 9410 Acidophilous spruce forests (*Picea*) from the mountain floor to the alpine one (*Vaccinio-Piceetea*) which sums up several categories of forest habitats.

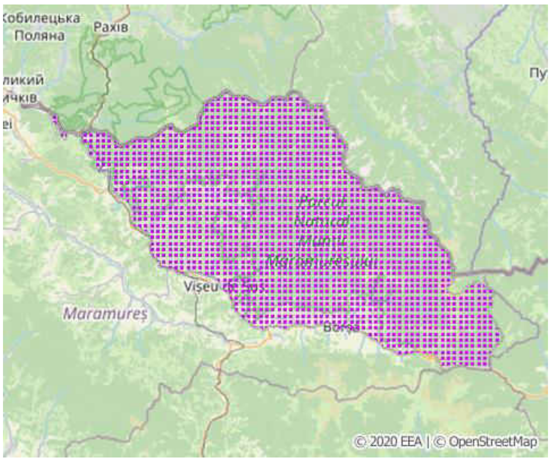

Fig. 1. Reference area of the Maramureș Mountains Natural Park [17]

The MMNP extends in the northern part of the Someş-Tisa hydrographic area. The hydrographic basins with the largest extension in the area of the protected natural area are Vaser, Viseu, and Ruscova. approximately 3.8-4% of the total area of PNMM. At the level of PNMM, within the three specific areas of any protected natural area, respectively ZPI - 17,619.25 ha, ZMD - 75,975.90 ha and ZDD - 40,025.85 ha (see Fig. 2) [19], there are the following categories of aquatic ecosystems:

- plots (763.1 ha) - permanent and non-permanent watercourses;
- lentic (24.44 ha) - natural lakes and accumulations;
- wetlands (4,356.77 ha) - swamps.

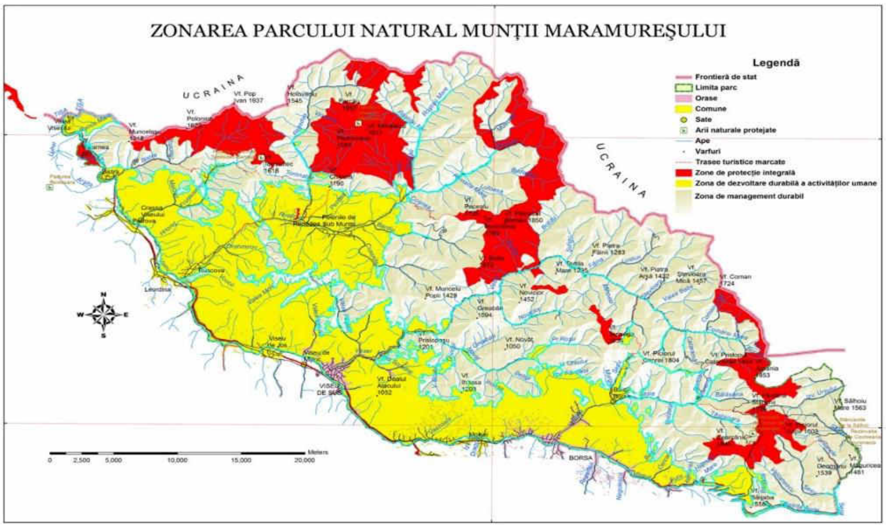

Fig. 2. Maramureș Mountains Natural Park zoning [19]

In the Maramureş Mountains, the continuity of the lotic systems is naturally interrupted sometimes by waterfalls of significant dimensions: Criva, Tomnatec, and Bardău. In the Vişeu basin, for example, water quality is influenced locally by mineral springs. The slow aquatic ecosystems in PNMM are less represented, for example, Lutoasa, Bârsânescu, Budescul Mare, Măgurii, Tăul Roşu, and Vinderel lakes. Representative wetlands are the Mejghi, Berescu swamps, the one on Vârtopul Mare, the one below Pietrosul Bardăului, etc.

3.3 Evaluation of the contribution of ecosystem services in the MMNP

Forest and aquatic ecosystems provide services, but they are not quantified and paid for at their true value, so their supply is guaranteed in the long run. Restrictions imposed by the management of protected years to ensure the conservation of natural ecosystems and the provision of ecosystem services are not properly assessed and, consequently, there is no chance of them being paid by the beneficiaries of the services generated.

The forestry sector, where about 50% of Romania's forests are privately owned, is underfunded and there are no subsidies or other means of support from the state budget or other funds to manage forests and maintain the role of protection. Besides, there are no compensation schemes for private forest owners in any protected natural area. This is one of the reasons why private owners are reluctant to support the implementation of management measures and very often resort to illegal practices. The assessment of the services provided by the forest ecosystems in the MMNP pilot area must take into account flood protection services, water supply services, soil erosion control, habitat establishment, and the provision of quiet areas specific to ecological transit corridors, provision of non-timber resources and ease of hunting activities. About the assessment of the services provided by aquatic ecosystems, this must include production services (water resources used for drinking and local economic activities, mineral water resources, etc.), regulation, and support services (flood control, biodiversity maintenance). and cultural services (the service of recreation and provision of aesthetic resources).

Table 1: Forest and aquatic ecosystem services and their beneficiaries

Beneficiaries of ecosystem services	Forest ecosystem services	Aquatic ecosystem services
Administrative-territorial units (ATU)	Flood protection Hydrological regularization Erosion control Aesthetic framework Non-wood resources Resources for pharmacology	Drinking water resource Mineral water resource Flood control Recreational resource (tourism)
Road infrastructure companies	Flood protection Erosion control against floods	Flood protection
Insurance companies	Flood protection	Flood protection
Energy sector	Hydrological regularization	Industrial water resource
Water bottling companies	Hydrological regularization	Drinking water resource Mineral water resource
Water dispensers	Hydrological regularization	Drinking water resource
Agricultural holdings	Flood protection Erosion control against floods	Industrial water resource Educational and scientific resource
Educational and research institutions	Educational and scientific resource	Educational and scientific resource
Tourism industry	Aesthetic framework Habitat and refuge	Drinking water resource Mineral water resource Fish resource Recreational resource (tourism)
Hunters' associations	Aesthetic framework Habitat and refuge Non-wood resources Genetic resources	Maintaining biodiversity Recreational resource (tourism)
Fish farms	-	Industrial water resource Fish resource
Non-timber products companies	Non-wood resources Genetic resources	-
Beekeepers	Habitat and refuge Non-wood resources Genetic resources	-
Pharmaceutical companies	Resources for pharmacology	Drinking water resource

In a participatory manner, a working methodology and a strategy on establishing and calculating compensations for forest owners with restrictions on timber harvesting were developed. Thus, it is desired that those forest owners with protection functions be compensated for the value of the services offered by the forest ecosystems, to maintain the protective functions of the forest. The methodology takes into account the loss of income of the owners, as well as the costs of active management for the forest areas restricted from felling. Similarly, we are working on a strategy that takes into account adequate pricing for the price of water that comes to serve users.
In the pilot area of PNMM, following the ranking of beneficiaries of ecosystem services for the two types of ecosystems according to Table 1, it can be seen that the administrative-territorial units prevail within the structure for forest ecosystem services for flood protection function, followed by hunting associations for the quiet area creation function. Among the aquatic ecosystems, the fish farms, together with the tourists and the administrative-territorial units benefit the most from the supply of the drinking water resource and for economic activities. For these categories of beneficiaries and not only should be followed the payment schemes (grants).
Park administrations (service provider) collect low revenues from visiting fees. The private sector (represented by tour operators, hotels, boarding houses, restaurants, transport companies, and souvenir manufacturers) is the main beneficiary of the ecosystem services provided by the protected area. The private sector is therefore the main stakeholder in getting involved in designing and adopting any possible payment mechanism for ecosystem services, thus keeping their productive potential (protected area) unaltered.
The lack of clear compensatory measures for landowners can also be an incentive for them to continue to use some of the resources (wood, stone, hay, etc.) in an unsustainable manner. This can lead to the degradation of ecosystems, which will negatively affect the supply of tourist services. Inadequate water management can also affect water quality and industry can affect air quality, while uncontrolled infrastructure development can lead to the loss of architectural styles so sought after by tourists.
Through this paper, we aimed to identify, describe, analyze and evaluate the services of forest and aquatic ecosystems in the MMNP ecosystem, by using for Romania the recommendations of the European Union, provided in the reports Mapping and Assessment of Ecosystem Services, on meeting the objectives of the EU Biodiversity Strategy.
The results obtained in the work in terms of identified ecosystem services are addressed to national and local public authorities and administrations, scientific communities, non-governmental organizations (NGOs), and the population. The final aim of the paper was to highlight the natural, scientific, recreational, and economic value of wetland ecosystems and the goods and services provided, as well as the role and importance of their sustainable management for biodiversity and socio-economic development of society.

4. Conclusions (and recommendations)

The evaluation of the services provided by the forest and aquatic ecosystems makes an important contribution to the estimation of the total economic value of the services in the area of the different protected areas. The identification, analysis, and valorization of the services provided by each category of the ecosystem cannot be always feasible, because, for certain categories of services, such as cultural ones, the analysis and valorization is performed at the level of the ecosystem complex, and not on each component unit in part. At the same time, economic evaluation (in other words monetary quantification) makes sense from the perspective of quantifying the value of nature to support human activities (the beneficiary principle pays), as well as quantifying the impact of these activities on ecosystems (the polluter pays principle).
In the sense of the above, there are at least two directions for promoting ecosystem services. On the one hand, we are talking about the compensations grant for ecosystem goods and services, and on the other hand, we are talking about the granting of incentive payments (as subsidies) for adopting a behavior that prevents and protects ecosystems.
The "polluter pays" principle is not enough to secure the provision of environmental services in the long run. Therefore, an attempt is made to establish a fair value for environmental services, based on impact and benefits, by applying the "beneficiary pays" principle. To sustainably manage

ecosystems in a protected area, an approach that integrates three pillars is needed: legislation - capacity - funding, and in these conditions no legislative framework is useful and effective in the absence of adequate implementation capacity and funding.
The approach we propose is that of shifting from a status of violation of the rules on the protection of ecosystems (forestry and/or aquatic) to a status of stimulating/rewarding practices that ensure the maintenance/restoration of their status. We believe that this forms a package of measures on ecosystem regulation (appropriate legislation), a form of administration and governance, and options for financing payment schemes. Under these conditions, the payments do not serve strictly restrictions or a certain status of ecosystems, but the shift of the behavior of landowners and/or users from actions damaging to natural ecosystems (negative impact) to behavior that sustainably integrates ecological systems. with the socio-economic ones (positive impact).

References

[1] ***. *Assessing the contribution of forest and aquatic ecosystems in the Maramureș Mountains Natural Park to the sustainable development of local communities. Biodiversity and ecosystem services.* SEE 2009-2014. Romanian.
[2] Stanciu, E., and F. Florescu. *Protected areas in Romania*. Braşov, "Green Steps" Publishing House, 2009. Available: https://propark.ro/images/uploads/file/manual arii protejate_net.pdf (Romanian).
[3] Mesaroș, M, B. Cioruța, and M. Coman. "Protected natural heritage on route from philosophy to environment engineering." *Scientific Bulletin of North University Center of Baia Mare, Mining, Mineral Processing, Non-ferrous Metallurgy, Geology & Environmental Engineering* 32, no. 1, (2018): 63-72.
[4] Pop, A.L., B. Cioruța, and M. Coman. "Considerations regarding the implications of philately in ecological education." *Scientific Bulletin of North University Center of Baia Mare, Mining, Mineral Processing, Non-ferrous Metallurgy, Geology & Environmental Engineering* 31, no. 1 (2017): 57-62.
[5] Cioruța, B., A.L. Pop, M. Coman, and A. Lauran. "Implications of philately in promoting the protected natural areas (I): Ceahlău National Park." *Scientific Bulletin of North University Center of Baia Mare, Series D, Mining, Mineral Processing, Non-ferrous Metallurgy, Geology and Environmental Engineering* 32, no. 1 (2018): 87-96.
[6] Pop, A.L., B. Cioruța, and M. Coman. "Implications of philately in promoting the protected natural areas (II): "Pețea Creek" Natural Reservation." *Scientific Bulletin of North University Center of Baia Mare, Series D, Mining, Mineral Processing, Non-ferrous Metallurgy, Geology and Environmental Engineering* 32, no. 2 (2018): 43-52.
[7] Rațiu, A. *Legal regime of protected natural areas - practical aspects*. Brașov, 2017. Available: www.juridice.ro/wp-content/uploads/2016/11/Regimul-juridic-al-ANP-aspecte-practice_Antoanela.pdf (Romanian).
[8] ***. Government Emergency Ordinance no. 57/2007 regarding the regime of protected natural areas, conservation of natural habitats, of wild flora and fauna. *Official Gazette* no. 442/2007. Available: https://aliantasportnatura.wordpress.com/legea-ariilor-protejate (Romanian).
[9] ***. Law no. 5/2000 on the approval of the National Spatial Planning Plan - Section III - protected areas. Available: www.cdep.ro/pls/legis/legis_pck.htp_act_text?idt=22636 (Romanian).
[10] ***. Decision no. 230 of March 4, 2003 on the delimitation of biosphere reserves, national parks and natural parks and the establishment of their administrations. Available: www.legex.ro/Hotararea-230-2003-36800.aspx (Romanian).
[11] ***. The Common International Classification of Ecosystem Services. Available: https://cices.eu.
[12] ***. "Maramureș Mountains Natural Park." *Wikipedia*. Accessed 08.07.2020. Available: https://ro.wikipedia.org/wiki/Parcul_Natural_Munții_Maramureșului (Romanian).
[13] ***. "Maramureș Mountains Maramureș Mountains Natural Park administration". Accessed 08.07.2020. Available: https://muntiimaramuresului.ro/index.php/ro (Romanian).
[14] ***. "Maramureș Mountains Natural Park." *Turist prin România*. Accessed 10.07.2020. Available: https://turistprinromania.com/2014/12/09/parcul-natural-muntii-maramuresului (Romanian).
[15] ***. "Maramureș Mountains Natural Park." *România sălbatică.* Accessed 13.07.2020. Available: https://romaniasalbatica.ro/ro/parc-natural/muntii-maramuresului (Romanian).
[16] ***. Available: http://d2ouvy59p0dg6k.cloudfront.net/downloads/metodologie_v2_final_1.pdf.
[17] ***. Available: https://eunis.eea.europa.eu/sites/193310.
[18] ***. Available: www.protectedplanet.net/parcul-natural-mun-ii-maramure-ului-natural-park.
[19] ***. Available: www.profudegeogra.eu/harta-turistica-a-muntilor-maramuresului/maramures.

Press of Parallelepiped-Shaped Briquettes

PhD Eng. **Gabriela MATACHE[1],** Dipl. Eng. **Valentin BARBU[1],** PhD Stud. Eng. **Ioan PAVEL[1],** Dipl. Eng. **Alina Iolanda POPESCU[1],** Physicist **Cristina Florina VOICU[2]**

[1] Hydraulics and Pneumatics Research Institute INOE 2000-IHP

[2] Caloris Group S.A.

*fluidas.ihp@fluidas.ro

Abstract: *The article analyses the basic elements necessary for the design of a press on which one can make medium-sized parallelepiped briquettes (150/60/60). First, the qualities of the raw material, the forest sawdust, the need and utility of making and using briquettes, as well as comparative elements with firewood are highlighted. The article presents a hydraulic solution of a medium sawdust briquette press and not only, of medium size (226kgf h), for which an indicative hydraulic scheme and an overall drawing are given, which is the basis of a future manufacturing.*

Keywords: *Press, briquettes, electrohydraulic, driving*

1. Introduction

1.1 The usefulness of sawdust

In recent years, it has been found that specialists around the world are facing the problem of diversifying energy sources while reducing the consumption of fossil fuels and forest wood. One of the resources that is easy to turn into energy is sawdust and other forest waste, or even straw waste resulting from the harvesting of cereal crops. The circular economy rule on the "zero waste" requirement is very successfully applied in both forestry and agriculture. Next, we will talk with priority about the processing of forest sawdust, which is easier to control and possible to extend the results to other types of raw materials from waste [1]. In our country there is a lot of sawdust, as waste at furniture factories, sawmills, wood cutting in forests, wood cutting in households, etc. On average, the density of the sawdust is 300 kg/m^3 even at a humidity of 55%. The most sought-after type of sawdust is beech. The density of the sawdust is usually estimated at 0.21 g /cm^3 or 210 kg/ m^3. Sawdust has some extremely dangerous characteristics, in addition to the ecological ones of environmental pollution and especially of the waters of mountain rivers. Among the most serious are those related to its danger as a carcinogen, but also as an element that attacks the skin, eyes and respiration. All these elements have contributed to finding technological solutions that highlight the qualities of a component for agricultural improvers, but especially those of fuel.

1.2 Useful items for the briquettes manufacturer and user

Briquettes are a solid fuel formed by pressing forest sawdust or straw vegetable, but also by pressing coal dust. In the process of burning, the briquettes increase their volume, so pay attention to the loading of the stoves, and consume more air than firewood. 95% of sawdust briquettes burn. In the end very little embers and very little ash result. There are rectangular briquettes on the market which, in addition to the forest sawdust, also include wood chips and which finally reach a calorific value of approx. 18.63 MJ/kg. The calorific value of the sawdust is 4,200-5,500 kcal/kg, wood used for fire, 1,600-2,800 kcal/kg. The professor from Brașov, Dragomir Peneș, once said that "a 1 Gcal gas power plant consumes twice as much as a similar power plant that uses sawdust briquettes".

1.3 The advantages of using sawdust briquettes [2]

Briquettes have already entered in our lives as a variant of replacing wood from the heating process with an equivalent, processed, obtained from forest or cereal vegetable waste, such as sawdust and chips. Does this solution have advantages or only disadvantages compared to wood?

The first advantage is that the moisture content of the sawdust, which is important in the heating process, is lower than that of wood. Forest sawdust briquettes have an approximate humidity of 5% to 10% compared to firewood which has a relative humidity of over 35% taking into account that wood fibre usually stores this amount of water in the atmosphere.
The second advantage is the calorific value of briquettes, which is 2-3 times higher than firewood.
The third advantage is that the briquettes burn longer, the burning being slower, very little ash remains, which in turn is a fertilizer. Finally, one of the intentions of the circular economy is fulfilled, that of carrying out processes that do not result in waste.
The fourth advantage is a complex, economical one, which results from the acceptable price, the ease of transport, the reduction of storage space and for many people the advantage of getting rid of cutting and cracking activities that require time, money and effort.
The fifth advantage is the ecological one, both by the fact that it takes an extremely aggressive raw material for the environment, but also by the fact that the combustion process is non-polluting.
The sixth advantage is that it succeeds in replacing coal, coke and natural gas, fossil fuels, non-renewable and with limited world reserves.
The comparative tests made by some specialists, regarding various fuels, showed that 10 kg of briquettes represent the equivalent of 5.5 l of oil, that 1 kg of briquettes has a calorific value of 4769 cal/kg or 19.97 MJ/kg and that a ton of briquettes is equal to 4 m^3 of firewood.

2. Constructively functional press solutions for the manufacture of sawdust briquettes

Briquetting is the technological process, which transforms the sawdust into briquettes, meaning presses it until the total evacuation of the contained air. Although, theoretically, briquettes can be made mechanically by plasticizing wood chips and then heat sintering them, or by mixing the sawdust with a chemical binder, the most used and almost the only solution used is by which the sawdust is pressed without introducing binders or other substances. In the case of a larger production of briquettes, a technological line consisting of a waste sorter, a thermal power plant, a sawdust dryer, a briquetting machine and auxiliary transport elements between machines is used. As the temperature at which the briquettes are removed is even 100 °C, they are often introduced into the technological and cooling line to reduce both manufacturing defects and the risk of fire.

2.1 Existing solutions on the press market

Several briquetting press solutions are currently known in various sizes and with a wide variety of functional and efficient features. An example is the Winter BP 60 briquetting press (https://www.winter-holztechnik.de/winter-maschinen/winter-brikettpresse-bp-60.html) which is hydraulically driven with a 5.5 kW motor having a productivity of 15-70 kg / h. Haba Hallenbausatz also produces a hydraulically operated press with a 7.5 kW motor, which has a productivity of 100 kg / h (https://habapellet.de.tl/Prese-bricheti.htm).

PRODECO Winter BP 60

Haba Hallenbausatz

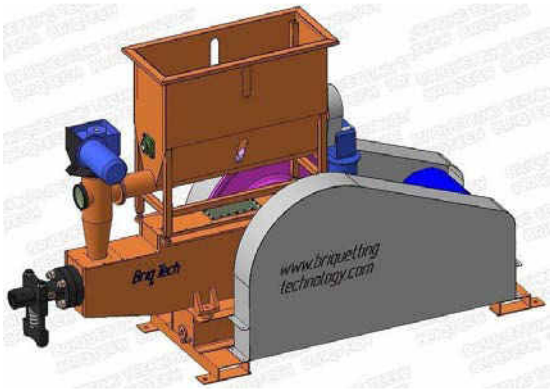

AGROBI BRICHET

Company: PRODECO - Italy produces a 4kW electrohydraulic press variant (NANO 55), but with a reduced productivity of only 15-50 kg/h, having only 7 cycles per minute (https://www.lemnsupermarket.ro/prese -de-briquetting-PRODECO-2298). The company AGROBI BRICHET produces electromechanical briquetting press BT-050-200 (https://agrobiobrichet.ro/presa-brichetat-mecanica-bt-050-200.html) with a capacity of 150-250 kg / h with main drive motor of 18.5 kW to which are added two other secondary motors under 3kW. Some manufacturers of briquetting presses out of a desire to display low energy consumption underestimate the installed power with the risk of achieving specific pressing forces in the mould at the limit, below 300 kgf /cm^2, resulting in insufficiently compacted, "elastic" briquettes that crumble in time. Another problem is that the technological process requires adjustments of forces and working speeds depending on the raw material used. Most of these presses use fixed flow hydraulic pumps, and for speed adjustment they use hydraulic throttles that are high energy consuming and heat the oil in the tank for cooling which is consumed again.

2.2 The chosen solution

The technical problem solved by the press for manufacturing parallelepiped briquettes, proposed, consists in the realization of a new solution of briquetting press with six parallelepiped moulds, located on a rotating plate, which are used simultaneously in the work process. Thus, the main cylinder on the pressing stroke also evacuates the previously pressed briquette, at the same time three mould nests are filled by the free fall of the raw material from the tank into the wells, and in the mould to be pressed, the material is prepressed with a screw, also placed in the tank which creates pressure on the material in the mould and constantly ensures the amount of raw material to achieve an approximately equal length of briquettes [3]. Thus, an increased productivity can be obtained by superimposing the working times on the phases preparatory to the final pressing. Practically the whole working process takes place at the same time as the final pressing, so the productivity is that regulated by the working frequency of the main cylinder plus the indexing time without other waiting times for filling moulds, prepressing and evacuation.

Figure 1 shows the realization of the hydraulic press of parallelepiped briquettes. It consists of a pressing cylinder **1**, which has mounted on the rod a double pressing and discharge punch **2**, a cylinder for indexing the moulded plate **3**, a raw material tank **4**, a prepress screw **5**, the frame **6**, a briquettes tray **7**, rotating plate with six parallelepiped dies **8**, and hydraulic station **9**.

Cylinder **3** rotates the mould plate **8** by actuating a ratchet mechanism in a fixed working position. Three of the six parallelepiped dies are located in front of the raw material tank **4** and are filled by its free fall during three work cycles until each of them reaches the pre-pressing station. The mould to be inserted on the pressing station is next to a screw **5**, which makes the pre-pressing and ensures an approximately equal volume of material for the final pressing. The material in the die on the pressing station is pressed by the cylinder **1**, which at the same time discharges the previously pressed briquette by means of the pressing / evacuation punch **2**. The cycle is resumed by a new indexing in a fixed position of work

.

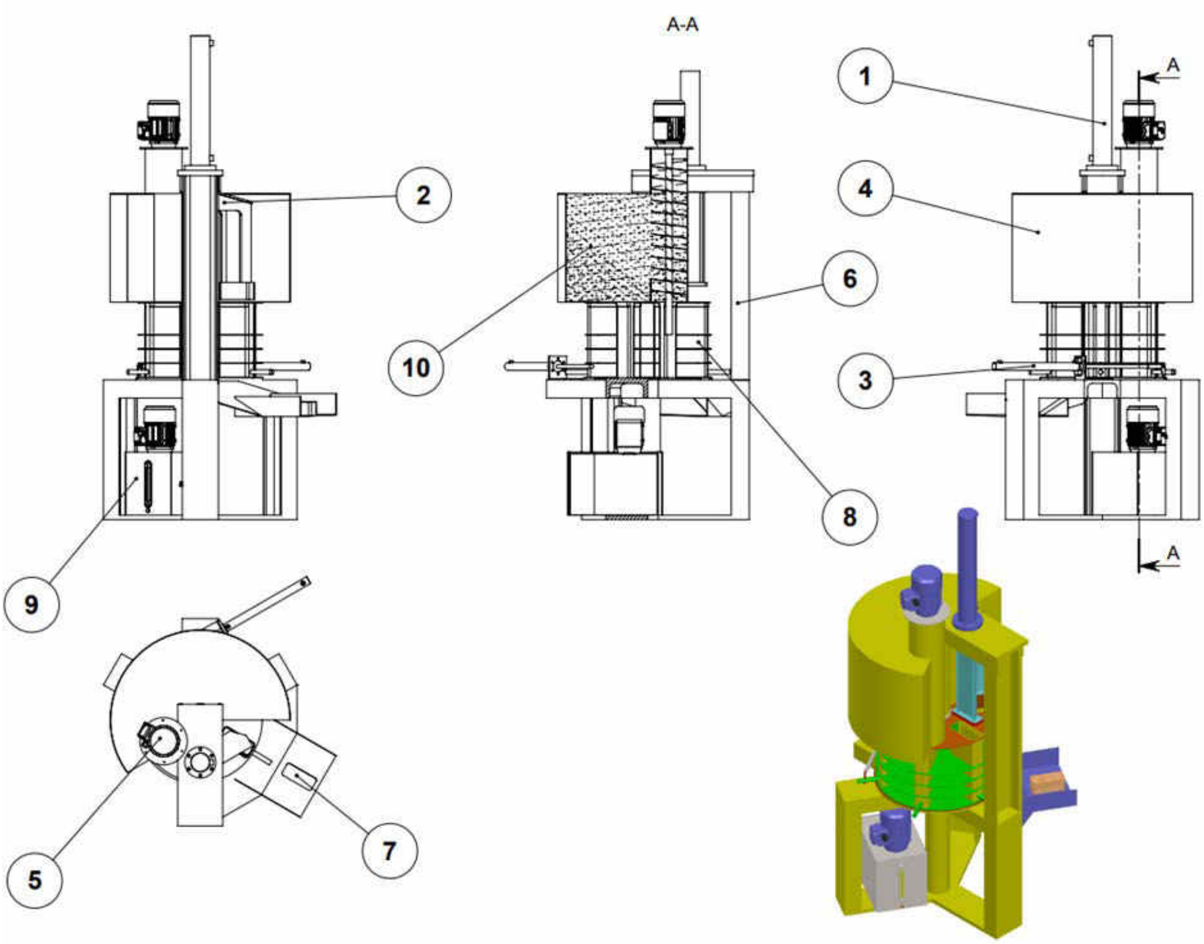

Fig. 1. Example of making the hydraulic press of parallelepiped-shaped briquettes

Component elements:

1. Pressing cylinder
2. Press / discharge punch
3. Indexing cylinder
4. Raw material tank
5. Prepress screw
6. Frame
7. Briquette tray
8. Rotating plate with parallelepiped dies
9. Hydraulic station

2.3 Hydraulic schematic diagram

The hydraulic scheme allows the adjustment of the working speed for the pressing and indexing cylinder by means of three-way flow regulators, which in the construction are not energy consuming, the excess flow being discharged to the basin at very low pressure [1].
Figure 2 shows the hydraulic scheme diagram for operating the hydraulic press of parallelepiped-shaped briquettes.
The hydraulic scheme diagram consists of electric pump **1,** which absorbs oil through the filter **2** and sends to the installation a fixed flow at the pressure set at valve **3**. The directional control valve **4** when is in the centre position allows the discharge of the flow to the tank without pressure, thus protecting the pump at start and energy saving in case of short work breaks. The same directional

control valve **4** alternates the pressing phase with the moulding plate indexing phase. The working speed for the pressing cylinder is adjustable with the flow regulator **5**, and by switching the directional control valve **6** the rod of the pressing cylinder is raised or lowered between the limiters L1 and L2. If accidentally the cylinder does not reach the limiter **L2** (for example too much material in the mould), although the compaction was done at the set pressure, the pressure switch **PR1** gives the command to continue the work cycle. The indexing cylinder **10** has the preferred position retracted and makes a return stroke by indexing the mould plate **3** by a ratchet mechanism in the next working position. The advance and retraction of the indexing cylinder rod is done through the directional control valve **9** between the limiters **L3** and **L4**. The indexing operating speed is adjustable with the flow controller **8**.

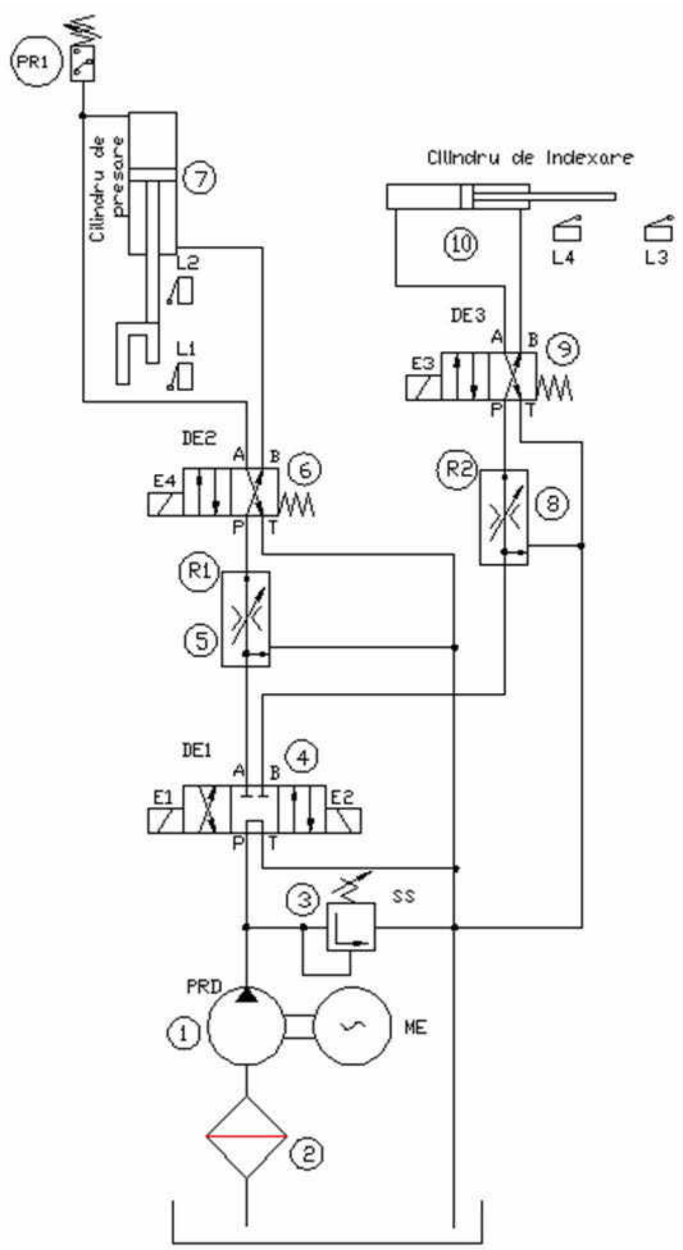

Hydraulic scheme structure

1. Electro pump
2. Suction filter
3. Pressure valve
4. Hydraulic press / index selection directional control valve
5. Three-way flow regulator
6. Hydraulic directional control valve for lifting / lowering press cylinder rod
7. Press / discharge cylinder
8. Three-way flow regulator
9. Hydraulic directional control valve for indexing cylinder control
10. Hydraulic cylinder for indexing

Fig. 2. Hydraulic scheme diagram for operating the hydraulic press of parallelepiped-shaped briquettes

3. Calculation elements for the sawdust briquetting press

The hydraulic system produces a specific pressing force of 700kg/cm^2 and a check is made at 900 kg/cm^2 during the briquetting process, thus ensuring a high quality of the briquette even in operating conditions at a fairly sufficient rate or with poor quality raw material on moisture, wood type or granulation.

Calculation starting elements [4]:
- Briquette size L-1-h (mm) 150 -60-60
- Press productivity 7 briquettes / min
- Density of R_{ob} briquette1000 kg/m^3 or 1 kg/dm^3 or 1g / cm^3
- Density of sawdust R_{or} 0.2 kg / dm^3
- Working pressure of the hydraulic installation, Pc, 200kgf /cm^2

Calculation of required forces:

- Briquette volume: $V_b = 15 \cdot 6 \cdot 6 = 540$ cm^3 (1)
- Briquette mass: $M=V_b \cdot R_{ob}= 540$ g = 0.54 kg (2)
- Briquette weight: G = 540 gf (3)
- Pressing surface, in the variant with the positioning of the briquette with h = 60 mm:

$$S_a= 60 \cdot 60 = 36 \text{ cm}^2 \quad (4)$$

- The specific pressing force is adopted:

$$F_s = 700 \text{ kgf /cm}^2 \quad (5)$$

- Required total pressing force:

$$F = 36 \cdot 700 = 25200 \text{kgf} \quad (6)$$

4. Design elements for the solution of the hydraulic briquetting press

Functional performance of presses:
a. The first performance of a press, the one that orients us to purchase is the production capacity.
b. The number of cycles per minute is between 5 and 10.
c. The calorific value of briquettes is between 4000 and 5500 kcal / kg.
d. The density varies quite a lot depending on the type of wood, from which the sawdust resulted, but also on the level of pressing. The density value is between 900 and 1400 kg / m^3.
e. The pressing force is between 700kgf / cm^2 and 2000 kgf / cm^2.
f. The burning temperature of the briquette is between 900 and 1200 °C.
g. The ash resulting from normal combustion is between 1.5% and 10% of the amount of briquettes used.

5. Conclusions

5.1 Briquettes from forest sawdust or from any other material is a useful and important fuel for a country's economy, with an energy value of more than 4400kcal / kg.
5.2 The burning of briquettes is not polluting as the manufacturing process excludes the use of additives of any kind.
5.3 The use of briquettes can save up to 30% compared to any other fuel.
5.4 The briquetting presses are complex equipment, hydraulically operated most of the time, and have capacities from 30kg/h to 250kg/h, and if they are organized in complex production lines, they can have much higher productivity.

Acknowledgments

This paper has been developed in INOE 2000-IHP, as part of a project co-financed by the European Union through the European Regional Development Fund, under Competitiveness Operational Programme 2014-2020, Priority Axis 1: Research, technological development and innovation (RD&I) to support economic competitiveness and business development, Action 1.2.3 – Partnerships for knowledge transfer, project title: Eco-innovative technologies for recovery of biomass wastes, project acronym: ECOVALDES, SMIS code: 105693-594, Financial agreement no. 129/23.09.2016.

References

[1] Maharani, Rizki, Tamai Yutaka, Takashi Yajima, and Terazawa Minoru. ”Scrutiny on physical properties of sawdust from tropical commercial wood species: effects of different mills and sawdust’s particle size.” *Indonesian Journal of Forestry Research* 7, no. 1 (2010): 20-32.
[2] http://www.brichete-din-rumegus.ro/avantaje/.
[3] Marin, Virgil, and Alexandru Marin. *Automatic hydraulic systems - Structure, adjustment, operation / Sisteme hidraulice automate - Constructie, reglare, exploatare*. Bucharest, Technical Publishing House, 1987.
[4] *** Assofluid Italian Association of Manufacturing and Trading Companies in Fluid Power Equipment Components*. Hydraulics in Industrial and Mobile Applications*. Brugherio (Milano), Grafiche Parole Nuove s.r.l. Publishing House, 2007.

FLUIDAS

NATIONAL PROFESSIONAL ASSOCIATION OF HYDRAULICS AND PNEUMATICS IN ROMANIA

fluidas@fluidas.ro